Data supplement for Norman et al., Subcortico-Cortical Dysconnectivity in ADHD: A Voxelwise Mega-Analysis Across Multiple Cohorts. Am J Psychiatry (doi: 10.1176/appi.ajp.20230026)

SUPPLEMENTARY METHODS

Study protocols for included datasets

Adolescent Brain Cognitive Development (ABCD)

The Adolescent Brain Cognitive Development (ABCD) study is an ongoing multisite, longitudinal neuroimaging study of N=~11,875 youths(1, 2). See a special issue of Developmental Cognitive Neuroscience (Volume 32, Pages 1-164, August 2018). Children were aged between 9 and 11 years old at baseline, and largely recruited via probability sampling of public and private elementary schools within the catchment areas of 21 research sites in the United States of America. Demographic data were monitored to ensure that the study met targets for sex, socioeconomic, ethnic, and racial diversity. Exclusion criteria for children included not being fluent in English or having a parent not fluent in English or Spanish, major medical or neurological conditions, gestational age <28 weeks or birthweight <1200 g, contraindications to MRI scanning, a history of traumatic brain injury, a current diagnosis of schizophrenia, moderate/severe autism spectrum disorder, intellectual disability, or alcohol/substance use disorder.

Clinical and demographic data were taken from the ABCD-BIDS (NDA Collection 3165) participants.tsv file and ABCD release 3.0. For subjects without usable data at baseline we used raw imaging data from the two-year follow-up. We first processed data from the ABCD-BIDS project (NDA Collection 3165)(3). We downloaded additional scans from the NDA Collection

#2573 using the ABCD-BIDS protocol(3). The raw data are available at https://nda.nih.gov/edit_collection.html?id=2573. We excluded scans recommended for exclusion according to the ABCD quality control protocol (exclusion criteria: imgincl_rsfmri_include=0)(1, 2).

ADHD diagnoses were made according to a validated computerized parent-answered Kiddie Schedule of Affective Disorders and Schizophrenia for DSM-5 (KSADS-COMP) (4). This included current-ADHD (ksads_14_853_p = 1), ADHD-NOS (ksads_14_856_p =1) and ADHD in partial remission (ksads_14_855_p = 1). A large number of subjects met criteria for past-ADHD only (ksads_14_854_p=1) at baseline (N=~1,100). Given the young age of the sample, this number is likely inaccurate and we did not include these subjects in the categorical analyses as ADHD cases, unless they were currently taking a psychostimulant medication, in line with previous work using the ABCD cohort (5). Lacking a full-scale IQ measure in ABCD, we assessed estimated general intelligence using WISC-V Matrix Reasoning total scale score [5]. Race and ethnicity were based on parent reported variables dem_003 and dem_004. Race, ethnicity, and sex for the child were reported by the parents (pdem02). Household income was assessed via parent report (demo_comb_income_v2).

All procedures were approved by a central Institutional Review Board (IRB) at the University of California, San Diego, and by individual site IRBs. Parents/guardians provided written informed consent and children assented before participation in the study. We have access to the genetic and phenotypic data from the NIMH data archive (NDA) Adolescent Brain Cognitive Development (ABCD) / Connectome Coordination Facility (CCF) permission group under a data use certification agreement.

Healthy Brain Network (HBN)

The HBN sample is enriched for emotional and behavioral problems, with ADHD diagnoses present in more than half of the subjects released to date (release 10). Exclusion criteria included serious neurological disorders, neurodegenerative disorders, acute encephalopathy, hearing or visual impairment, lifetime substance abuse necessitating chemical replacement therapy/acute intoxication at time of study, recent diagnosis of a severe mental disorder or manic/psychotic episode within the last 6 months without ongoing treatment, in addition to the onset of suicidality/homicidality where there is no current, ongoing treatment. All participants > 18 years provided signed informed consent, while parents/legal guardians signed informed consent for participants < 18, in addition to minors giving a written assent. The Chesapeake Institutional Review Board approved the study (https://www.chesapeakeirb.com/). Brain imaging data for the Healthy Brain Network (HBN) study are publicly available. We accessed additional phenotypic data via a signed data use agreement with the Child Mind Institute.

ADHD diagnoses were determined via the Diagnosis_ClinicianConsensus spreadsheet, which considered the outcomes of parent, child and (where collected) teacher KSADS-COMP. For some early subjects in the study, a non-computerized version of the KSADS was completed. A team of licensed clinicians also formed “consensus diagnoses” based on other study assessments, notes, the automated K-SADS diagnoses and their own clinical judgement. Medication status was based on the DailyMeds spreadsheet. The sex, race and ethnicity of the child were based on interview with parents (PreInt_Demos_Fam).

Human Connectome Project – Developmental (HCP-D)

The HCP-D is an accelerated longitudinal study of healthy brain development (age range 5-21 years old at baseline) (6, 7). We included data from HCP-Development Lifespan 2.0. This is a multi-site study with sites in four locations (Boston, Los Angeles, Minneapolis, St. Louis). Diagnostic data were unavailable at the time of data analysis, but the cohort was described as largely healthy at baseline. While medication data were unavailable, we modeled subjects in this dataset as unmedicated given the healthy nature of the sample and the fact that prolonged use of medications for psychiatric disorders was an exclusion criterion. Further exclusion criteria included the subject or subject's parent having insufficient English abilities to complete screening and consent procedures, premature birth (more than 3 weeks early), low birth weight (<5 lb), lifetime history of serious medical conditions, a history of head injuries, hospitalization for two or more days, receiving special services at school and MRI contraindications. We used data from release 2.0 (https://www.humanconnectome.org/study/hcp-lifespan-development/data-releases). Sex of the subjects at birth, race and ethnicity were taken from ndar_subject01. We have access to the phenotypic data from the NIMH data archive (NDA) Adolescent Brain Cognitive Development (ABCD) / Connectome Coordination Facility (CCF) permission group under a data use certification agreement. Subjects provided written informed consent and assent, although parents of participants under 18 years provided written informed consent for their child's participation. All procedures were approved by a central Institutional Review Board administered at Washington University in St. Louis (IRB #201603135).

Neurobehavioral Clinical Research (NCR)

The NCR study was enriched for ADHD symptoms by targeting the recruitment of children and adolescents with ADHD traits in addition to children and adolescents with existing ADHD diagnoses and unaffected controls(8). ADHD diagnoses were based on the Parent Diagnostic Interview for Children and Adolescents (DICA-IV), conducted by two experienced clinicians (interrater reliabilities of $\kappa > 0.9$), and made according to DSM-IV-TR criteria(9). A symptom was defined as present if it had an adverse impact on functioning at school, home and/or with peers (with a range from 0 to a maximum of 9 symptoms in each category). Attention-deficit/hyperactivity disorder combined type was diagnosed when the subject had both six or more symptoms of inattention and six or more symptoms of hyperactivity/impulsivity. The inattentive or hyperactive/impulsive subtypes were diagnosed when symptom counts ≥6 were confined to one of these domains. ADHD-NOS was considered when subjects had 5 impairing symptoms in either domain, but less than six symptoms in both domains. Diagnoses of past-ADHD/ADHD in partial remission were assigned for subjects who met criteria for ADHD or ADHD-NOS at an earlier timepoint of the study but not at the time of their included scan. The unaffected subjects did not meet criteria for ADHD at the time of their scan or at any previous assessment. Parents were asked the sex, race and ethnicity of their child. Exclusion criteria for all subjects included IQ<70, evidence of medical or neurological disorders affecting cerebral anatomy, psychosis or bipolar disorder. The study was approved by the IRB of the NIH. Parents or guardians of children gave written consent and children gave assent.

National Consortium on Alcohol and Neurodevelopment in Adolescence (NCANDA)

The NCANDA cohort is from an accelerated longitudinal study of roughly 830 youths and young adults, aged 12 to 21 years old(10–15). There are five data collection sites: Duke University, University of Pittsburgh Medical Center, Oregon Health & Science University, University of California, San Diego, and SRI International. Each site aimed to recruit a community sample that was reflective of local racial/ethnic distributions of the surrounding area with equal sex proportions in each age group. Exclusion criteria for children included not being fluent in English or having a parent not fluent in English or Spanish, major medical or neurological conditions, IQ<70, gestational age <30 weeks or low birth weight, contraindications to MRI scanning, a history of traumatic brain injury, prenatal alcohol/drug exposure, a current or persistent major Axis I psychiatric disorder that would interfere with valid completion of the protocol including psychosis, substance dependence, parental history of psychotic disorder, intellectual disability, or use of psychotropic medications. Subject sex, race and ethnicity were assessed at baseline via a demographics interview(10).

Given the small number of subjects with ADHD in this dataset, we did not include it in the categorical analyses. All subjects were free from psychostimulant medication. The institutional review board at each site approved the study. Adult participants consented to participating, and minors provided written assent along with consent from a parent/legal guardian. We used data from NCANDA_PUBLIC_4Y_REDCAP_V01 (https://dx.doi.org/10.7303/syn22216455), NCANDA_PUBLIC_BASE_RESTINGSTATE_V01 (https://dx.doi.org/10.7303/syn11605291) and NCANDA_PUBLIC_BASE_STRUCTURAL_V01 (https://dx.doi.org/10.7303/syn11541569). We accessed the de-identified NCANDA dataset via

adata use agreement in place with the National Institute on Alcohol Abuse and Alcoholism (NIAAA) (http://www.ncanda.org/datasharing.php).

NKI-Rockland cohort

The NKI-Rockland cohort is comprised of N=1500 child, adolescent and adult subjects from Rockland County, population of 311,687 per the 2010 census, located 15 miles northwest of New York City. The racial and socioeconomic demographics of Rockland County approximately resemble those of the United States census(16). Recruitment was made via a number of sources, including flyers posted at schools, shops, community centers and community events (e.g., street fairs) within Rockland County, as well as via appeals for word-of-mouth recommendations. A team of clinicians discussed data from all study assessments, including clinician administered K-SADS interviews, and formed “consensus diagnoses” based on these assessments, that incorporated impressions of impairment due to symptoms, and their own clinical judgements (16, 17). Full-scale IQ was assessed via the Wechsler intelligence scale (int_14) (18). Socioeconomic status was defined according to household income (demos_02). Race and ethnicity were based on parent reported variables dem_003 and dem_004. Sex was based on dem_002 (What is your sex? (Male = 1, Female = 2, ‘Don't Know’ = Missing Data)).

Institutional Review Board Approval was obtained for this project at the Nathan Kline Institute. Written informed consent was obtained from legal guardians and written assent was obtained from the participants.

MRI Acquisition

ABCD

Full details regarding imaging acquisition are available elsewhere and the details are discussed in brief here(1, 2). Four separate resting-state scans were acquired per subject (TR = 800 ms, TE=30ms, flip angle=52°, multiband acceleration factor=6, FOV=216 × 216, slices=60, acquisition voxel size 2.4 x 2.4 x 2.4mm, ~380 volumes [~5 minutes]). During the scan, subjects were instructed to relax and focus on the fixation cross. A 3D T1w inversion prepared RF-spoiled gradient echo scan was also acquired (TR= 2500 ms, TE= range 2-2.9ms (depending on site), flip angle= 8°, FOV= 256 × 256 mm, voxel size at acquisition= 1 × 1 × 1 mm, slices=range 176-225, depending on site). Where possible, anatomical images were acquired using prospective motion correction (1, 2). Resting-state data were acquired with eyes open and passive viewing of a cross hair.

Healthy Brain Network

For more information about the MRI parameters, see http://fcon_1000.projects.nitrc.org/indi/cmi_healthy_brain_network/MRI%20Protocol.html. Two runs of resting-state fMRI data were collected using a T2*-weighted BOLD echo-planar imaging sequence (TR=800ms, TE=30ms, multiband acceleration factor = 6, number of slices =60, voxel size= 2.4×2.4×2.4 mm, 375 volumes [5 minutes]). For all included sites, anatomic T1 images were acquired using 3-D Magnetization-Prepared Rapid Gradient-Echo Imaging (MPRAGE) sequences (TR= 2.5 s, TE= 3.15 ms, flip angle= 8°, FOV= 256 mm, slice thickness= 0.8 mm, slices=224). In addition, CBIC acquired an MPRAGE structural scan based on the ABCD and HCP-D study protocols including prospective motion correction (TR = 2.5 s, TE = 2.88 ms, flip

angle= 8°, FOV= 256 mm, slice thickness= 173 mm, slices= 176). Where possible, we used the structural scans with prospective motion correction as has been recommended by HBN authors for studies of 'hyperkinetic' populations(19). Specific instructions for the resting-state scan were as follows: "Please lie quietly with your eyes open, and direct your gaze towards the plus symbol. During this scan let your mind wander. If you notice yourself focusing on a particular stream of thoughts, let your mind wander away."

Human Connectome Project – Development

Full details and rationales are provided elsewhere(6, 7). Data were collected on a Siemens 3T Prisma MRI using a 64-channel head coil. Four resting-state runs were collected per subject. These functional scans were acquired with a gradient-recalled echo-planar imaging sequence (TR=800ms, TE=37ms, multiband factor=8, flip angle = 52°, 2.0 mm isotropic voxels, 488 volumes [~6 minutes 30 seconds]). A high-resolution, MPRAGE T1w image was also acquired using prospective motion correction (TR=2,400ms, TE=2.18ms, flip angle= 8°, FOV = 256 × 240 × 167 mm, 0.8 mm isotropic voxels, 208 slices). During the resting-state scan, participants were asked to lie with eyes open, and look at white fixation cross presented on a dark background. They were further asked to "think of nothing in particular", and not to fall asleep.

NCANDA

Imaging data was collected via 3T General Electric (GE) Discovery MR750 at 3 sites (University of California San Diego, SRI International, and Duke University) and via 3T Siemens TIM TRIO scanners at 2 sites (University of Pittsburgh and Oregon Health & Sciences

University). The parameters for the resting state scans were as follows: TR=2,200ms, TE=30ms, flip angle = 79°, voxel size=3.75mm, 3.75mm, 5mm, slices= 32, 275 volumes [~10 minutes]. Regarding structural images, the GE sites used an Array Spatial Sensitivity Encoding Technique (ASSET) for parallel and accelerated imaging with an 8-channel head coil and acquired an Inversion Recovery-Spoiled Gradient Recalled (IR-SPGR) echo sequence (TR = 5.904 ms, TI = 400 ms, TE = 1.932 ms, flip angle = 11°, NEX = 1, matrix = 256 × 256, FOV = 24 cm, slice dimensions = 1.2 × 0.9375 × 0.9375 mm, slices=146). The Siemens sites used a 12-channel head coil and parallel imaging and temporal acceleration with iPAT and acquired an MPRAGE sequence (TR = 1900 ms, TI = 900 ms, TE = 2.92 ms, flip angle = 9°, NEX = 1, matrix = 256 × 256, FOV = 24 cm, slice dimensions = 1.2 × 0.9375 × 0.9375 mm, slice=160). During resting-state scans, participants kept their eyes open and focused on a white fixation cross that appeared on a black background.

NCR

Up to two runs of resting-state fMRI data for the NCR cohort were acquired using a gradient-echo-planar series acquisition procedure (TR = 2,500 ms; echo time = 27 ms; flip angle = 90°; 44 axial contiguous interleaved slices per volume; 2.8-mm slice thickness; field of view = 22 cm; 64 × 64 acquisition matrix; single-voxel volume = 3.4 mm, 3.4 mm, 2.8 mm, volumes=120 [5mins]) with whole-brain coverage on a 3-T General Electric MR 750 scanner. Subjects were instructed to lie in the scanner at rest and look at a fixation cross. A baseline-weighted anatomical image [magnetization prepared rapid acquisition gradient recalled echo sequence (MP RAGE): 124 axial slices, 1.3-mm slice thickness, field of view = 22 cm, 224 × 224 acquisition matrix] was acquired to assist with the alignment of the functional image with

normalization to stereotaxic space. Participants were instructed to lie in the scanner at rest, looking at a fixation cross.

NKI-Rockland cohort

Neuroimaging data were collected on a Siemens Magnetom TrioTim syngo MR B17. We used the two ~10-minute multiband runs of resting-state fMRI (Run 1: TR = 645 ms, TE = 30 ms, multi-band factor = 4, slice thickness = 3.0 mm, FA=60°, FOV = 222 × 222 mm, voxel size=3mm × 3mm × 3mm, slices=40, volumes=900; Run 2: TR = 1400 ms, TE = 30 ms, multi-band factor = 4, slice thickness = 2.0 mm, flip angle = 65°, FOV = 224 mm × 224mm, slices = 64, volumes=404). Acquisition of the MPRAGE images followed the following scanning parameters: TR = 1,900 ms, TE = 2.52 ms, flip angle = 9°, FOV = 250mm, slice thickness = 1.0 mm, voxel size = 1.0 × 1.0 × 1.0 mm, and slices = 176). Detailed scanning parameters are provided on the NKI-Rockland website (http://fcon_1000.projects.nitrc.org/indi/enhanced/mri_protocol.html). During the resting-state scan, participants were asked to keep their eyes open and fixated on a fixation cross, stay still, and not think of anything in particular.

Preprocessing of fMRI images

Data were preprocessed using fMRIPrep version 20.2.3, a Nipype based tool (20, 21). Each T1w (T1-weighted) volume was corrected for intensity non-uniformity using N4BiasFieldCorrection v2.1.0 (22) and skull-stripped using antsBrainExtraction.sh v2.1.0 (using the OASIS template). Brain tissue segmentation of cerebrospinal fluid, white-matter and gray-matter was performed on the brain-extracted T1w using fast (FSL 5.0.9,

RRID:SCR_002823, Zhang, Brady, and Smith 2001). Freesurfer's recon-all was used to reconstruct brain surfaces (FreeSurfer 6.0.1, RRID:SCR_001847, Dale, Fischl, and Sereno 1999). The previously estimated brain mask was refined with a custom variation of the method to reconcile ANTs-derived and FreeSurfer-derived segmentations of the cortical gray-matter of Mindboggle (RRID:SCR_002438, Klein et al. 2017). Volume-based spatial normalization to MNI152NLin2009cAsym space was performed using brain-extracted versions of both T1w reference and the T1w template via nonlinear registration with antsRegistration (ANTs 2.3.3). Functional data were motion corrected using mcflirt (FSL v5.0.9) (23).

The final preprocessing steps used the xcpengine toolbox version 2.2.3 (https://xcpengine.readthedocs.io), and the 36-parameter + despiking functional design(24–28). Despiking refers to the removal of and interpolation over intensity outliers in each voxel's time series using AFNI's 3DDESPIKE utility(29). We then performed de-meaning and removal of any linear or quadratic trends. The 36-parameters regressed from the timeseries included the 6 motion estimates, global signal, and white matter and cerebrospinal fluid-derived time series), and then their derivatives, quadratic terms, and squares of derivatives(24, 25). Temporal filtering was performed using a bandpass filter of 0.01–0.08 Hz (first-order Butterworth filter(30)) and images were smoothed in FSL using a Gaussian-weighted kernel with 6 mm FWHM(31). We excluded subjects where <50% collected data (neuroimaging runs) were usable. Runs/subjects were excluded if they failed to complete the preprocessing pipeline. Note that while in most cases this was likely due to problems with the data, for instance missing or poor quality T1 preventing completion of the Freesurfer pipeline or missing or incorrect header information in the jsons received from the study sites, some failures may have been due to computer cluster

failures or exceeded cluster walltime limits. Given the size of the dataset we were not able to assess the reasons for such failures for all subjects.

Resting-state connectivity

We examined robustness of findings across two sets of seed regions. First, primary analyses were based on seeds for the caudate nucleus, putamen, nucleus accumbens and amygdala, selected from the Harvard-Oxford probabilistic anatomical atlas (threshold ≥25% probability) (32).

The second set of subcortical seeds correspond to those used in our previous work(33, 34). These seeds also allowed us to examine for potential functional heterogeneity between subregions of the subcortical seeds. Seeds for the dorsal caudate (MNI: x = ±13, y = 15, z = 9), ventral caudate (MNI: x = ±10, y = 15, z = 0), nucleus accumbens (MNI: x = ±9, y = 9, z = −8), dorsal putamen (MNI: x = ±28, y = 1, z = 3) and ventral putamen (MNI: x = ±20, y = 12, z = −3) were adopted from work by Di Martino and colleagues(25). We included ventral (MNI: x = ±21, y = −3, z = −23) and dorsal (MNI: x = ±21, y = −4, z = −13) seeds for the amygdala. These corresponded with the basolateral and centromedial amygdala, respectively(36). Mean timeseries were extracted from voxels included within 5mm radius spherical masks placed around the central coordinates for each region of interest.

Mean region of interest timeseries were then correlated with the timeseries of each cortical and subcortical gray matter voxel in the brain, thereby creating subject-level voxelwise connectivity maps for each region of interest, which were subsequently Fisher-z transformed.

We found that ADHD-related connectivity patterns were similar across the different striatal seeds. This suggests that these seeds are sharing a considerable amount of variance in their time-series, and results are therefore non-specific. Therefore, partial correlation analyses were performed to test for potentially more direct associations. Specifically, for the Harvard-Oxford seeds, we examined associations between the seed timeseries and the remaining voxels of the brain while controlling for the timeseries of the remaining three seed regions. This modeling was performed using the ppcor package for R(37).

In the first instance, we examined bilateral seed regions. However, in follow-up analyses we also examined for potential hemispheric heterogeneity using hemispheric-specific seeds for the Harvard-Oxford regions of interest.

Modeling approach

Mixed-model mega-analysis

Prior to analysis, race and ethnicity variables were re-coded to the following categories: non-Hispanic White, Hispanic/Latino, Black/African American, Mixed/Other/Declined/Missing, Asian). Socioeconomic status (household income) was re-coded as follows: <$50,000, $50,000-$100,000, $100,001-$200,000, >$200,000. The primary model was based on the following syntax in the lmerTest (version 3.1-3) package(38), where Y is replaced by each voxel as part of a simple for-loop in R.

```
m1 <- lmer(Y  ~ ADHD_controls +Age + Sex + Minutes +
CBCL_internalizing_raw_score + CBCL_externalizing_raw_score+ SES+ race_ethnicity+
MeanRMS +I(MeanRMS^2) +(1|Study/Scanner-ID/family_ID), data=group_dataframe)
```

For the CBCL model, similar syntax was used.

m1 <- lmer(Y ~ CBCL_Attention_Problems_Raw_score +Age + Sex + Minutes

+ CBCL_internalizing_raw_score + CBCL_externalizing_raw_score + SES+ race_ethnicity+

MeanRMS +I(MeanRMS^2) +(1|Study/Scanner-ID/family_ID), data=CBCL_dataframe)

Within the group-level voxelwise images, t-values were converted to z values with Hughett's transform(39). Effect sizes maps were also generated. Effect sizes were estimated from the mixed-effects models t-values using the package effectsize (version 0.5) for R (40). Cohen's d was estimated for case-control comparisons, and partial-r was calculated for associations with CBCL (40).

We were concerned that inclusion of the three CBCL subscales in the model would produce multicollinearity. To test this, we ran models on extracted significant clusters and examined the variance inflation factor (VIF) using the car package (41). All VIF <5.

We used the linear hypothesis function from the car package to test whether the strength of the associations between Fisher-z transformed correlation coeeficients at each voxel and raw scores on the Attention Problems scale differed significantly from those involving Fisher-z transformed correlation coeeficients and the Internalizing and Externalizing broadband scales.

Example syntax, applied at each voxel, is given below for the comparison between CBCL_Attention_Problems_Raw_score and CBCL_internalizing_raw_score.

linearHypothesis(m1, " CBCL_Attention_Problems_Raw_score - CBCL_internalizing_raw_score = 0").

Resultant voxelwise chi-square statistics were transformed to z-scores, to facilitate image thresholding.

Group-level statistical maps were thresholded using Gaussian random field theory via FSL's Cluster command(31). AFNI's @chauffeur_afni and custom code was used to generate brain images and results tables (https://afni.nimh.nih.gov/pub/dist/doc/program_help/@chauffeur_afni.html). Supplementary images were also created using DPABI(42).

Sensitivity analyses and robustness checks

To ensure the robustness of the findings, several sensitivity analyses and robustness checks were conducted. To remove the correlation between ADHD diagnosis/Attention Problem scores and in-scanner motion, we employed a greedy matching algorithm(43). In each loop, the correlations between ADHD diagnosis or attention problems and mean-RMS and mean-RMS^2 were calculated excluding each subject one at a time, and the subject whose exclusion resulted in the biggest decrease in correlation coefficients was removed from the sample. The algorithm stopped when associations with both mean-RMS and mean-RMS^2 $p \geq 0.5$.

As estimated intelligence may in part be impacted by ADHD, and not just temporally antecedent, we performed analyses both with and without this covariate. The covariate was calculated by z-scoring either measures of intelligence quotient (IQ; NCR, HBN, NKI-Rockland

and NCANDA datasets) or scaled matrix (ABCD, HCP cohorts) within cohort, depending on the metric that was available(44).

Psychostimulants are widely held to act via a modulation of functioning within fronto-striatal circuits(45, 46). We therefore examined whether findings held in psychostimulant-free youth with ADHD. By examining this specific subgroup, we aimed to explore the potential neural mechanisms underlying ADHD beyond the influence of medication.

Associations with neuropsychological task performance.

We focus on cognitive features consistently associated with ADHD through meta-analyses, namely working memory, processing speed, attention/interference control and impulsive decision making(47–55). These cognitive domains have also been tied to subcortico-cortical functioning(45, 46, 56–58). Performance in the working memory, processing speed, interference control domains was tested using composite variables from the NIH toolbox(59). The specific modules used were the List Sorting Working Memory module (working memory), the Pattern Comparison Processing Speed module (processing speed), and the Flanker Inhibitory Control & Attention module (attention and interference control). Decision making impulsivity was measured using the Cash Choice task. The single-item Cash Choice Task, a measure of delayed reward discounting, asked children, 'Let's pretend a kind person wanted to give you some money. Would you rather have $75 in three days or $115 in 3 months?'. We chose to use this measurement of decision making in place of the delay discounting task collected in later waves of the ABCD study because it aligned with the age of participants during scanning.

Models examining associations between neurosychological and subcortical-cortical connectivity took the following form, where Y is replaced by each voxel as part of a simple for loop. neurosych_parameter is replaced by the neuropsychology parameter for each cognitive domain.

```
m1 <- lmer(Y ~ neurosych_parameter+ Age + Sex +SES+ race_eth +
Minutes+MeanRMS+I(MeanRMS^2)+(1|Scanner-ID/family_ID), data=neurosych_dataframe)
```

Forest plots for brain findings

Mean Fisher-z values for each significant cluster were extracted for each subject, and we re-ran models within each cohort to produce mega-analytic forest plots. Importantly, the data contained in the plots were extracted from clusters that were already found to be significant in the whole-brain analyses. In addition, the plots are based on extracted cluster data whereas the primary analysis was performed separately at each voxel. Therefore, these plots were produced only to illustrate the relative influence of each dataset in driving the significant associations and do not themselves provide exact representations of the tests performed in the primary analyses.

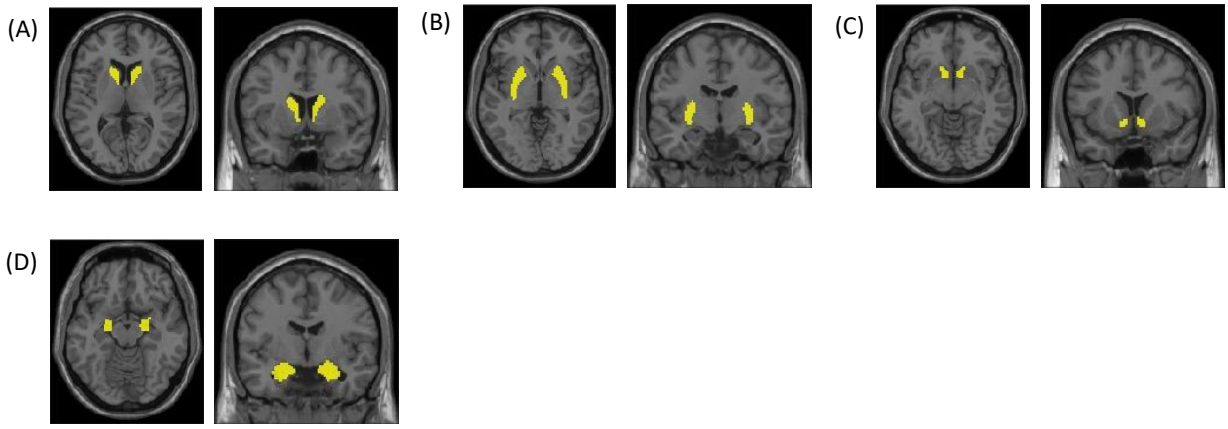

FIGURE S1. Shows the spatial locations of the Harvard-Oxford subcortical seeds used in primary analyses. (A) Caudate. (B) Putamen. (C) Nucleus Accumbens. (D) Amygdala.

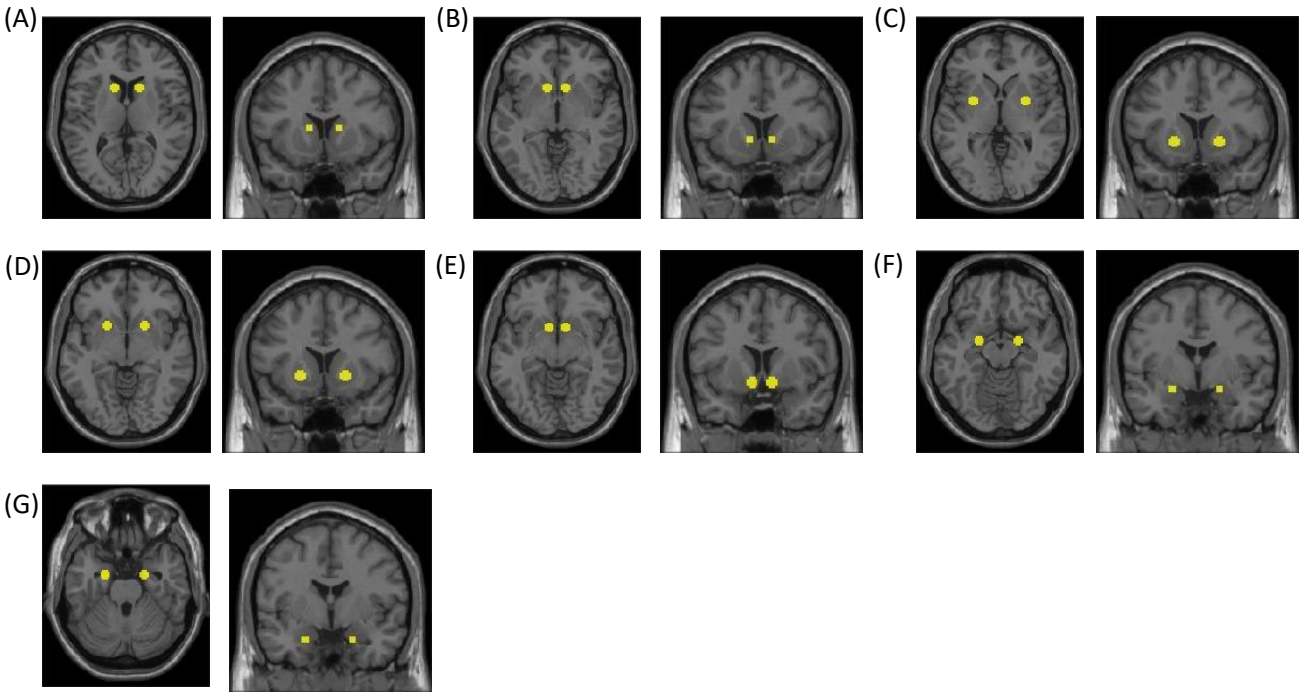

FIGURE S2. Shows the spatial locations of the alternative subcortical seed definitions. **(**A) Dorsal Caudate. (B) Ventral Caudate. (C) Dorsal Putamen (D) Ventral Putamen (E) Nucleus Accumbens (F) Dorsal Amygdala (G) Ventral Amygdala. DiMartino et al (35) and Gianaros et al (36) provide detailed discussions on how these region of interest seeds were created and defined.

SUPPLEMENTARY RESULTS

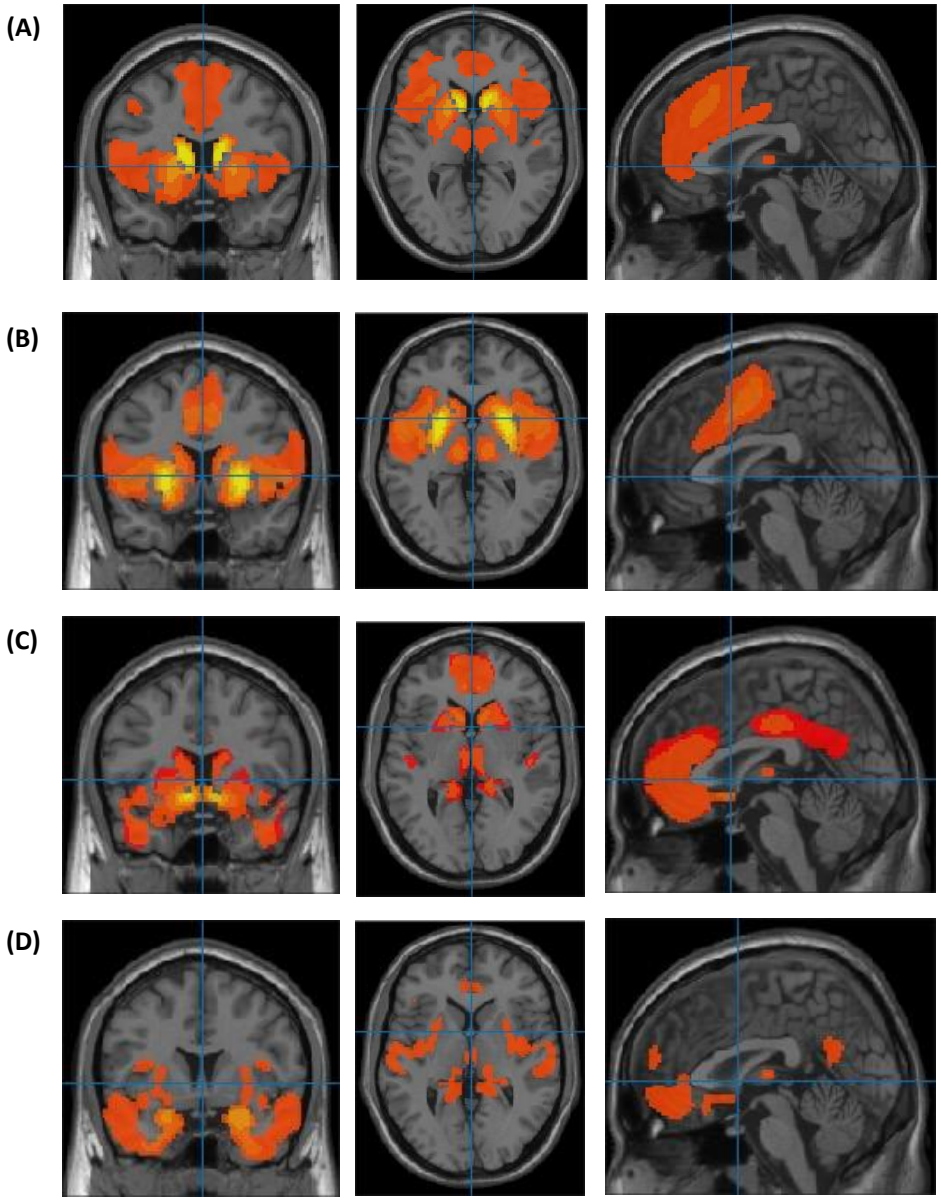

FIGURE S3. Results of one-sample t-tests across all N=9980 subjects. Shows the group average top 15% most connected voxels for each Harvard-Oxford subcortical seed region. (A) Caudate. (B) Putamen. (C) Nucleus Accumbens. (D) Amygdala.

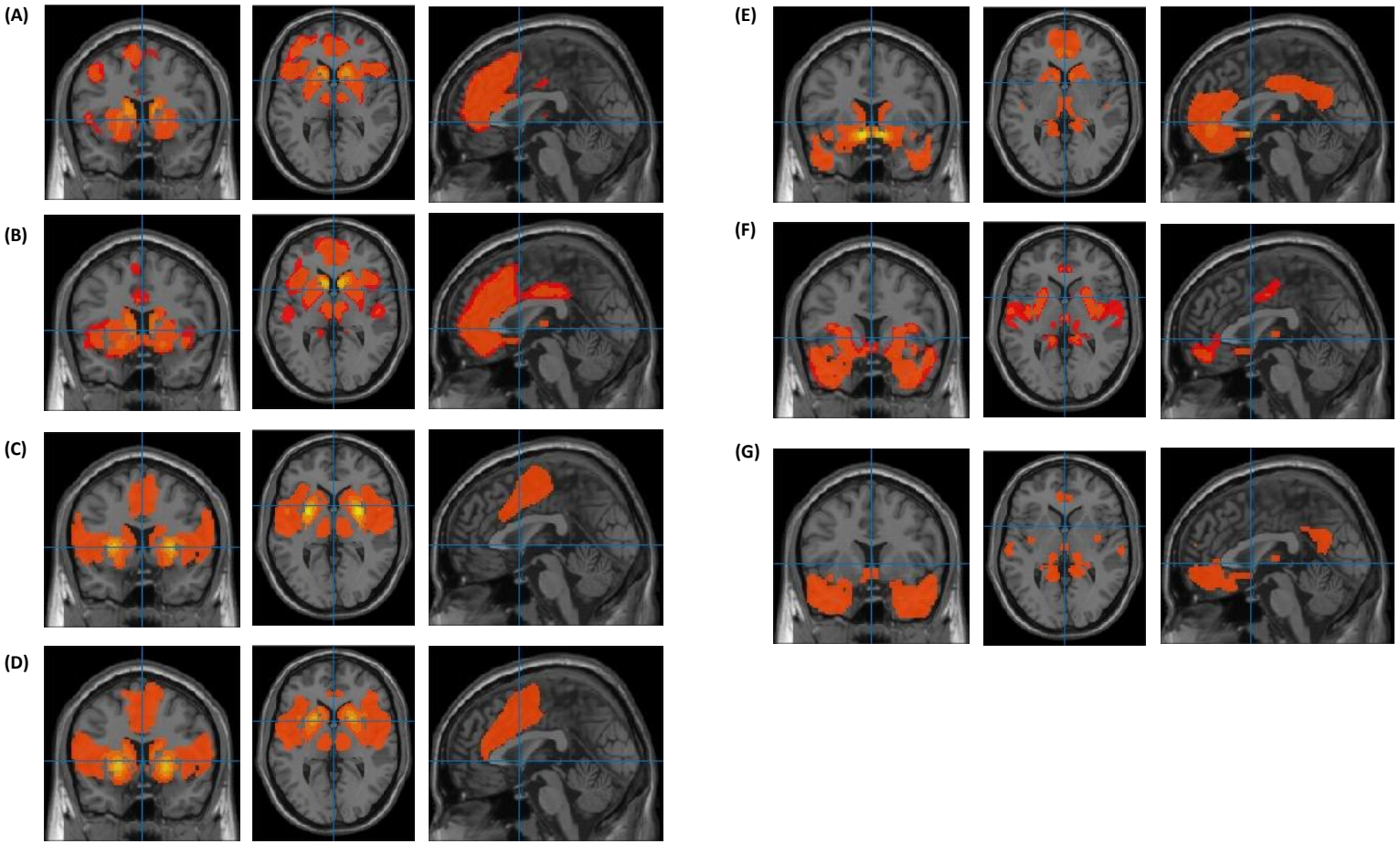

FIGURE S4. Results of one-sample t-tests across all N=9980 subjects. Shows the group average top 15% most connected voxels for each of the alternative subcortical seed region. **(A)** Dorsal Caudate. **(B)** Ventral Caudate. **(C)** Dorsal Putamen **(D)** Ventral Putamen **(E)** Nucleus Accumbens **(F)** Dorsal Amygdala **(G)** Ventral Amygdala.

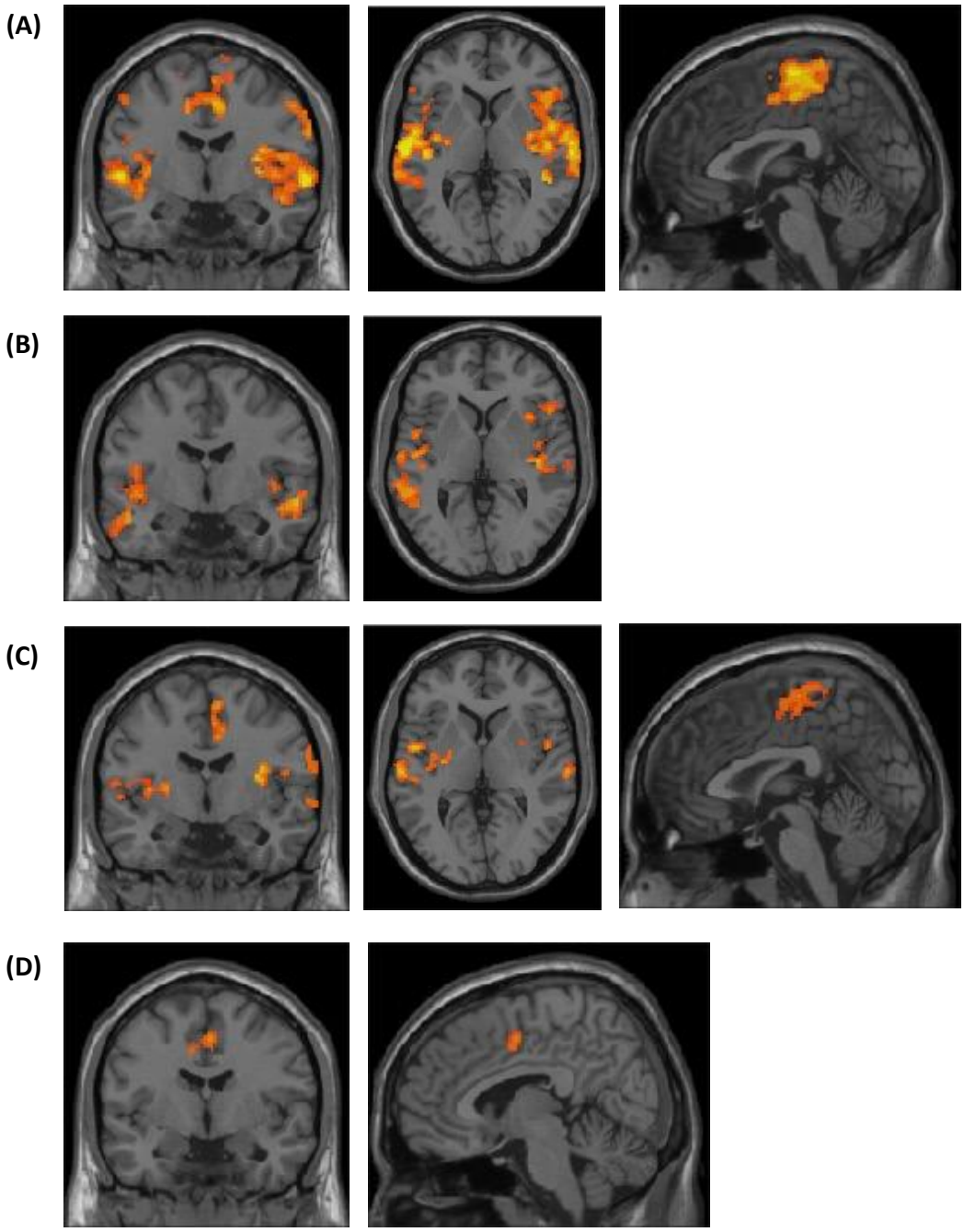

FIGURE S5. Alternative presentation of findings from a mega-analysis of differences in seed-based subcortico-cortical connectivity in youth with attention deficit/hyperactivity disorder (ADHD) and unaffected controls. **(A)** Caudate. **(B)** Putamen. **(C)** Nucleus Accumbens. **(D)** Amygdala.

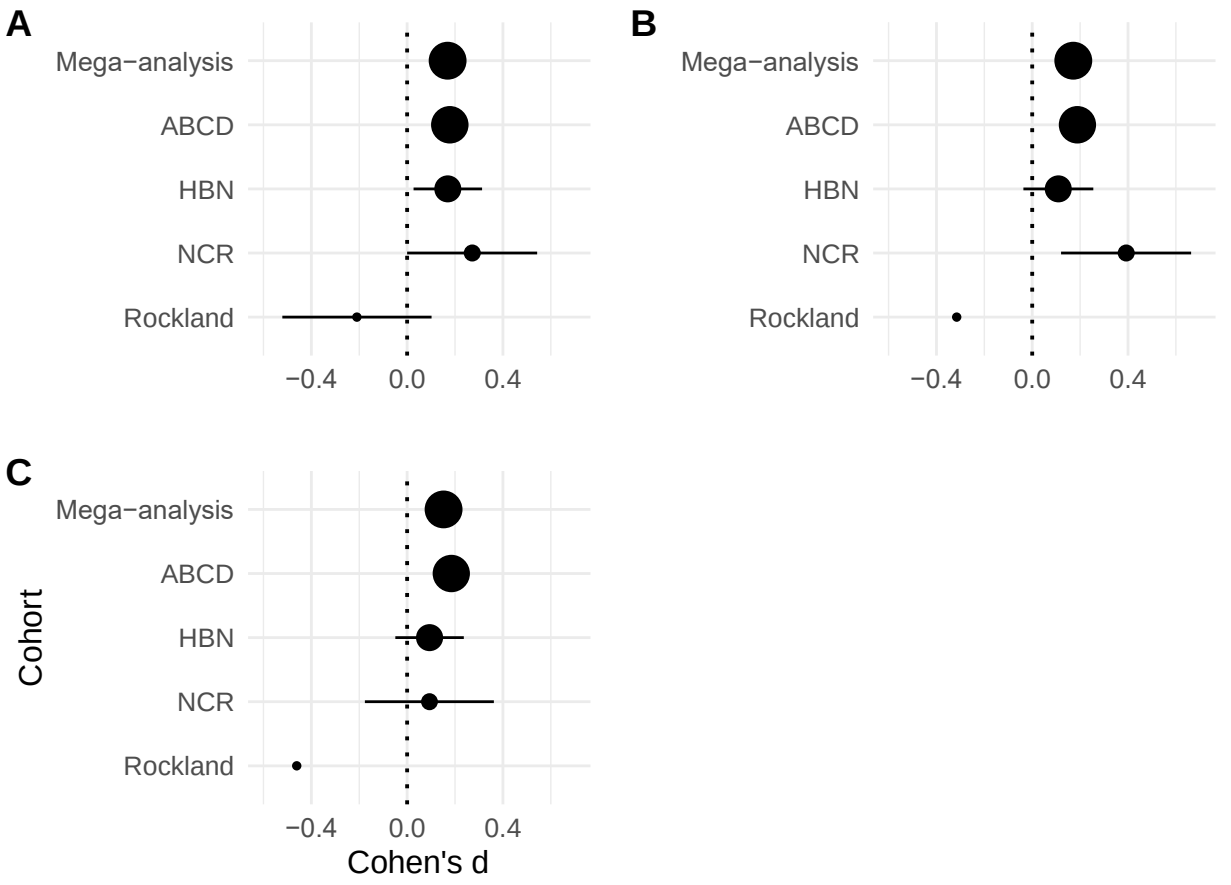

FIGURE S6. Forest plot showing the group difference in functional connectivity between the caudate seed and (a) right temporal lobe/insula/inferior frontal gyrus, (b) left temporal lobe/insula/inferior frontal gyrus and (c) bilateral supplementary motor cortex/precentral/postcentral gyrus. Note that at the primary threshold of $p<0.0001$, these regions formed a single large cluster. Therefore, thresholding was performed at <0.00001 for the purposes of plotting discrete clusters.

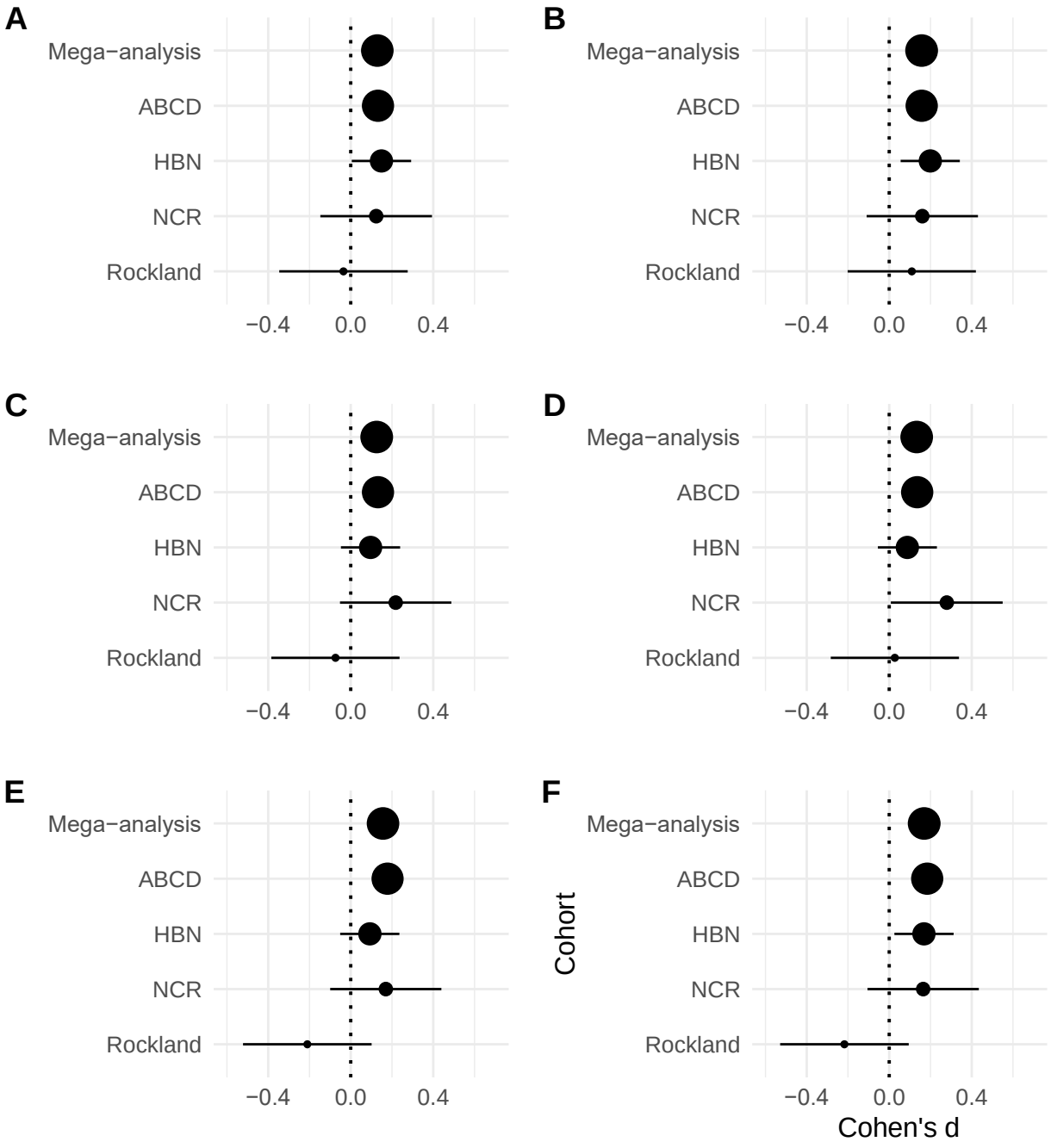

FIGURE S7. Forest plot showing the group difference in functional connectivity between the putamen seed and (a) right inferior frontal gyrus, (b) right inferior frontal gyrus/insula/temporal gyrus, (c) right precentral/postcentral gyrus, (d) left inferior parietal lobe/precentral gyrus/postcentral gyrus, (e) right superior temporal gyrus/middle temporal gyrus, (f) left superior temporal gyrus/middle temporal gyrus.

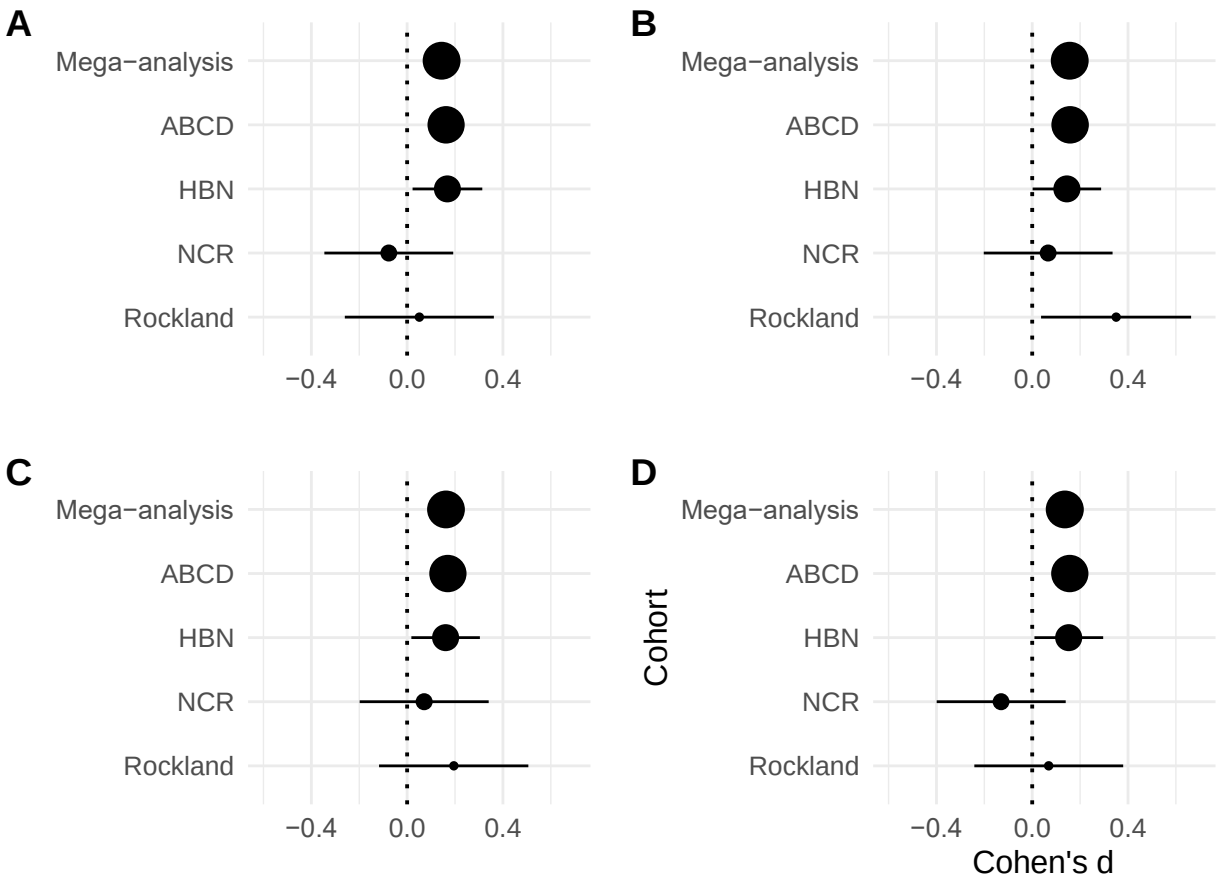

FIGURE S8. Forest plot showing the group difference in functional connectivity between the nucleus accumbens seed and (a) left precentral gyrus, (b) left superior temporal gyrus/insula/putamen, (c) right precentral gyrus/postcentral gyrus/insula/superior temporal gyrus, (d) supplementary motor area/precentral gyrus/postcentral gyrus.

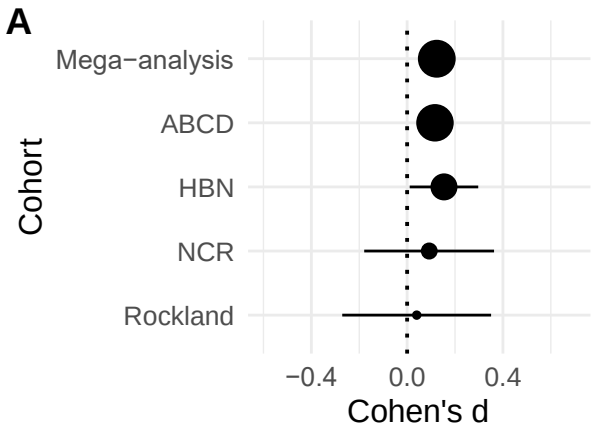

FIGURE S9. Forest plot showing the group difference in functional connectivity between the amygdala seed and (a) bilateral cingulate gyrus/left superior frontal gyrus.

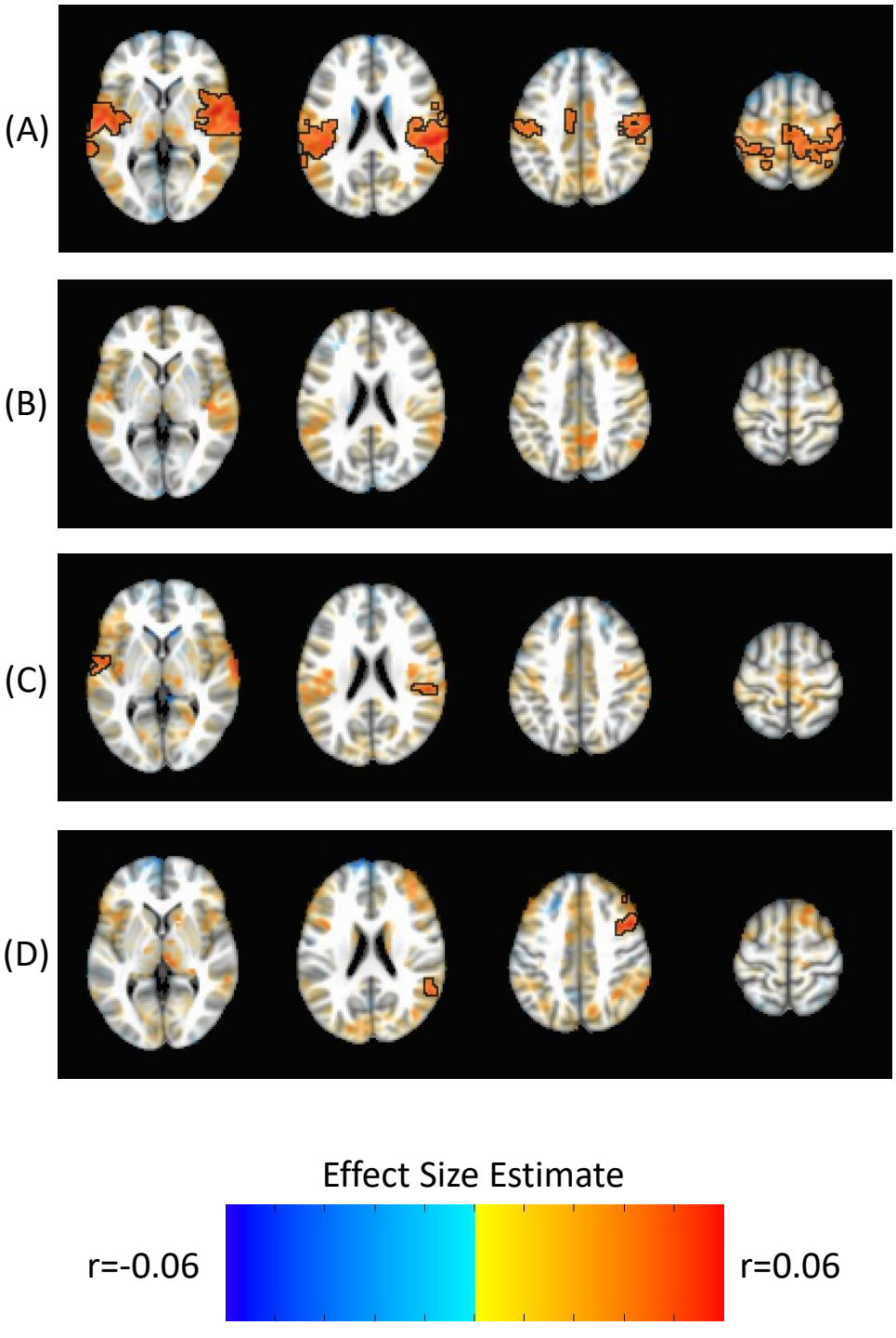

FIGURE S10. Findings from a mega-analysis of associations between seed-based subcortico-cortical connectivity and scores on the Attention Problems scale. **(A)** Caudate. **(B)** Putamen. **(C)** Nucleus Accumbens. **(D)** Amygdala. Positive effect sizes indicate ADHD>controls. Voxels in significant clusters are opaque and boxed. Subthreshold voxels are presented translucently.

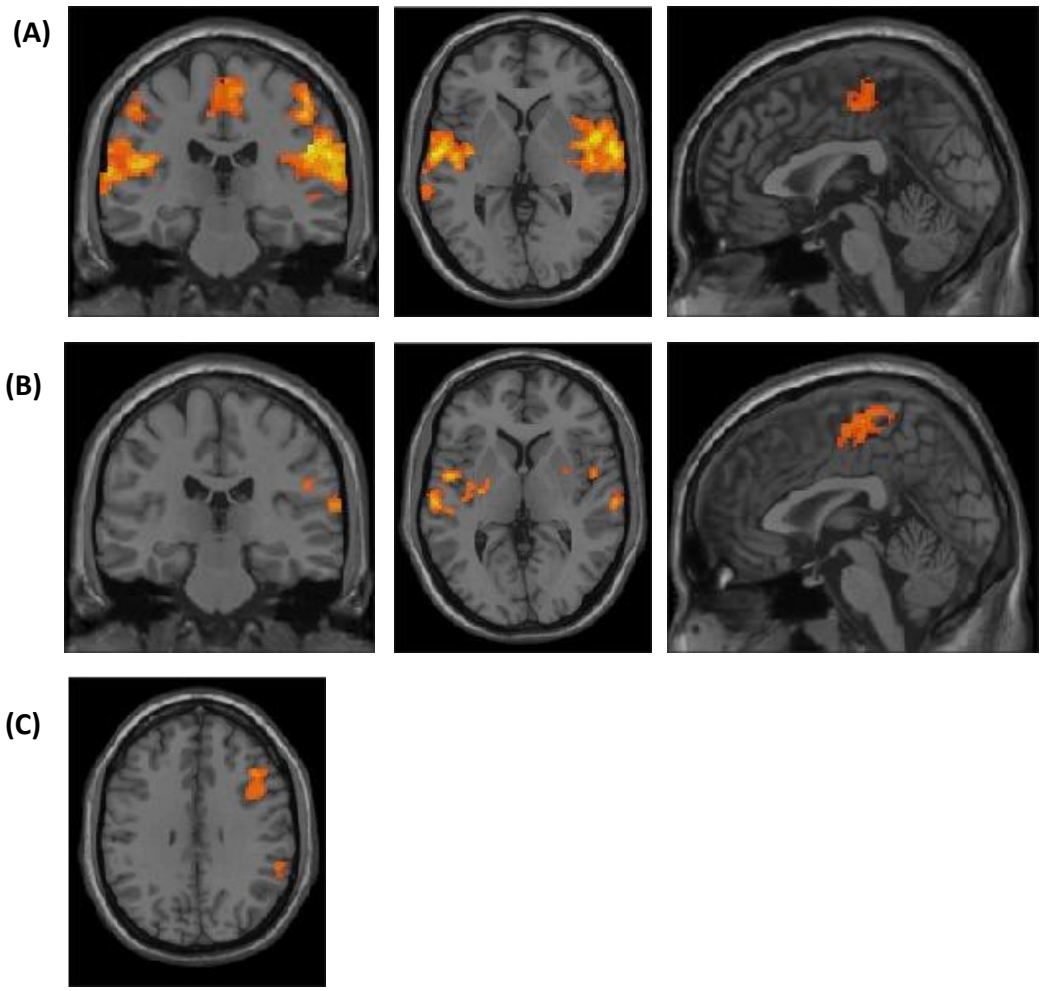

FIGURE S11. Findings from a mega-analysis of associations between seed-based subcortico-cortical connectivity and scores on the Attention Problems scale. **(A)** Caudate. **(B)** Nucleus Accumbens. **(C)** Amygdala. Positive effect sizes indicate ADHD>controls.

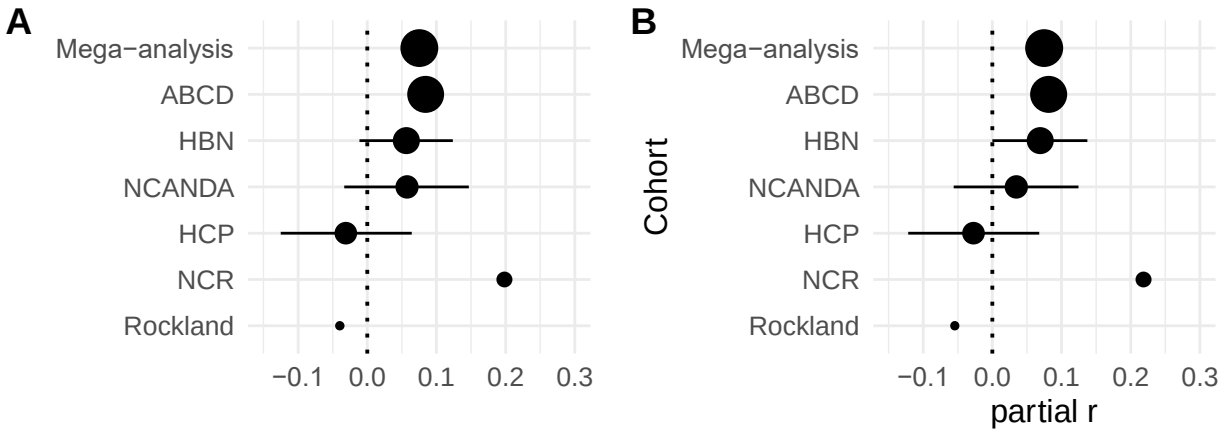

FIGURE S12. Forest plot showing the associations between scores on the Attention Problems Scale and functional connectivity between the caudate and (a) left superior temporal gyrus/postcentral gyrus/insula, (b) right superior temporal gyrus/postcentral gyrus/insula.

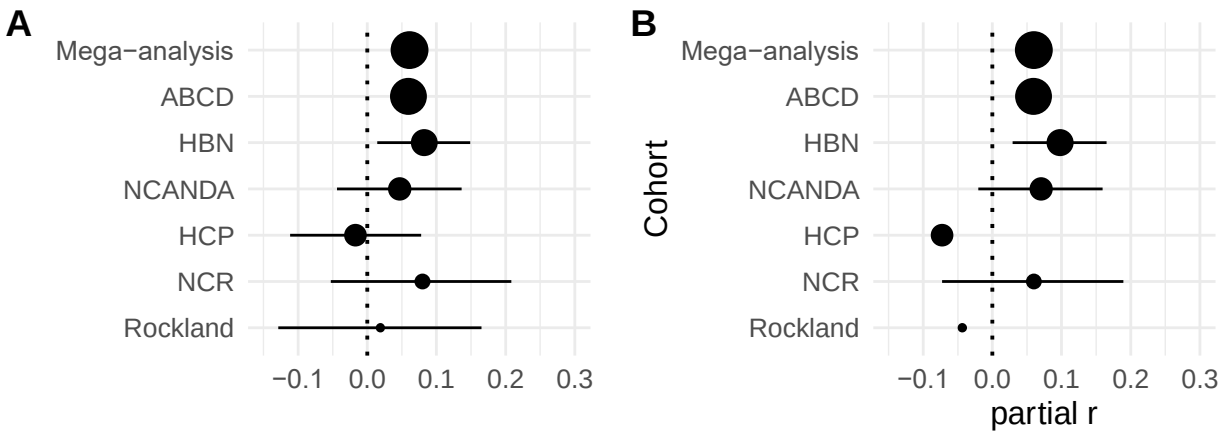

FIGURE S13. Forest plot showing the associations between scores on the Attention Problems Scale and functional connectivity between the nucleus accumbens and (a) left superior temporal gyrus/precentral gyrus/insula, (b) right inferior parietal lobe/superior temporal gyrus/postcentral gyrus/insula.

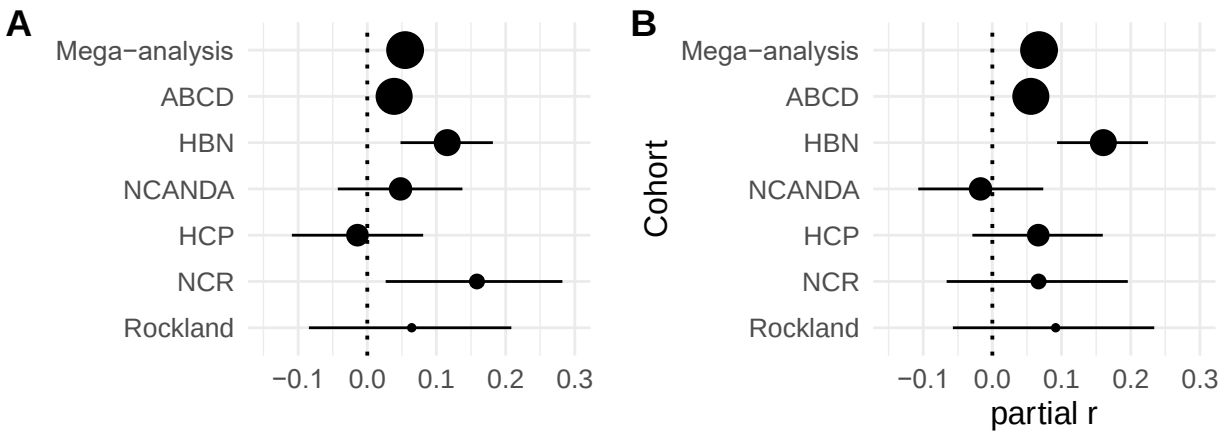

FIGURE S14. Forest plot showing the associations between scores on the Attention Problems Scale and functional connectivity between the amygdala and (a) right supramarginal gyrus/right superior temporal gyrus/right inferior parietal lobe, (b) right middle frontal gyrus/right precentral gyrus.

TABLE S1. Significant associations between Attention Problems scores and subcortico-cortical connectivity. n= 9890.

Cluster	X	Y	Z	Peak *partial-r*	Mean *patrial-r*	Size (voxels)	Overlap	Talairach label
Bilateral Caudate								
1	50	-1	-1	0.07	0.04	7338	20.70%	Right Superior Temporal Gyrus
							18.40%	Right Postcentral Gyrus
							13.90%	Right Insula
							11.00%	Right Precentral Gyrus
							6.80%	Right Inferior Parietal Lobule
							2.90%	Right Paracentral Lobule
							2.50%	Left Medial Frontal Gyrus
							1.90%	Right Medial Frontal Gyrus
2	-59	-13	10	0.07	0.04	4599	33.70%	Left Superior Temporal Gyrus
							17.70%	Left Postcentral Gyrus
							12.50%	Left Insula
							7.50%	Left Inferior Parietal Lobule
							7.40%	Left Precentral Gyrus
							4.80%	Left Middle Temporal Gyrus
							2.90%	Left Transverse Temporal Gyrus
Bilateral Nucleus Accumbens								
1	68	-25	14	0.05	0.04	348	48.40%	Right Inferior Parietal Lobule
							23.40%	Right Superior Temporal Gyrus
							11.60%	Right Insula
							10.40%	Right Postcentral Gyrus
2	-49	-1	12	0.05	0.04	277	51.50%	Left Superior Temporal Gyrus

							26.50%	Left Precentral Gyrus
							8.80%	Left Transverse Temporal Gyrus
							8.70%	Left Insula
							1.40%	Left Postcentral Gyrus
Bilateral Amygdala								
1	48	10	44	0.06	0.04	508	86.40%	Right Middle Frontal Gyrus
							8.90%	Right Precentral Gyrus
							3.00%	Right Inferior Frontal Gyrus
2	56	-53	22	0.05	0.04	221	65.40%	Right Supramarginal Gyrus
							20.10%	Right Superior Temporal Gyrus
							14.40%	Right Inferior Parietal Lobule

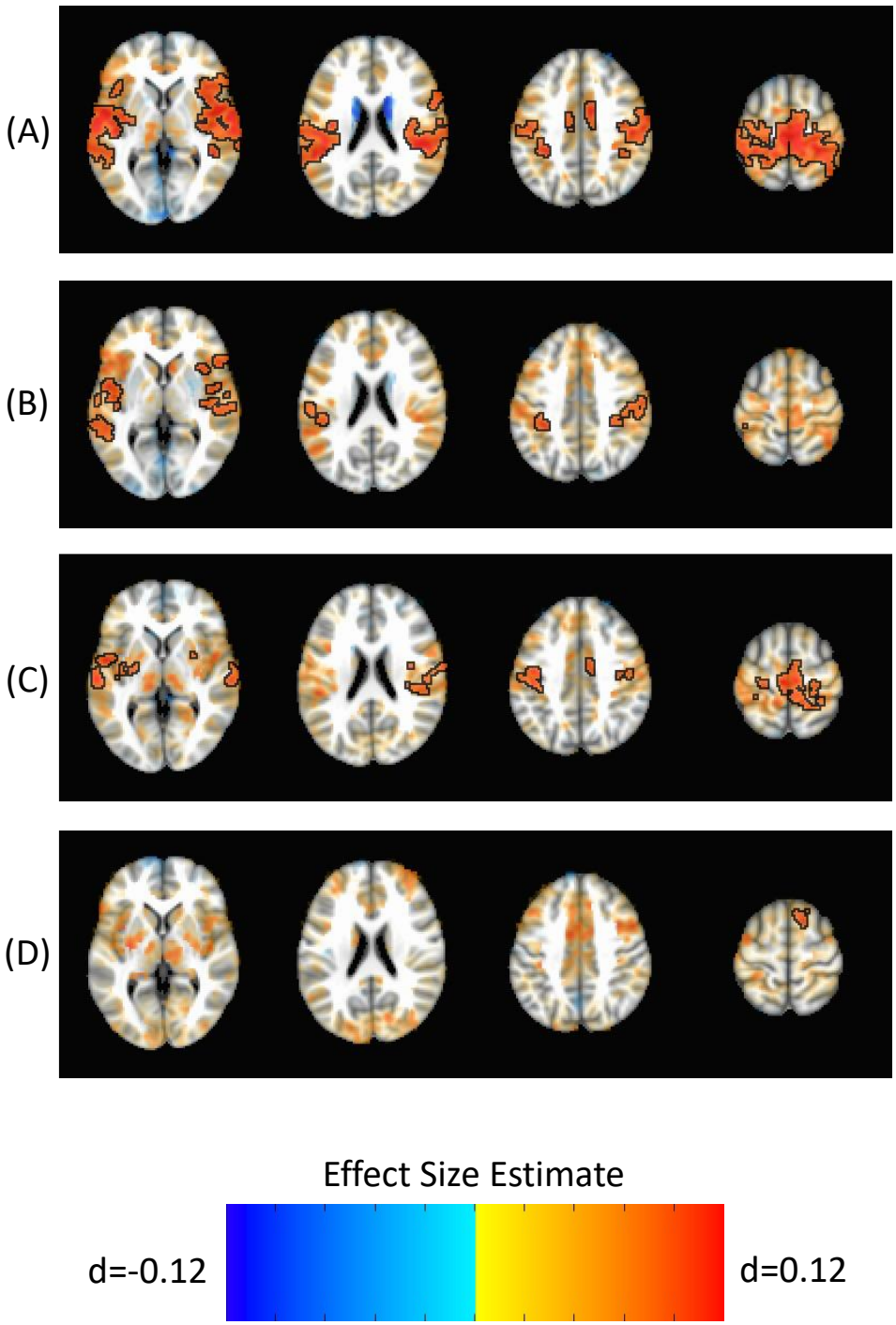

FIGURE S15. Findings from a mega-analysis of differences in seed-based subcortico-cortical connectivity in youth with attention deficit/hyperactivity disorder (ADHD) and unaffected control subjects after matching groups on in-scanner motion. **(A)** Caudate. **(B)** Putamen. **(C)** Nucleus Accumbens. **(D)** Amygdala. Positive effect sizes indicate ADHD>controls. Voxels in significant clusters are opaque and boxed. Subthreshold voxels are presented translucently.

TABLE S2. Show results of case-control comparison after matching groups on in-scanner motion. n=1642 patients with ADHD and n=6737 unaffected controls.

Cluster	X	Y	Z	Peak-*d*	Mean-*d*	Size (voxels)	Overlap	Talairach label
Bilateral Caudate								
1	64	-7	-3	0.16	0.10	18389	9.70%	Left Superior Temporal Gyrus
							8.70%	Right Superior Temporal Gyrus
							8.40%	Right Postcentral Gyrus
							6.10%	Left Postcentral Gyrus
							6.10%	Right Insula
							5.00%	Right Precentral Gyrus
							4.20%	Left Insula
							3.80%	Left Precentral Gyrus
							3.20%	Right Inferior Parietal Lobule
							2.90%	Right Medial Frontal Gyrus
							2.80%	Left Inferior Parietal Lobule
							2.70%	Left Middle Temporal Gyrus
							2.30%	Left Medial Frontal Gyrus
							2.00%	Right Inferior Frontal Gyrus
							1.70%	Right Paracentral Lobule
							1.60%	Left Paracentral Lobule
Bilateral Putamen								
1	-51	-3	-1	0.13	0.09	2099	41.00%	Left Superior Temporal Gyrus
							28.60%	Left Middle Temporal Gyrus
							10.80%	Left Insula
							3.80%	Left Postcentral Gyrus
							1.60%	Left Inferior Temporal Gyrus

							1.20%	Left Precentral Gyrus
							1.10%	Left Inferior Parietal Lobule
							1.00%	Left Fusiform Gyrus
							1.00%	Left Transverse Temporal Gyrus
2	44	-25	8	0.13	0.09	872	37.70%	Right Superior Temporal Gyrus
							32.20%	Right Middle Temporal Gyrus
							10.00%	Right Transverse Temporal Gyrus
							6.60%	Right Insula
							2.90%	Right Postcentral Gyrus
							2.10%	Right Inferior Temporal Gyrus
3	30	20	-21	0.12	0.09	858	63.40%	Right Inferior Frontal Gyrus
							18.00%	Right Insula
							7.10%	Right Superior Temporal Gyrus
							3.80%	Right Uncus
4	52	-29	36	0.12	0.09	517	56.40%	Right Postcentral Gyrus
							10.70%	Right Precentral Gyrus
							10.00%	Right Inferior Parietal Lobule
5	-31	-39	44	0.11	0.09	409	49.80%	Left Inferior Parietal Lobule
							3.20%	Left Postcentral Gyrus
							2.20%	Left Superior Parietal Lobule
Bilateral Nucleus Accumbens								
1	-39	-15	50	0.13	0.09	2020	17.30%	Left Postcentral Gyrus
							16.90%	Right Medial Frontal Gyrus
							15.90%	Left Precentral Gyrus

							6.60%	Left Medial Frontal Gyrus
							5.90%	Right Paracentral Lobule
							5.10%	Right Postcentral Gyrus
							3.10%	Right Cingulate Gyrus
							2.30%	Left Inferior Parietal Lobule
							2.30%	Right Precentral Gyrus
							1.40%	Left Paracentral Lobule
2	34	-3	12	0.13	0.09	924	20.20%	Right Postcentral Gyrus
							19.80%	Right Insula
							19.40%	Right Precentral Gyrus
							14.50%	Right Superior Temporal Gyrus
							4.60%	Right Inferior Parietal Lobule
							3.20%	Right Middle Temporal Gyrus
							2.10%	Right Claustrum
3	-63	-19	2	0.12	0.09	379	63.90%	Left Superior Temporal Gyrus
							25.00%	Left Precentral Gyrus
							6.30%	Left Insula
							4.20%	Left Middle Temporal Gyrus
4	-29	-11	8	0.12	0.09	258	38.30%	Left Insula
							37.40%	Left Lentiform Nucleus
							5.70%	Left Claustrum
Bilateral Amygdala								
1	8	20	56	0.11	0.09	204	81.70%	Right Superior Frontal Gyrus
							4.10%	Right Medial Frontal Gyrus
							1.20%	Right Middle Frontal Gyrus

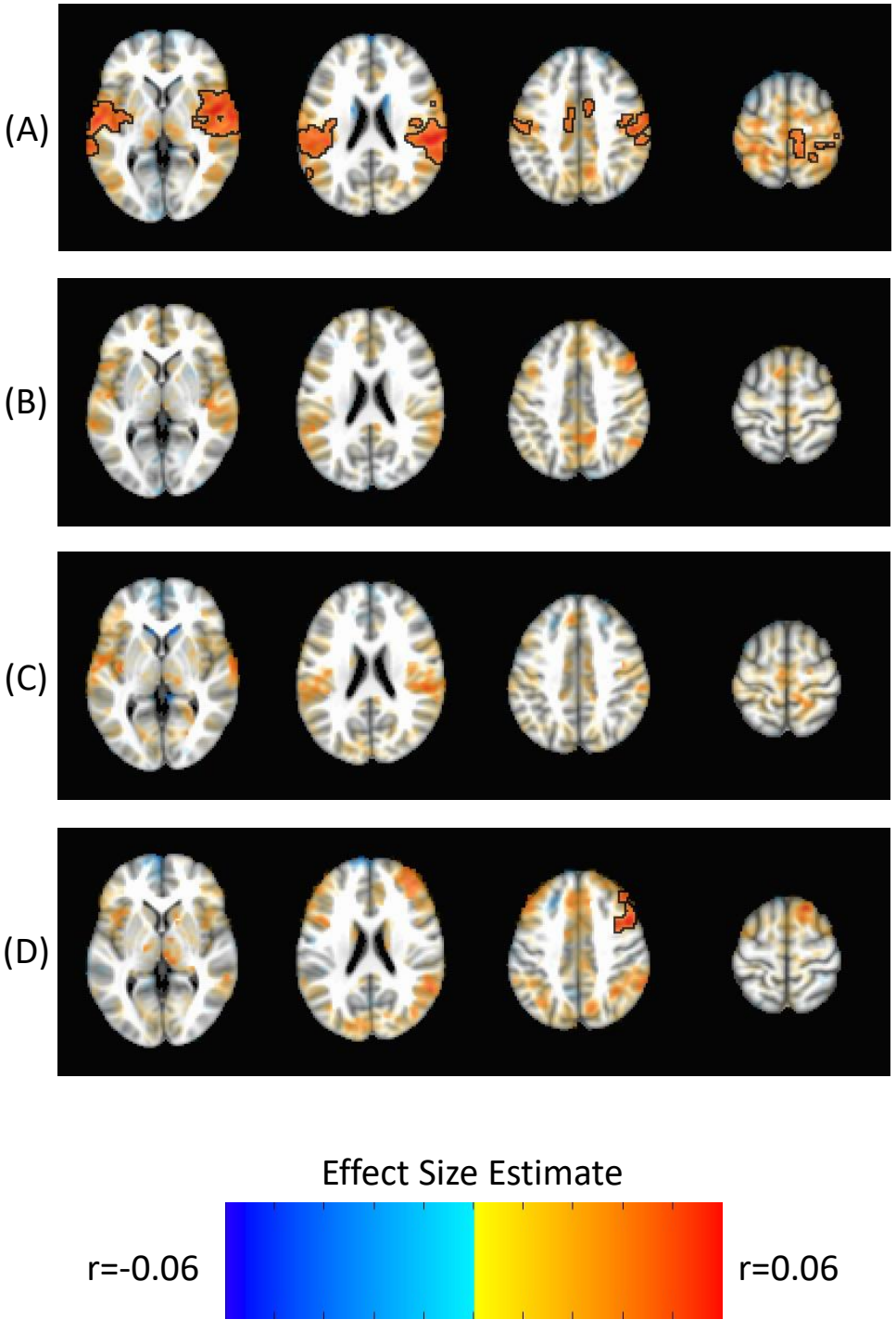

FIGURE S16. Findings from a mega-analysis of associations between seed-based subcortico-cortical connectivity and scores on the Attention Problems scale after removing associations with in-scanner motion. **(A)** Caudate. **(B)** Putamen. **(C)** Nucleus Accumbens. **(D)** Amygdala. Voxels in significant clusters are opaque and boxed. Subthreshold voxels are presented translucently.

TABLE S3. Significant associations between Attention Problems scores and subcortico-cortical connectivity after removing associations with in-scanner motion. n= 9867.

Cluster	X	Y	Z	Peak *partial-r*	Mean *patrial-r*	Size (voxels)	Overlap	Talairach label
Bilateral Caudate								
1	56	-29	26	0.07	0.05	6389	22.40%	Right Superior Temporal Gyrus
							16.70%	Right Postcentral Gyrus
							14.30%	Right Insula
							10.70%	Right Precentral Gyrus
							8.80%	Right Inferior Parietal Lobule
							3.00%	Right Paracentral Lobule
							2.00%	Right Middle Temporal Gyrus
							1.40%	Right Transverse Temporal Gyrus
							1.40%	Right Cingulate Gyrus
							1.30%	Right Medial Frontal Gyrus
							1.10%	Left Medial Frontal Gyrus
							1.10%	Left Paracentral Lobule
2	-59	-13	8	0.07	0.04	3463	41.00%	Left Superior Temporal Gyrus
							13.70%	Left Insula
							13.40%	Left Postcentral Gyrus
							9.30%	Left Inferior Parietal Lobule
							6.40%	Left Precentral Gyrus
							6.10%	Left Middle Temporal Gyrus
							3.40%	Left Transverse Temporal Gyrus
							0.20%	Left Supramarginal Gyrus

							0.20%	Left Claustrum
							0.10%	Left Lentiform Nucleus
Bilateral Amygdala								
1	48	10	44	0.07	0.05	831	83.20%	Right Middle Frontal Gyrus
							8.70%	Right Precentral Gyrus
							3.30%	Right Inferior Frontal Gyrus

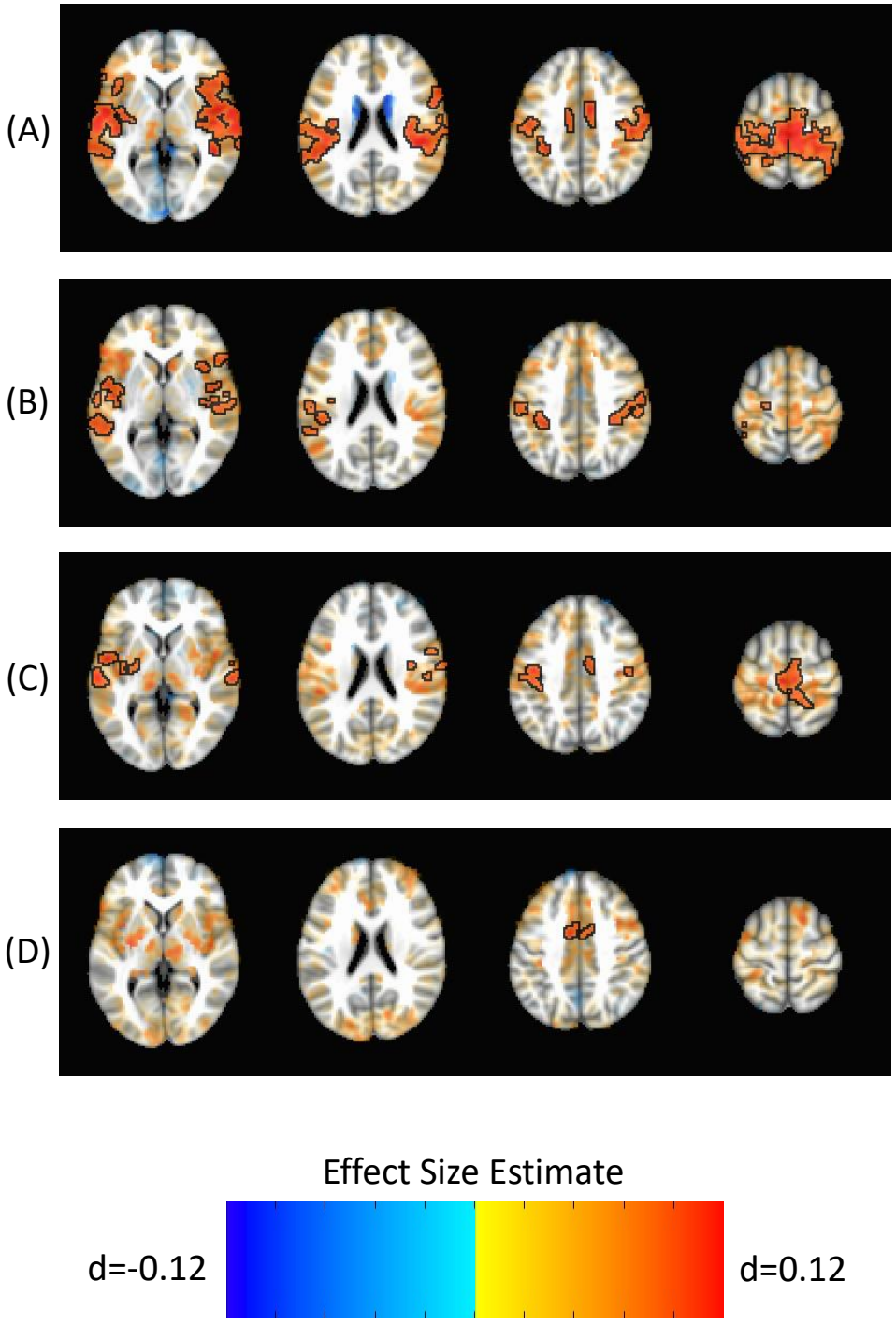

FIGURE S17. Findings from a mega-analysis of differences in seed-based subcortico-cortical connectivity in youth with attention deficit/hyperactivity disorder (ADHD) and unaffected control subjects after controlling for IQ. **(A)** Caudate. **(B)** Putamen. **(C)** Nucleus Accumbens. **(D)** Amygdala. Positive effect sizes indicate ADHD>controls. Voxels in significant clusters are opaque and boxed. Subthreshold voxels are presented translucently.

TABLE S4. Show results of case-control comparison after controlling for IQ. n=1678 patients with ADHD and n=6540 unaffected controls.

Cluster	X	Y	Z	Peak-*d*	Mean-*d*	Size (voxels)	Overlap	Talairach label
Bilateral Caudate								
1	64	-7	-3	0.15	0.10	12488	12.60%	Right Superior Temporal Gyrus
							9.80%	Right Postcentral Gyrus
							8.10%	Right Insula
							6.60%	Right Precentral Gyrus
							5.60%	Left Postcentral Gyrus
							3.80%	Left Precentral Gyrus
							3.80%	Right Medial Frontal Gyrus
							3.40%	Right Inferior Parietal Lobule
							3.40%	Left Medial Frontal Gyrus
							3.20%	Right Inferior Frontal Gyrus
							2.40%	Right Paracentral Lobule
							2.10%	Right Middle Temporal Gyrus
							2.10%	Left Paracentral Lobule
							1.30%	Left Inferior Parietal Lobule
							1.00%	Right Cingulate Gyrus
2	-55	-5	-1	0.15	0.10	3708	41.70%	Left Superior Temporal Gyrus
							18.20%	Left Insula
							11.00%	Left Middle Temporal Gyrus
							6.00%	Left Postcentral Gyrus
							4.90%	Left Inferior Parietal Lobule
							3.50%	Left Precentral Gyrus

							3.40%	Left Transverse Temporal Gyrus
							1.80%	Left Inferior Frontal Gyrus
							1.80%	Left Supramarginal Gyrus
Bilateral Putamen								
1	-51	-3	-1	0.13	0.09	2122	36.20%	Left Superior Temporal Gyrus
							31.00%	Left Middle Temporal Gyrus
							11.00%	Left Insula
							3.80%	Left Inferior Parietal Lobule
							3.00%	Left Postcentral Gyrus
							2.20%	Left Supramarginal Gyrus
							1.30%	Left Inferior Temporal Gyrus
							1.00%	Left Fusiform Gyrus
							1.00%	Left Precentral Gyrus
2	-31	-39	44	0.12	0.09	521	25.00%	Left Postcentral Gyrus
							22.20%	Left Inferior Parietal Lobule
							14.80%	Left Precentral Gyrus
3	52	-29	36	0.12	0.09	484	52.70%	Right Postcentral Gyrus
							12.60%	Right Precentral Gyrus
							11.10%	Right Inferior Parietal Lobule
4	56	-9	-9	0.12	0.09	473	67.50%	Right Middle Temporal Gyrus
							15.50%	Right Superior Temporal Gyrus
							3.20%	Right Inferior Temporal Gyrus
5	24	4	-25	0.12	0.09	460	39.20%	Right Inferior Frontal Gyrus
							30.80%	Right Insula
							12.20%	Right Superior Temporal Gyrus

							8.40%	Right Uncus
							1.10%	Right Middle Frontal Gyrus
6	44	-25	8	0.12	0.09	413	63.20%	Right Superior Temporal Gyrus
							16.60%	Right Transverse Temporal Gyrus
							9.60%	Right Insula
							3.80%	Right Postcentral Gyrus
							2.60%	Right Middle Temporal Gyrus
							1.30%	Right Claustrum
7	58	24	12	0.11	0.09	302	96.10%	Right Inferior Frontal Gyrus
Bilateral Nucleus Accumbens								
1	6	-23	68	0.12	0.09	884	33.90%	Right Medial Frontal Gyrus
							11.80%	Left Medial Frontal Gyrus
							10.30%	Right Paracentral Lobule
							7.10%	Right Cingulate Gyrus
							3.40%	Right Postcentral Gyrus
							2.40%	Left Paracentral Lobule
2	-39	-15	50	0.13	0.09	488	44.30%	Left Precentral Gyrus
							39.00%	Left Postcentral Gyrus
							9.30%	Left Inferior Parietal Lobule
3	70	-21	14	0.13	0.09	477	29.10%	Right Postcentral Gyrus
							26.90%	Right Superior Temporal Gyrus
							20.40%	Right Precentral Gyrus
							7.20%	Right Middle Temporal Gyrus
							2.80%	Right Transverse Temporal Gyrus

4	-63	-19	2	0.13	0.09	326	73.50%	Left Superior Temporal Gyrus
							15.40%	Left Precentral Gyrus
							5.80%	Left Insula
							5.00%	Left Middle Temporal Gyrus
5	34	-5	12	0.13	0.09	294	44.40%	Right Insula
							24.90%	Right Precentral Gyrus
							7.50%	Right Inferior Frontal Gyrus
							5.90%	Right Claustrum
6	-35	-19	10	0.12	0.09	247	40.10%	Left Insula
							36.00%	Left Lentiform Nucleus
							5.30%	Left Claustrum
Bilateral Amygdala								
1	-9	-1	42	0.11	0.09	205	54.50%	Left Cingulate Gyrus
							25.70%	Right Cingulate Gyrus
							14.80%	Right Medial Frontal Gyrus
							5.00%	Left Medial Frontal Gyrus

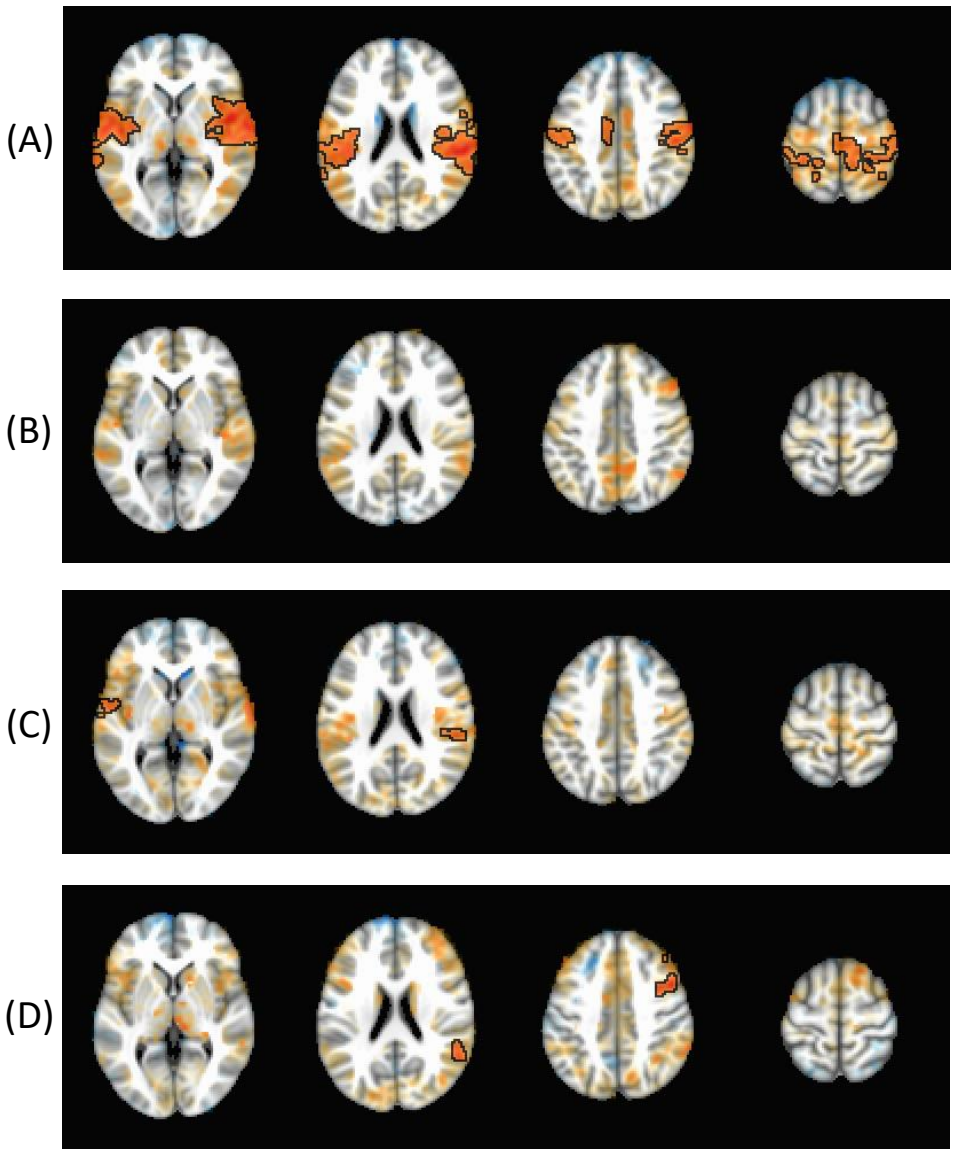

FIGURE S18. Findings from a mega-analysis of associations between seed-based subcortico-cortical connectivity and scores on the Attention Problems scale after controlling for IQ. **(A)** Caudate. **(B)** Putamen. **(C)** Nucleus Accumbens. **(D)** Amygdala. Voxels in significant clusters are opaque and boxed. Subthreshold voxels are presented translucently.

TABLE S5. Significant associations between Attention Problems scores and subcortico-cortical connectivity after controlling for IQ. n=9706.

Cluster	X	Y	Z	Peak *partial-r*	Mean *patrial-r*	Size (voxels)	Overlap	Talairach label
Bilateral Caudate								
1	50	-1	-1	0.07	0.04	6802	21.10%	Right Superior Temporal Gyrus
							17.40%	Right Postcentral Gyrus
							14.50%	Right Insula
							11.50%	Right Precentral Gyrus
							6.60%	Right Inferior Parietal Lobule
							2.80%	Right Paracentral Lobule
							2.50%	Left Medial Frontal Gyrus
							1.90%	Right Medial Frontal Gyrus
							1.50%	Right Transverse Temporal Gyrus
							1.50%	Right Middle Temporal Gyrus
							1.20%	Left Paracentral Lobule
							1.00%	Left Cingulate Gyrus
2	-59	-13	10	0.07	0.04	4097	35.20%	Left Superior Temporal Gyrus
							16.50%	Left Postcentral Gyrus
							13.90%	Left Insula
							8.20%	Left Precentral Gyrus
							6.60%	Left Inferior Parietal Lobule
							4.10%	Left Middle Temporal Gyrus
Bilateral Nucleus Accumbens								
1	68	-23	16	0.05	0.04	282	46.90%	Right Inferior Parietal Lobule

							22.80%	Right Superior Temporal Gyrus
							11.70%	Right Postcentral Gyrus
							11.30%	Right Insula
2	-49	-1	12	0.05	0.04	233	46.40%	Left Superior Temporal Gyrus
							29.40%	Left Precentral Gyrus
							11.90%	Left Insula
							7.80%	Left Transverse Temporal Gyrus
							1.50%	Left Postcentral Gyrus
Bilateral Amygdala								
1	48	10	44	0.06	0.04	391	85.90%	Right Middle Frontal Gyrus
							9.90%	Right Precentral Gyrus
							2.70%	Right Inferior Frontal Gyrus
2	56	-53	22	0.05	0.04	241	65.80%	Right Supramarginal Gyrus
							19.10%	Right Superior Temporal Gyrus
							15.10%	Right Inferior Parietal Lobule

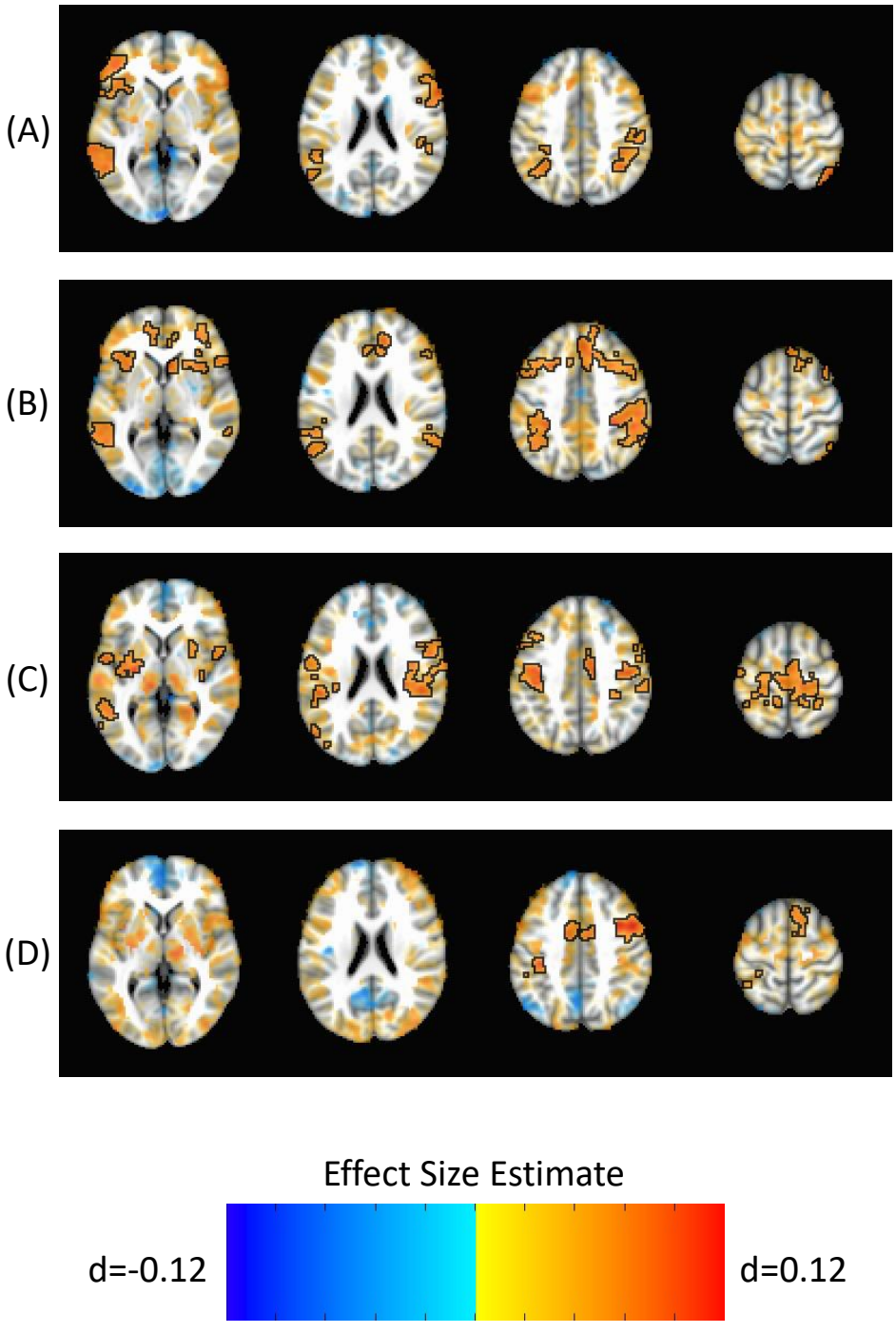

FIGURE S19. Findings from a mega-analysis of differences in seed-based subcortico-cortical connectivity in youth with attention deficit/hyperactivity disorder (ADHD) and unaffected control subjects after removing subjects receiving psychostimulant medication. **(A)** Caudate. **(B)** Putamen. **(C)** Nucleus Accumbens. **(D)** Amygdala. Positive effect sizes indicate ADHD>controls. Voxels in significant clusters are opaque and boxed. Subthreshold voxels are presented translucently. Findings presented at a liberal cluster forming threshold of $p<0.005$.

TABLE S6. Show results of case-control comparison. n=1114 psychostimulant-free patients with ADHD and n=6737 unaffected controls.

Cluster	X	Y	Z	Peak-*d*	Mean-*d*	Size (voxels)	Overlap	Talairach label
Findings presented at a liberal cluster forming threshold of p<0.005.								
Bilateral Caudate								
1	-63	-39	-5	0.13	0.07	1853	47.20%	Left Middle Temporal Gyrus
							14.10%	Left Superior Temporal Gyrus
							10.20%	Left Inferior Parietal Lobule
							8.40%	Left Supramarginal Gyrus
							2.60%	Left Superior Parietal Lobule
							1.70%	Left Angular Gyrus
2	32	-59	56	0.12	0.07	1287	45.60%	Right Inferior Parietal Lobule
							11.40%	Right Superior Parietal Lobule
							9.00%	Right Postcentral Gyrus
							5.90%	Right Supramarginal Gyrus
3	-45	42	2	0.10	0.07	757	64.40%	Left Inferior Frontal Gyrus
							14.10%	Left Middle Frontal Gyrus
							5.40%	Left Insula
							5.10%	Left Precentral Gyrus
4	38	4	26	0.11	0.07	659	58.80%	Right Inferior Frontal Gyrus
							22.40%	Right Middle Frontal Gyrus
							8.00%	Right Precentral Gyrus

Bilateral Putamen								
1	26	18	-21	0.12	0.07	8098	15.40%	Right Inferior Frontal Gyrus
							11.80%	Right Middle Frontal Gyrus
							9.30%	Right Superior Frontal Gyrus
							6.70%	Right Medial Frontal Gyrus
							5.20%	Left Medial Frontal Gyrus
							4.80%	Left Inferior Frontal Gyrus
							4.40%	Right Anterior Cingulate
							4.30%	Right Middle Temporal Gyrus
							3.60%	Left Middle Frontal Gyrus
							3.60%	Left Anterior Cingulate
							2.50%	Left Superior Frontal Gyrus
							2.10%	Right Superior Temporal Gyrus
							2.00%	Right Parahippocampal Gyrus
							1.50%	Right Uncus
							1.00%	Left Insula
							1.00%	Right Inferior Temporal Gyrus
2	-45	4	-37	0.10	0.07	3508	34.40%	Left Middle Temporal Gyrus
							18.60%	Left Superior Temporal Gyrus
							17.50%	Left Inferior Parietal Lobule
							4.00%	Left Supramarginal Gyrus
							2.00%	Left Angular Gyrus
							1.70%	Left Insula

3	52	-29	38	0.12	0.07	1852	29.30%	Right Inferior Parietal Lobule
							17.10%	Right Supramarginal Gyrus
							14.00%	Right Postcentral Gyrus
							11.00%	Right Superior Temporal Gyrus
							7.60%	Right Middle Temporal Gyrus
							2.50%	Right Superior Parietal Lobule
							1.40%	Right Precentral Gyrus
Bilateral Nucleus Accumbens								
1	-29	-13	8	0.12	0.07	2288	35.30%	Left Precentral Gyrus
							17.10%	Left Postcentral Gyrus
							8.90%	Left Insula
							8.70%	Left Lentiform Nucleus
							8.30%	Left Middle Frontal Gyrus
							5.10%	Left Superior Temporal Gyrus
							1.90%	Left Claustrum
							1.20%	Left Middle Temporal Gyrus
2	54	-3	18	0.11	0.07	2282	33.90%	Right Precentral Gyrus
							12.60%	Right Insula
							12.60%	Right Inferior Parietal Lobule
							11.50%	Right Postcentral Gyrus
							9.40%	Right Inferior Frontal Gyrus
							2.90%	Right Middle Frontal Gyrus

							1.90%	Right Lentiform Nucleus
							1.70%	Right Superior Temporal Gyrus
							1.60%	Right Claustrum
3	24	-21	68	0.11	0.07	1457	22.20%	Right Medial Frontal Gyrus
							10.50%	Left Medial Frontal Gyrus
							9.60%	Right Cingulate Gyrus
							7.90%	Right Paracentral Lobule
							6.90%	Right Postcentral Gyrus
							6.80%	Right Precentral Gyrus
							1.50%	Left Paracentral Lobule
							1.10%	Right Superior Parietal Lobule
4	-51	-47	-3	0.10	0.07	1121	63.50%	Left Middle Temporal Gyrus
							12.40%	Left Inferior Parietal Lobule
							9.10%	Left Superior Temporal Gyrus
							3.80%	Left Middle Occipital Gyrus
							2.70%	Left Insula
							1.80%	Left Inferior Temporal Gyrus
5	-19	-43	72	0.09	0.07	833	24.30%	Left Postcentral Gyrus
							12.50%	Left Precentral Gyrus
							10.40%	Left Inferior Parietal Lobule
							2.80%	Left Paracentral Lobule
							1.50%	Left Superior Parietal Lobule

Bilateral Amygdala								
1	36	8	40	0.13	0.08	1061	61.70%	Right Middle Frontal Gyrus
							25.00%	Right Precentral Gyrus
							7.10%	Right Inferior Frontal Gyrus
							1.10%	Right Superior Frontal Gyrus
2	8	18	54	0.10	0.07	847	39.40%	Right Superior Frontal Gyrus
							16.70%	Left Cingulate Gyrus
							16.50%	Right Medial Frontal Gyrus
							15.20%	Right Cingulate Gyrus
							3.70%	Left Medial Frontal Gyrus
3	-37	-29	42	0.11	0.07	620	38.00%	Left Inferior Parietal Lobule
							33.80%	Left Postcentral Gyrus
							2.50%	Left Supramarginal Gyrus

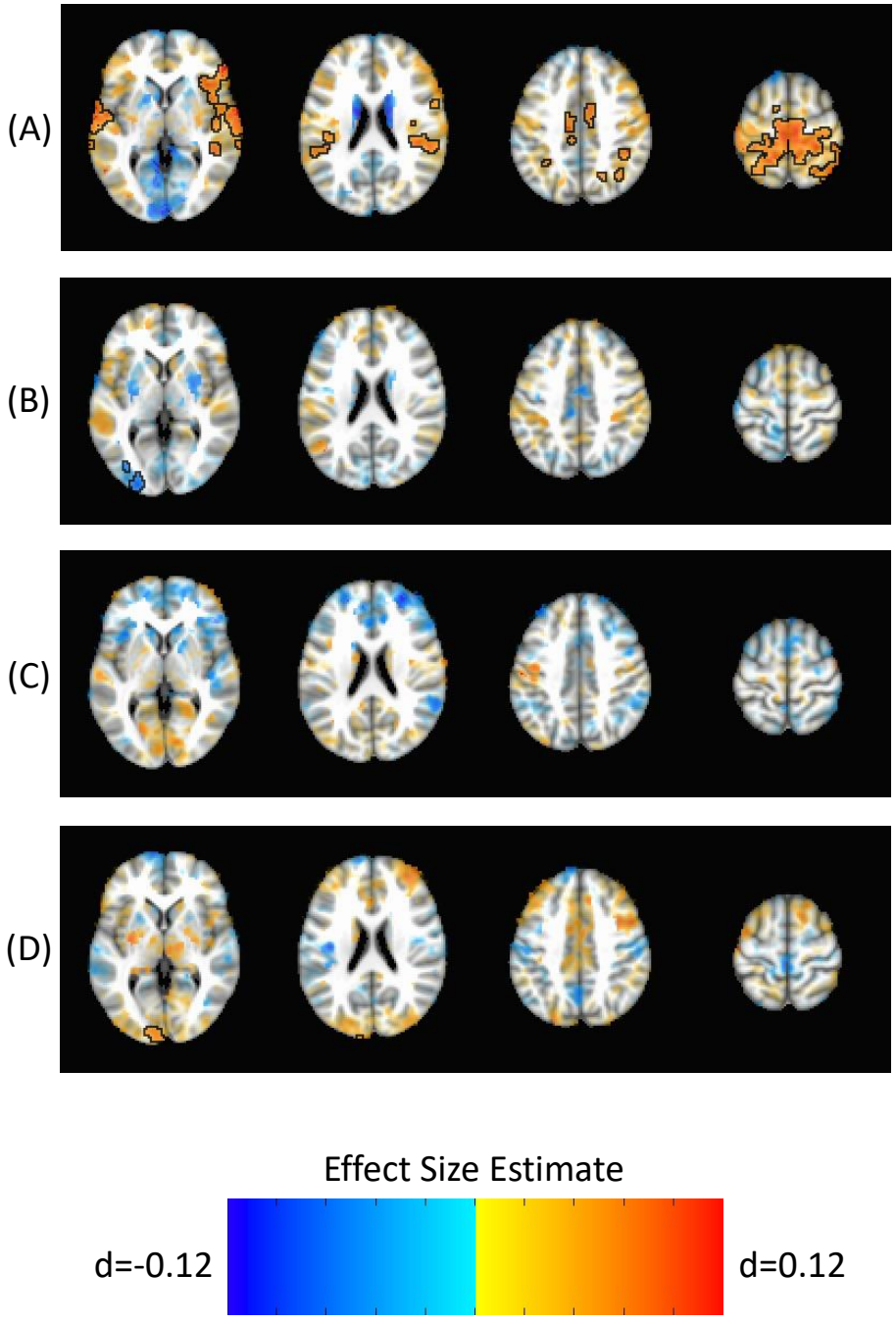

FIGURE S20. Findings from a mega-analysis of differences in seed-based subcortico-cortical connectivity in youth with attention deficit/hyperactivity disorder (ADHD) and unaffected control subjects after applying partial correlation models at the single subject level. **(A)** Caudate. **(B)** Putamen. **(C)** Nucleus Accumbens. **(D)** Amygdala. Positive effect sizes indicate ADHD>controls. Voxels in significant clusters are opaque and boxed. Subthreshold voxels are presented translucently. Findings presented at a liberal cluster forming threshold of $p<0.005$.

TABLE S7. Show results of case-control comparison after applying partial correlation models at the single subject level. n=1696 patients with ADHD and n=6737 unaffected controls.

Cluster	X	Y	Z	Peak-*d*	Mean-*d*	Size (voxels)	Overlap	Talairach label
Findings presented at the strict cluster forming threshold of p<0.0001.								
Bilateral Caudate								
1	14	-7	78	0.38	0.09	761	19.40%	Right Medial Frontal Gyrus
							12.40%	Left Medial Frontal Gyrus
							9.10%	Right Paracentral Lobule
							7.80%	Right Postcentral Gyrus
							5.90%	Left Paracentral Lobule
2	-19	-33	78	0.14	0.09	250	14.50%	Left Postcentral Gyrus
							7.70%	Left Precentral Gyrus
3	14	-5	22	-0.19	-0.10	175	52.80%	Right Caudate
4	-9	4	16	-0.15	-0.10	165	49.30%	Left Caudate
							16.10%	Left Lentiform Nucleus
5	62	-37	8	0.11	0.09	125	86.30%	Right Superior Temporal Gyrus
							3.40%	Right Middle Temporal Gyrus
6	42	-45	54	0.24	0.09	99	39.60%	Right Inferior Parietal Lobule
Findings presented at a liberal cluster forming threshold of p<0.005.								
Bilateral Caudate								
1	14	-7	78	0.38	0.07	6672	5.30%	Left Postcentral Gyrus
							5.30%	Right Medial Frontal Gyrus
							5.30%	Right Inferior Parietal Lobule
							5.00%	Left Medial Frontal Gyrus
							4.90%	Left Paracentral Lobule
							4.70%	Right Postcentral Gyrus

							4.10%	Right Paracentral Lobule
							4.00%	Right Superior Parietal Lobule
							3.00%	Right Precentral Gyrus
							2.30%	Left Superior Parietal Lobule
							1.80%	Left Precentral Gyrus
							1.60%	Right Cingulate Gyrus
							1.10%	Right Precuneus
							1.10%	Left Inferior Parietal Lobule
2	66	-3	-3	0.26	0.07	2136	45.10%	Right Superior Temporal Gyrus
							11.90%	Right Insula
							10.70%	Right Inferior Frontal Gyrus
							7.20%	Right Inferior Parietal Lobule
							6.20%	Right Precentral Gyrus
							5.00%	Right Middle Temporal Gyrus
							2.70%	Right Transverse Temporal Gyrus
							1.20%	Right Postcentral Gyrus
3	-71	-21	6	0.21	0.07	763	60.70%	Left Superior Temporal Gyrus
							6.70%	Left Insula
							6.30%	Left Transverse Temporal Gyrus
							5.60%	Left Inferior Parietal Lobule
							5.20%	Left Postcentral Gyrus
							2.60%	Left Middle Temporal Gyrus
Bilateral Putamen								
1	-27	-95	-3	-0.11	-0.07	369	37.50%	Left Inferior Occipital Gyrus
							12.70%	Left Cuneus

							10.50%	Left Lingual Gyrus
							10.10%	Left Middle Occipital Gyrus
							4.50%	Left Fusiform Gyrus
Bilateral Amygdala								
1	-25	-87	10	0.08	0.06	452	42.90%	Left Cuneus
							24.20%	Left Lingual Gyrus
							21.80%	Left Middle Occipital Gyrus
							1.00%	Left Inferior Occipital Gyrus

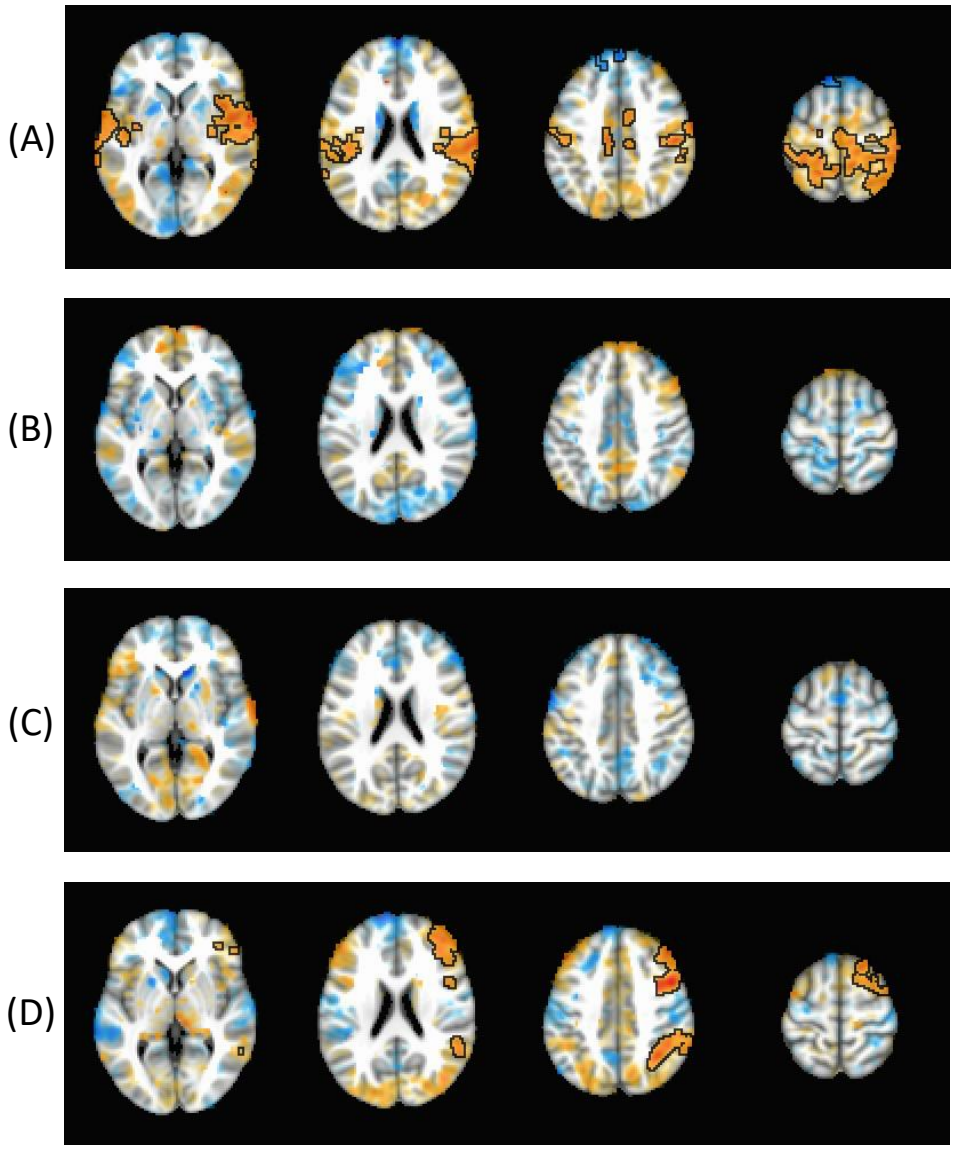

FIGURE S21. Findings from a mega-analysis of associations between seed-based subcortico-cortical connectivity and scores on the Attention Problems scale after applying partial correlation models at the single subject level. **(A)** Caudate. **(B)** Putamen. **(C)** Nucleus Accumbens. **(D)** Amygdala. Voxels in significant clusters are opaque and boxed. Subthreshold voxels are presented translucently.

TABLE S8. Significant associations between Attention Problems scores and subcortico-cortical connectivity after applying partial correlation models at the single subject level. n= 9890.

Cluster	X	Y	Z	Peak *partial-r*	Mean *patrial-r*	Size (voxels)	Overlap	Talairach label
Findings presented at the strict cluster forming threshold of p<0.0001.								
Bilateral Caudate								
1	70	-13	8	0.08	0.04	692	52.40%	Right Superior Temporal Gyrus
							22.00%	Right Inferior Parietal Lobule
							7.50%	Right Postcentral Gyrus
							5.30%	Right Transverse Temporal Gyrus
							4.00%	Right Precentral Gyrus
							2.50%	Right Insula
							2.20%	Right Middle Temporal Gyrus
2	-63	-11	12	0.05	0.04	200	56.90%	Left Superior Temporal Gyrus
							21.10%	Left Transverse Temporal Gyrus
							19.20%	Left Postcentral Gyrus
							1.60%	Left Precentral Gyrus
3	50	-25	50	0.12	0.05	158	81.30%	Right Postcentral Gyrus
							3.10%	Right Precentral Gyrus
4	24	-45	76	0.08	0.04	122	12.30%	Right Postcentral Gyrus
Findings presented at a liberal cluster forming threshold of p<0.005.								
Bilateral Caudate								
1	-29	-41	74	0.18	0.03	5801	13.10%	Right Postcentral Gyrus
							9.30%	Left Postcentral Gyrus
							5.00%	Right Paracentral Lobule

							4.70%	Right Precentral Gyrus
							3.80%	Left Paracentral Lobule
							3.30%	Right Medial Frontal Gyrus
							3.30%	Left Medial Frontal Gyrus
							3.30%	Right Superior Parietal Lobule
							3.10%	Left Precentral Gyrus
							2.20%	Right Cingulate Gyrus
							2.10%	Right Inferior Parietal Lobule
							2.10%	Left Precuneus
							1.40%	Right Precuneus
							1.40%	Left Superior Parietal Lobule
2	70	-13	8	0.08	0.03	3544	35.80%	Right Superior Temporal Gyrus
							18.90%	Right Insula
							11.50%	Right Inferior Parietal Lobule
							9.90%	Right Postcentral Gyrus
							6.80%	Right Precentral Gyrus
							3.10%	Right Transverse Temporal Gyrus
							2.10%	Right Middle Temporal Gyrus
3	-69	-27	8	0.06	0.03	2111	50.80%	Left Superior Temporal Gyrus
							14.10%	Left Insula
							11.50%	Left Postcentral Gyrus
							5.80%	Left Inferior Parietal Lobule
							5.30%	Left Transverse Temporal Gyrus
							3.10%	Left Middle Temporal Gyrus
							1.70%	Left Precentral Gyrus

4	4	18	54	-0.05	-0.03	777	24.90%	Right Superior Frontal Gyrus
							12.80%	Left Superior Frontal Gyrus
							1.00%	Right Medial Frontal Gyrus
Bilateral Nucleus Accumbens								
1	-3	34	-15	0.04	0.03	322	44.20%	Left Medial Frontal Gyrus
							19.30%	Right Medial Frontal Gyrus
							8.40%	Left Subcallosal Gyrus
							7.20%	Left Anterior Cingulate
							4.00%	Left Rectal Gyrus
							2.00%	Right Anterior Cingulate
							1.90%	Left Orbital Gyrus
Bilateral Amygdala								
1	48	10	44	0.07	0.03	3170	56.10%	Right Middle Frontal Gyrus
							13.20%	Right Superior Frontal Gyrus
							11.20%	Right Inferior Frontal Gyrus
							4.30%	Right Precentral Gyrus
							2.50%	Right Medial Frontal Gyrus
2	34	-57	44	0.05	0.03	1251	42.50%	Right Inferior Parietal Lobule
							20.00%	Right Supramarginal Gyrus
							11.40%	Right Superior Temporal Gyrus
							5.90%	Right Middle Temporal Gyrus
							3.50%	Right Superior Parietal Lobule
							2.50%	Right Precuneus
							1.10%	Right Angular Gyrus

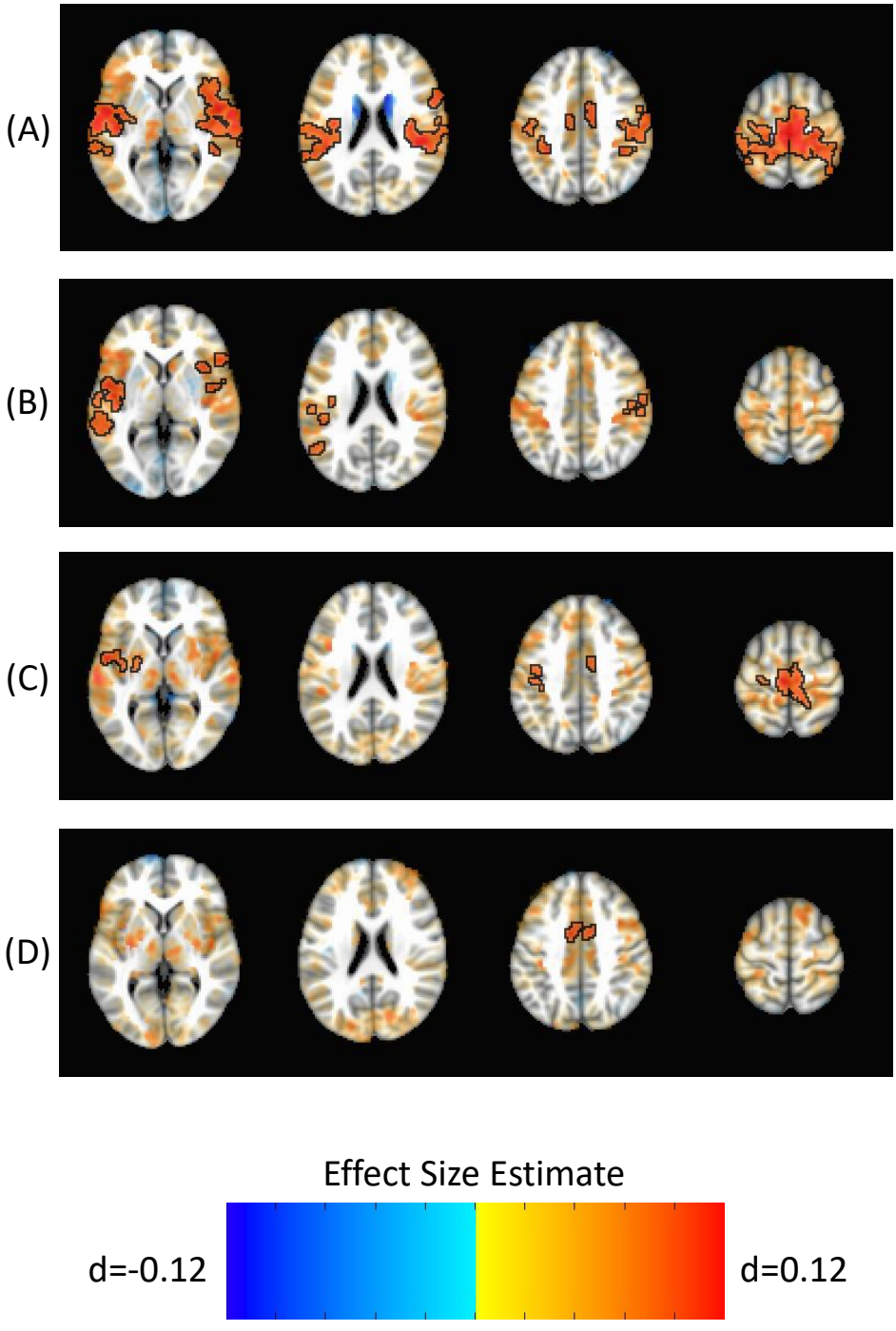

FIGURE S22. Findings from a mega-analysis of differences in seed-based subcortico-cortical connectivity in youth with attention deficit/hyperactivity disorder (ADHD) and unaffected control subjects using left hemisphere subcortical seeds. **(A)** Caudate. **(B)** Putamen. **(C)** Nucleus Accumbens. **(D)** Amygdala. Positive effect sizes indicate ADHD>controls. Voxels in significant clusters are opaque and boxed. Subthreshold voxels are presented translucently.

TABLE S9. Show results of case-control comparison using left hemisphere subcortical seeds. n=1696 patients with ADHD and n=6737 unaffected controls.

Cluster	X	Y	Z	Peak-*d*	Mean-*d*	Size (voxels)	Overlap	Talairach label
Left Caudate								
1	-5	-27	62	0.15	0.10	5584	8.60%	Right Medial Frontal Gyrus
							7.70%	Right Postcentral Gyrus
							7.40%	Left Postcentral Gyrus
							6.90%	Left Medial Frontal Gyrus
							5.30%	Left Paracentral Lobule
							5.30%	Right Paracentral Lobule
							4.90%	Left Precentral Gyrus
							3.00%	Left Inferior Parietal Lobule
							2.80%	Right Precentral Gyrus
							1.90%	Right Inferior Parietal Lobule
							1.70%	Right Cingulate Gyrus
							1.00%	Right Superior Frontal Gyrus
2	64	-7	-3	0.15	0.10	4779	29.10%	Right Superior Temporal Gyrus
							18.40%	Right Insula
							14.40%	Right Postcentral Gyrus
							9.80%	Right Precentral Gyrus
							8.30%	Right Inferior Parietal Lobule
							5.00%	Right Inferior Frontal Gyrus
							3.20%	Right Middle Temporal Gyrus
							2.40%	Right Transverse Temporal Gyrus
3	-55	-5	-1	0.16	0.10	3668	39.90%	Left Superior Temporal Gyrus

							19.40%	Left Insula
							10.30%	Left Postcentral Gyrus
							8.20%	Left Middle Temporal Gyrus
							6.20%	Left Precentral Gyrus
							4.30%	Left Inferior Parietal Lobule
							2.10%	Left Transverse Temporal Gyrus
Left Putamen								
1	-51	-3	-1	0.14	0.09	2299	38.40%	Left Superior Temporal Gyrus
							30.70%	Left Middle Temporal Gyrus
							13.70%	Left Insula
							1.60%	Left Inferior Temporal Gyrus
							1.50%	Left Postcentral Gyrus
							1.30%	Left Precentral Gyrus
							1.00%	Left Fusiform Gyrus
2	36	16	4	0.11	0.09	783	60.40%	Right Inferior Frontal Gyrus
							21.90%	Right Insula
							6.20%	Right Superior Temporal Gyrus
							4.10%	Right Uncus
3	52	6	-25	0.11	0.09	355	68.90%	Right Middle Temporal Gyrus
							17.90%	Right Superior Temporal Gyrus
							1.90%	Right Inferior Temporal Gyrus
4	52	-29	36	0.12	0.09	313	65.60%	Right Postcentral Gyrus
							24.90%	Right Precentral Gyrus
							8.50%	Right Inferior Parietal Lobule

Left Nucleus Accumbens								
1	-5	-25	62	0.13	0.09	974	27.10%	Right Medial Frontal Gyrus
							15.40%	Left Medial Frontal Gyrus
							9.90%	Right Paracentral Lobule
							8.20%	Left Precentral Gyrus
							5.40%	Right Cingulate Gyrus
							4.30%	Left Paracentral Lobule
							3.70%	Right Postcentral Gyrus
							1.30%	Left Postcentral Gyrus
2	-29	-11	8	0.12	0.09	528	29.40%	Left Insula
							24.30%	Left Superior Temporal Gyrus
							20.00%	Left Lentiform Nucleus
							6.90%	Left Precentral Gyrus
							5.30%	Left Middle Temporal Gyrus
							2.30%	Left Claustrum
3	-39	-13	50	0.15	0.09	324	55.70%	Left Precentral Gyrus
							19.00%	Left Postcentral Gyrus
							13.00%	Left Inferior Parietal Lobule
Left Amygdala								
1	-9	-1	44	0.11	0.09	245	49.00%	Left Cingulate Gyrus
							31.60%	Right Cingulate Gyrus
							9.60%	Right Medial Frontal Gyrus
							9.50%	Left Medial Frontal Gyrus

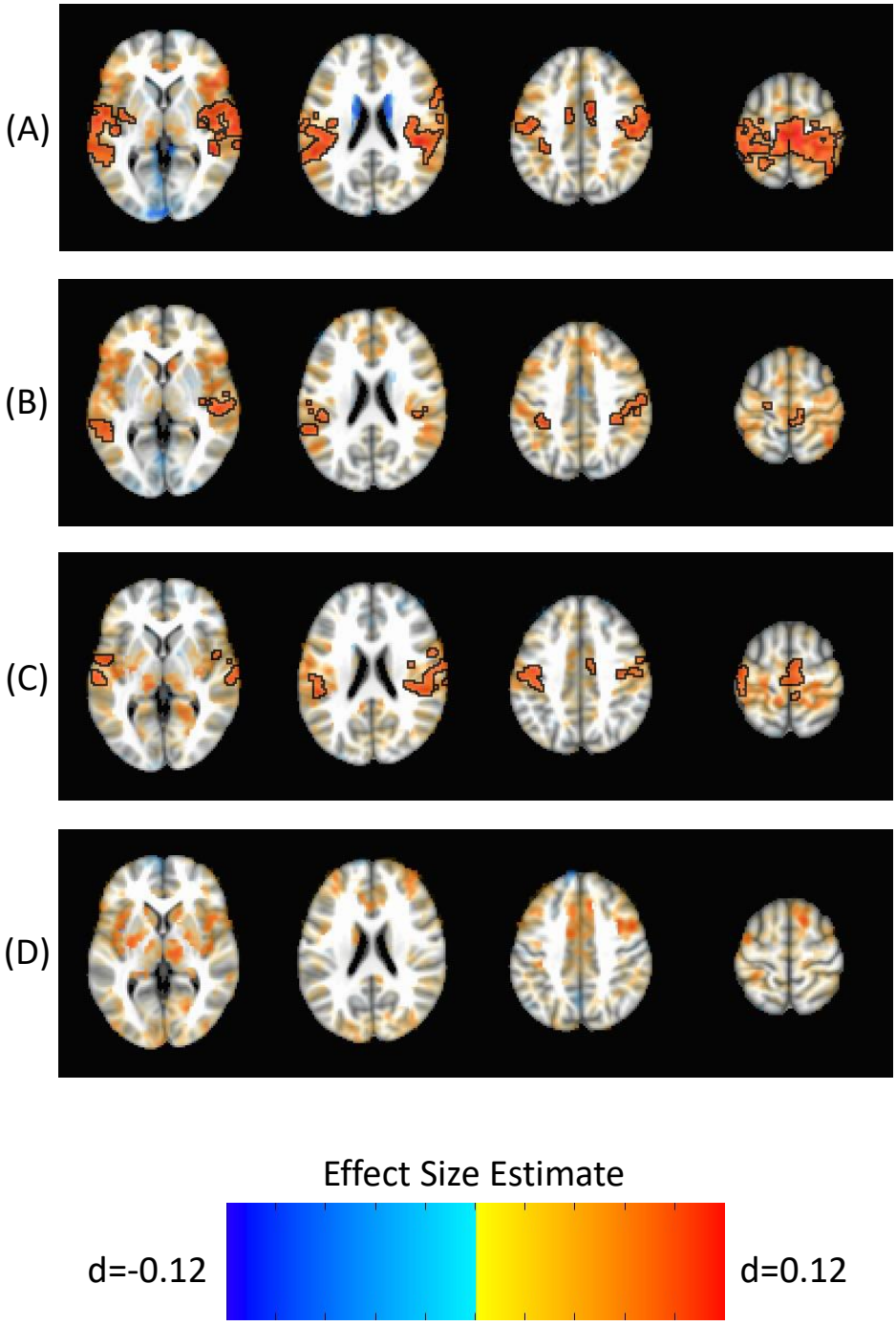

FIGURE S23. Findings from a mega-analysis of differences in seed-based subcortico-cortical connectivity in youth with attention deficit/hyperactivity disorder (ADHD) and unaffected control subjects using right hemisphere subcortical seeds. **(A)** Caudate. **(B)** Putamen. **(C)** Nucleus Accumbens. **(D)** Amygdala. Positive effect sizes indicate ADHD>controls. Voxels in significant clusters are opaque and boxed. Subthreshold voxels are presented translucently.

TABLE S10. Show results of case-control comparison using right hemisphere subcortical seeds. n=1696 patients with ADHD and n=6737 unaffected controls.

Cluster	X	Y	Z	Peak-*d*	Mean-*d*	Size (voxels)	Overlap	Talairach label
Right Caudate								
1	64	-7	-3	0.14	0.09	11438	13.40%	Right Superior Temporal Gyrus
							10.00%	Right Postcentral Gyrus
							7.80%	Right Precentral Gyrus
							5.80%	Right Insula
							5.50%	Left Postcentral Gyrus
							4.40%	Left Precentral Gyrus
							3.70%	Right Inferior Parietal Lobule
							3.60%	Right Medial Frontal Gyrus
							3.40%	Left Medial Frontal Gyrus
							2.90%	Right Middle Temporal Gyrus
							2.40%	Right Paracentral Lobule
							1.90%	Left Paracentral Lobule
							1.30%	Right Superior Parietal Lobule
							1.00%	Left Inferior Parietal Lobule
							1.00%	Right Cingulate Gyrus
2	-37	-17	12	0.13	0.09	2989	39.40%	Left Superior Temporal Gyrus
							16.10%	Left Middle Temporal Gyrus
							15.80%	Left Insula
							7.50%	Left Postcentral Gyrus
							6.30%	Left Inferior Parietal Lobule

							4.20%	Left Transverse Temporal Gyrus
							2.30%	Left Supramarginal Gyrus
							1.70%	Left Precentral Gyrus
Right Putamen								
1	56	-9	-9	0.12	0.09	1032	40.60%	Right Middle Temporal Gyrus
							32.80%	Right Superior Temporal Gyrus
							6.30%	Right Transverse Temporal Gyrus
							4.30%	Right Insula
							2.40%	Right Postcentral Gyrus
							2.20%	Right Inferior Temporal Gyrus
2	-61	-45	20	0.11	0.09	1005	40.80%	Left Middle Temporal Gyrus
							38.20%	Left Superior Temporal Gyrus
							6.50%	Left Inferior Parietal Lobule
							4.40%	Left Supramarginal Gyrus
							4.20%	Left Postcentral Gyrus
							4.10%	Left Insula
3	56	-15	44	0.11	0.09	382	71.40%	Right Postcentral Gyrus
							13.10%	Right Precentral Gyrus
							4.00%	Right Inferior Parietal Lobule
4	-29	-39	46	0.12	0.09	342	43.60%	Left Inferior Parietal Lobule
							14.80%	Left Precentral Gyrus
							9.30%	Left Postcentral Gyrus
5	4	-39	72	0.11	0.09	274	16.40%	Right Paracentral Lobule
							5.30%	Right Medial Frontal Gyrus
							2.50%	Right Postcentral Gyrus

Right Nucleus Accumbens								
1	70	-21	14	0.13	0.09	1597	25.10%	Right Precentral Gyrus
							18.90%	Right Insula
							18.80%	Right Postcentral Gyrus
							10.70%	Right Superior Temporal Gyrus
							6.60%	Right Inferior Parietal Lobule
							3.20%	Right Middle Temporal Gyrus
							2.20%	Right Transverse Temporal Gyrus
							1.30%	Right Inferior Frontal Gyrus
							1.30%	Right Claustrum
2	-45	-15	44	0.12	0.09	750	49.60%	Left Postcentral Gyrus
							28.80%	Left Precentral Gyrus
							1.90%	Left Inferior Parietal Lobule
3	-59	-7	10	0.12	0.09	598	53.70%	Left Superior Temporal Gyrus
							16.50%	Left Precentral Gyrus
							11.20%	Left Inferior Parietal Lobule
							7.80%	Left Insula
							6.60%	Left Postcentral Gyrus
							2.30%	Left Transverse Temporal Gyrus
							1.10%	Left Middle Temporal Gyrus
4	8	-5	60	0.12	0.09	559	45.90%	Right Medial Frontal Gyrus
							7.30%	Left Medial Frontal Gyrus
							6.70%	Right Cingulate Gyrus
							6.70%	Right Paracentral Lobule

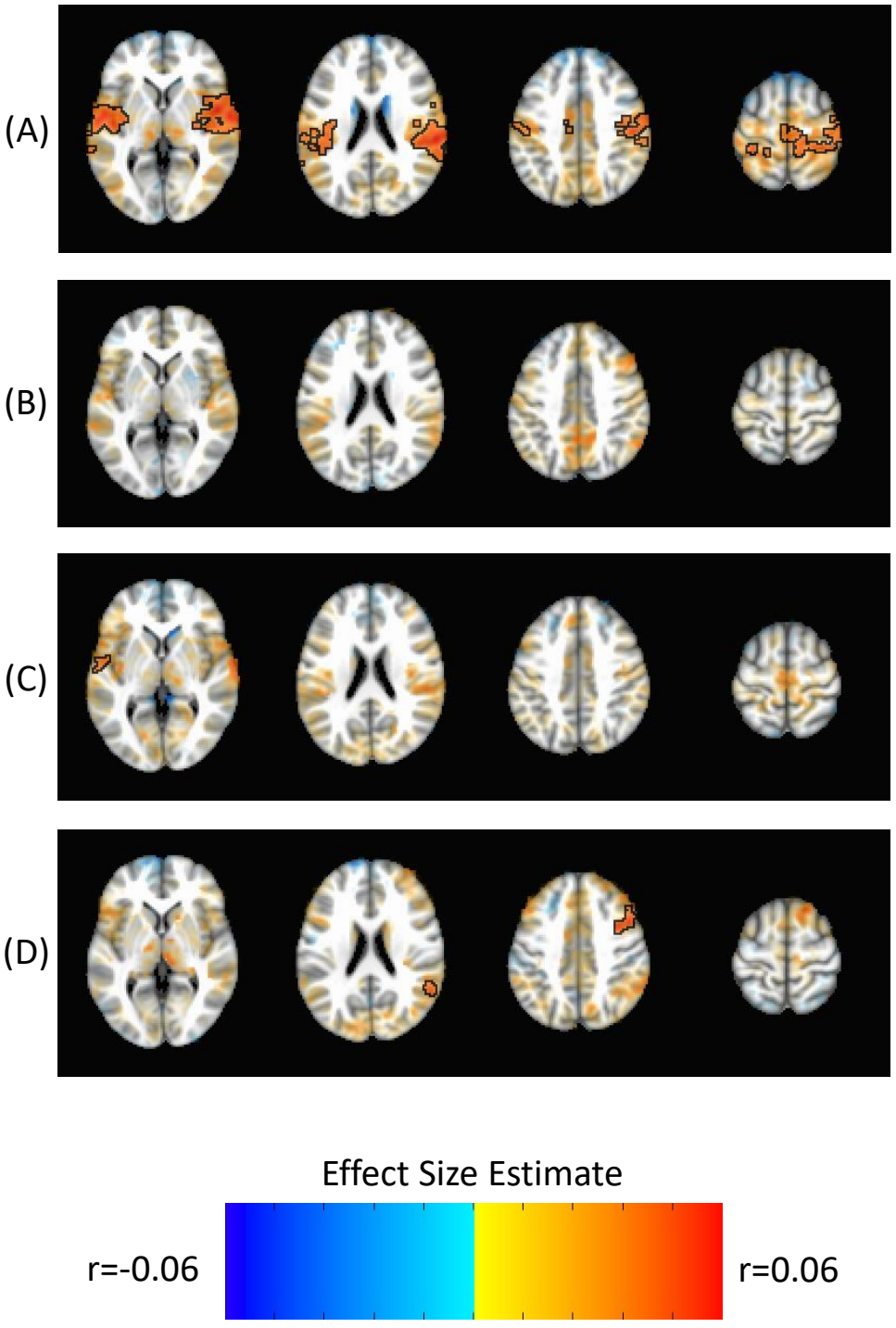

FIGURE S24. Findings from a mega-analysis of associations between seed-based subcortico-cortical connectivity and scores on the Attention Problems scale using left hemisphere subcortical seeds. **(A)** Caudate. **(B)** Putamen. **(C)** Nucleus Accumbens. **(D)** Amygdala. Voxels in significant clusters are opaque and boxed. Subthreshold voxels are presented translucently.

TABLE S11. Significant associations between Attention Problems scores and subcortico-cortical connectivity using left hemisphere subcortical seeds. n= 9890.

Cluster	X	Y	Z	Peak *partial-r*	Mean *patrial-r*	Size (voxels)	Overlap	Talairach label
Left Caudate								
1	66	-15	8	0.06	0.04	5440	22.10%	Right Postcentral Gyrus
							21.60%	Right Superior Temporal Gyrus
							12.60%	Right Insula
							11.20%	Right Precentral Gyrus
							8.20%	Right Inferior Parietal Lobule
							2.60%	Right Paracentral Lobule
							2.10%	Right Transverse Temporal Gyrus
							1.90%	Left Medial Frontal Gyrus
							1.70%	Right Medial Frontal Gyrus
2	-49	-11	-3	0.07	0.04	2574	45.90%	Left Superior Temporal Gyrus
							17.20%	Left Insula
							12.20%	Left Postcentral Gyrus
							6.60%	Left Precentral Gyrus
							5.00%	Left Inferior Parietal Lobule
							4.30%	Left Middle Temporal Gyrus
							3.80%	Left Transverse Temporal Gyrus
3	-33	-37	62	0.05	0.04	296	37.80%	Left Postcentral Gyrus
							16.80%	Left Inferior Parietal Lobule
Left Nucleus Accumbens								
1	-49	-1	12	0.05	0.04	132	48.60%	Left Superior Temporal Gyrus

							34.30%	Left Precentral Gyrus
							10.90%	Left Insula
Left Amygdala								
1	48	12	44	0.06	0.04	275	88.30%	Right Middle Frontal Gyrus
							6.90%	Right Precentral Gyrus
2	58	-49	26	0.05	0.04	248	73.90%	Right Supramarginal Gyrus
							14.80%	Right Superior Temporal Gyrus
							11.30%	Right Inferior Parietal Lobule

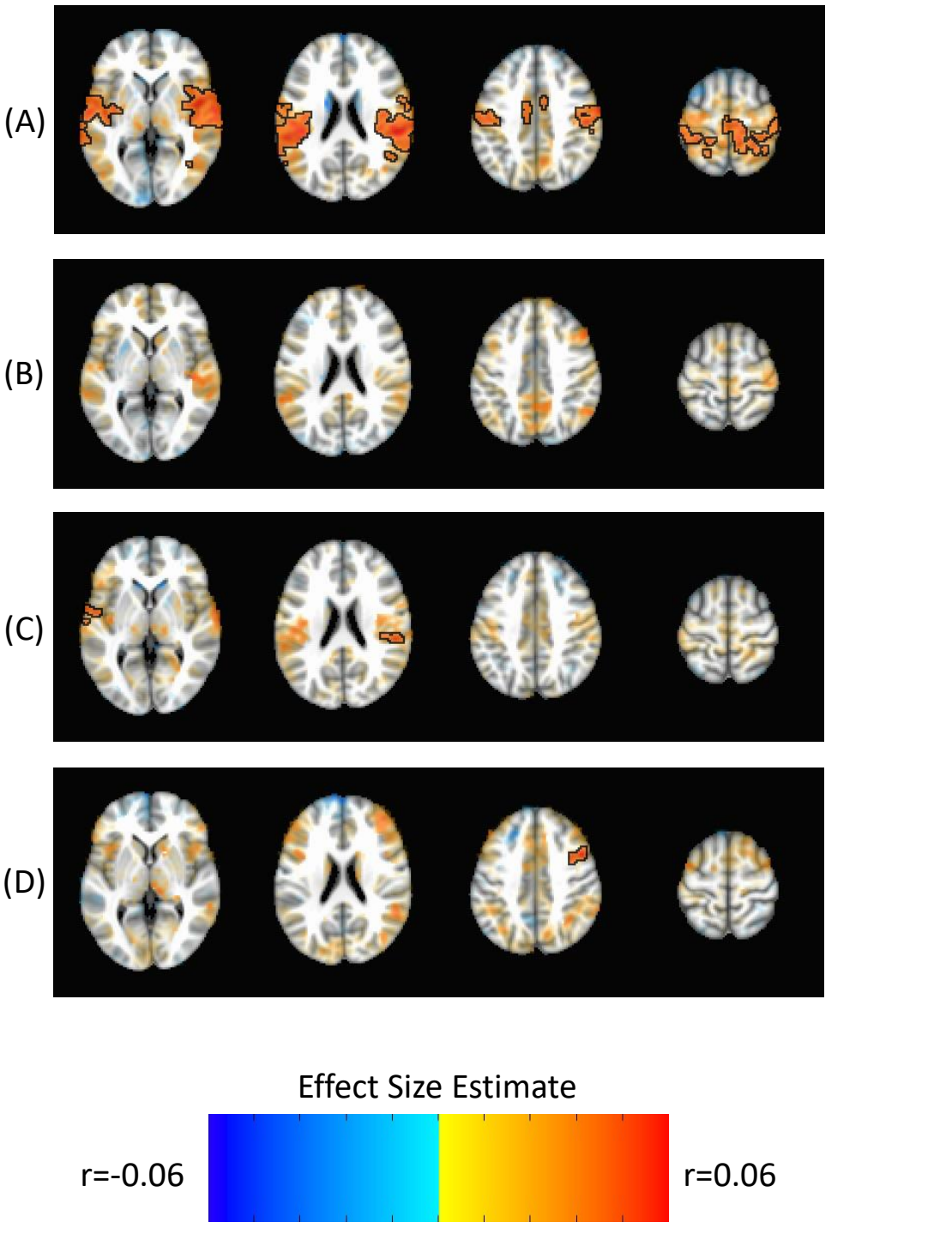

FIGURE S25. Findings from a mega-analysis of associations between seed-based subcortico-cortical connectivity and scores on the Attention Problems scale using right hemisphere subcortical seeds. **(A)** Caudate. **(B)** Putamen. **(C)** Nucleus Accumbens. **(D)** Amygdala. Voxels in significant clusters are opaque and boxed. Subthreshold voxels are presented translucently.

TABLE S12. Significant associations between Attention Problems scores and subcortico-cortical connectivity using right hemisphere subcortical seeds. n= 9890.

Cluster	X	Y	Z	Peak *partial-r*	Mean *patrial-r*	Size (voxels)	Overlap	Talairach label
Right Caudate								
1	50	-1	-1	0.06	0.04	6984	21.60%	Right Superior Temporal Gyrus
							15.20%	Right Postcentral Gyrus
							13.80%	Right Insula
							11.40%	Right Precentral Gyrus
							6.60%	Right Inferior Parietal Lobule
							2.90%	Right Paracentral Lobule
							2.30%	Left Medial Frontal Gyrus
							2.00%	Right Medial Frontal Gyrus
							1.90%	Right Middle Temporal Gyrus
							1.20%	Right Transverse Temporal Gyrus
							1.20%	Left Paracentral Lobule
							1.00%	Left Cingulate Gyrus
							1.00%	Right Superior Parietal Lobule
2	-59	-13	10	0.07	0.04	4976	29.10%	Left Superior Temporal Gyrus
							19.50%	Left Postcentral Gyrus
							11.10%	Left Precentral Gyrus
							10.70%	Left Insula
							7.30%	Left Inferior Parietal Lobule
							4.60%	Left Middle Temporal Gyrus

							2.80%	Left Transverse Temporal Gyrus
3	46	-63	8	0.05	0.04	370	64.50%	Right Middle Temporal Gyrus
							16.90%	Right Middle Occipital Gyrus
							14.20%	Right Superior Temporal Gyrus
Right Nucleus Accumbens								
1	68	-23	16	0.05	0.04	296	35.10%	Right Superior Temporal Gyrus
							31.30%	Right Inferior Parietal Lobule
							14.70%	Right Insula
							11.90%	Right Postcentral Gyrus
2	-51	-3	10	0.05	0.04	292	43.70%	Left Superior Temporal Gyrus
							24.30%	Left Precentral Gyrus
							14.60%	Left Transverse Temporal Gyrus
							11.00%	Left Postcentral Gyrus
							3.30%	Left Insula
Right Amygdala								
1	46	10	40	0.06	0.04	476	80.70%	Right Middle Frontal Gyrus
							9.80%	Right Precentral Gyrus
							6.40%	Right Inferior Frontal Gyrus
2	8	12	54	0.05	0.04	155	86.20%	Right Superior Frontal Gyrus
							11.60%	Right Medial Frontal Gyrus
							1.00%	Left Superior Frontal Gyrus

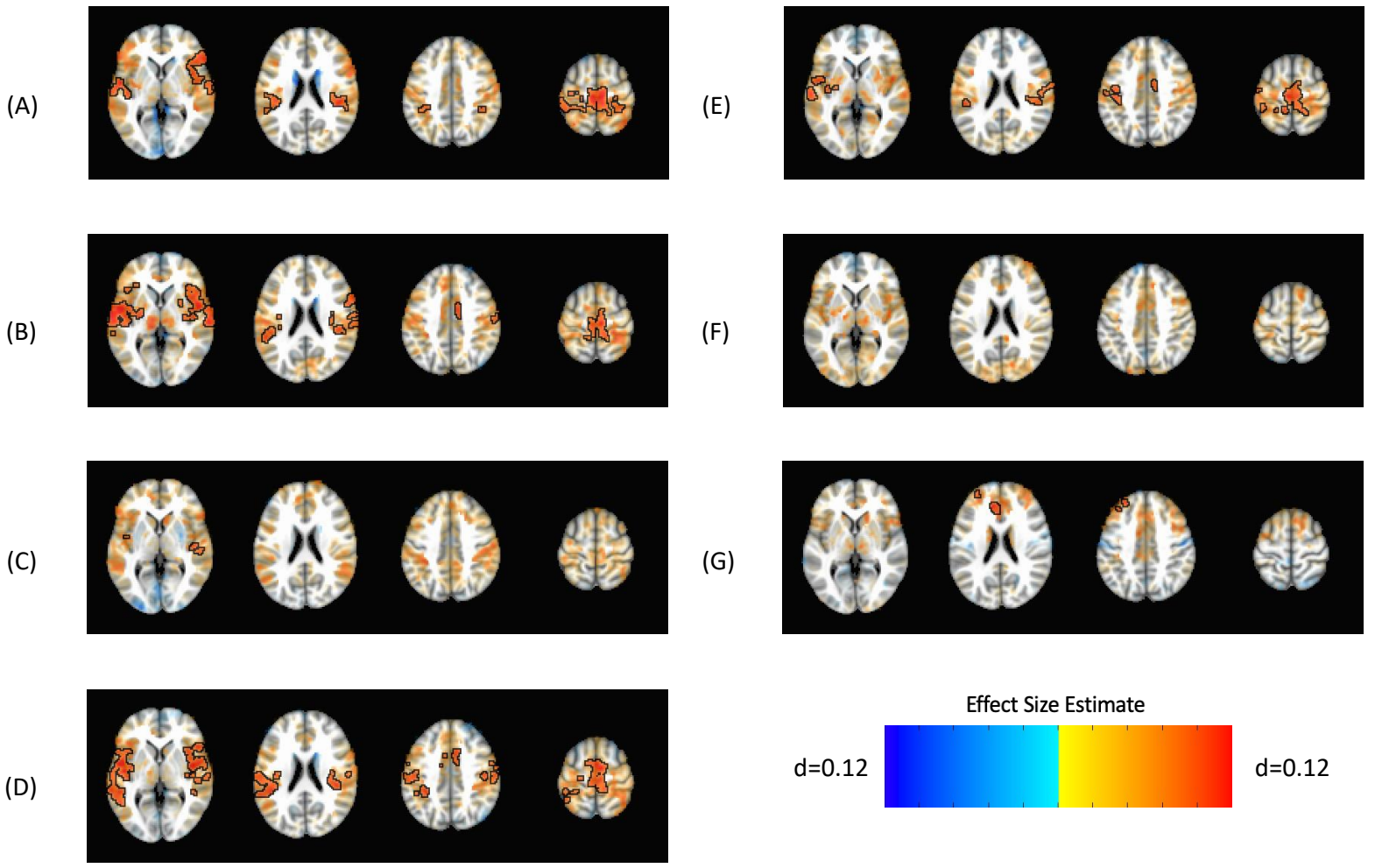

FIGURE S26. Findings from a mega-analysis of differences in seed-based subcortico-cortical connectivity in youth with attention deficit/hyperactivity disorder (ADHD) and unaffected control subjects when adopting alternative seed definitions. **(A)** Dorsal Caudate. **(B)** Ventral Caudate. **(C)** Dorsal Putamen **(D)** Ventral Putamen **(E)** Nucleus Accumbens **(F)** Dorsal Amygdala **(G)** Ventral Amygdala. Positive effect sizes indicate ADHD>controls. Voxels in significant clusters are opaque and boxed. Subthreshold voxels are presented translucently.

TABLE S13. Show results of case-control comparison. n=1696 patients with ADHD and n=6737 unaffected controls when adopting alternative seed definitions.

Cluster	X	Y	Z	Peak-*d*	Mean-*d*	Size (voxels)	Overlap	Talairach label
Bilateral Dorsal Caudate								
1	6	-21	62	0.14	0.09	3197	8.80%	Right Medial Frontal Gyrus
							8.00%	Left Medial Frontal Gyrus
							7.20%	Right Paracentral Lobule
							6.20%	Right Postcentral Gyrus
							6.00%	Left Inferior Parietal Lobule
							5.30%	Left Paracentral Lobule
							4.70%	Left Postcentral Gyrus
							3.90%	Right Inferior Parietal Lobule
							3.50%	Left Precentral Gyrus
							1.20%	Right Precentral Gyrus
2	46	-29	24	0.13	0.09	1554	30.40%	Right Superior Temporal Gyrus
							25.10%	Right Insula
							20.20%	Right Inferior Frontal Gyrus
							7.70%	Right Inferior Parietal Lobule
							4.20%	Right Precentral Gyrus
							2.20%	Right Middle Temporal Gyrus
							2.00%	Right Transverse Temporal Gyrus
3	-57	-5	-1	0.12	0.09	683	71.50%	Left Superior Temporal Gyrus
							10.50%	Left Insula
							7.10%	Left Inferior Parietal Lobule
							4.60%	Left Postcentral Gyrus

							1.50%	Left Transverse Temporal Gyrus
							1.40%	Left Middle Temporal Gyrus
Bilateral Ventral Caudate								
1	50	2	4	0.13	0.09	2683	24.20%	Right Superior Temporal Gyrus
							23.20%	Right Insula
							12.50%	Right Precentral Gyrus
							8.30%	Right Postcentral Gyrus
							8.20%	Right Inferior Frontal Gyrus
							4.00%	Right Inferior Parietal Lobule
							2.50%	Right Middle Temporal Gyrus
							1.90%	Right Lentiform Nucleus
							1.90%	Right Transverse Temporal Gyrus
2	-55	-5	2	0.14	0.09	1982	42.90%	Left Superior Temporal Gyrus
							21.70%	Left Insula
							7.40%	Left Middle Temporal Gyrus
							6.10%	Left Precentral Gyrus
							5.80%	Left Inferior Frontal Gyrus
							4.80%	Left Lentiform Nucleus
							4.10%	Left Inferior Parietal Lobule
3	8	-23	60	0.12	0.09	1025	33.50%	Right Medial Frontal Gyrus
							13.20%	Right Paracentral Lobule
							11.80%	Left Medial Frontal Gyrus
							7.30%	Right Cingulate Gyrus
							6.30%	Left Paracentral Lobule
							4.00%	Right Postcentral Gyrus

Bilateral Dorsal Putamen								
1	58	-3	-15	0.13	0.09	731	51.40%	Right Middle Temporal Gyrus
							21.80%	Right Superior Temporal Gyrus
							5.70%	Right Inferior Temporal Gyrus
							4.70%	Right Transverse Temporal Gyrus
							4.50%	Right Insula
							1.40%	Right Postcentral Gyrus
2	-49	-13	-7	0.11	0.09	351	31.90%	Left Middle Temporal Gyrus
							25.60%	Left Superior Temporal Gyrus
							7.30%	Left Insula
							6.60%	Left Fusiform Gyrus
							5.30%	Left Inferior Temporal Gyrus
Bilateral Ventral Putamen								
1	-51	-3	-1	0.14	0.09	4647	27.90%	Left Superior Temporal Gyrus
							15.90%	Left Middle Temporal Gyrus
							13.70%	Left Insula
							10.60%	Left Postcentral Gyrus
							8.90%	Left Inferior Parietal Lobule
							6.90%	Left Precentral Gyrus
							1.80%	Left Supramarginal Gyrus
							1.30%	Left Transverse Temporal Gyrus
2	44	-23	8	0.13	0.09	2707	26.40%	Right Insula
							22.70%	Right Superior Temporal Gyrus
							15.30%	Right Postcentral Gyrus

							13.40%	Right Precentral Gyrus
							5.70%	Right Inferior Parietal Lobule
							5.20%	Right Inferior Frontal Gyrus
							2.70%	Right Transverse Temporal Gyrus
							1.90%	Right Middle Temporal Gyrus
3	8	-9	62	0.12	0.09	1557	26.50%	Right Medial Frontal Gyrus
							22.50%	Left Medial Frontal Gyrus
							9.20%	Right Paracentral Lobule
							4.60%	Right Cingulate Gyrus
							4.00%	Left Cingulate Gyrus
							2.80%	Left Paracentral Lobule
							2.60%	Left Superior Frontal Gyrus
							1.50%	Right Postcentral Gyrus
							1.10%	Right Superior Frontal Gyrus
Bilateral Nucleus Accumbens								
1	-39	-13	52	0.13	0.09	1118	34.00%	Left Postcentral Gyrus
							22.30%	Left Precentral Gyrus
							8.90%	Left Inferior Parietal Lobule
							1.00%	Left Paracentral Lobule
							0.40%	Left Superior Parietal Lobule
2	-5	-23	64	0.12	0.09	1108	27.10%	Right Medial Frontal Gyrus
							17.50%	Left Medial Frontal Gyrus
							10.20%	Right Paracentral Lobule
							4.80%	Right Cingulate Gyrus
							3.40%	Right Postcentral Gyrus
							2.80%	Left Paracentral Lobule
3	-35	-19	8	0.12	0.09	676	33.60%	Left Superior Temporal Gyrus

							26.10%	Left Insula
							10.50%	Left Lentiform Nucleus
							10.30%	Left Precentral Gyrus
							3.10%	Left Claustrum
							3.10%	Left Inferior Parietal Lobule
							1.90%	Left Middle Temporal Gyrus
4	62	-21	36	0.11	0.09	439	40.60%	Right Postcentral Gyrus
							24.10%	Right Precentral Gyrus
							21.00%	Right Inferior Parietal Lobule
							9.80%	Right Insula
Bilateral Ventral Amygdala								
1	-31	50	28	0.11	0.10	304	53.80%	Left Middle Frontal Gyrus
							42.50%	Left Superior Frontal Gyrus
2	4	32	16	0.12	0.10	161	63.10%	Left Anterior Cingulate
							13.10%	Right Anterior Cingulate
							10.60%	Left Medial Frontal Gyrus
							8.30%	Left Cingulate Gyrus

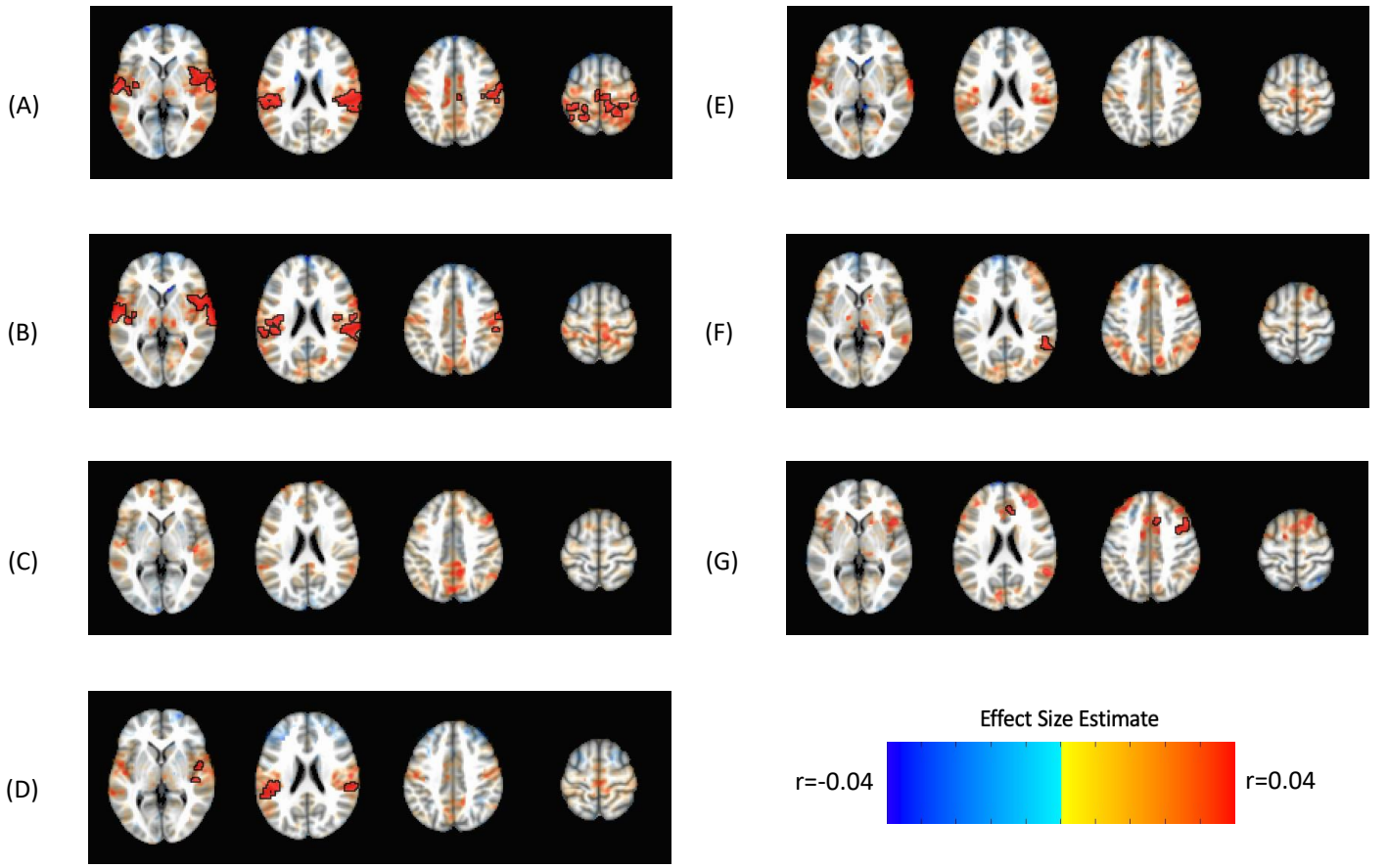

FIGURE S27. Findings from a mega-analysis of associations between seed-based subcortico-cortical connectivity and scores on the Attention Problems scale when adopting alternative seed definitions. **(A)** Dorsal Caudate. **(B)** Ventral Caudate. **(C)** Dorsal Putamen **(D)** Ventral Putamen **(E)** Nucleus Accumbens **(F)** Dorsal Amygdala **(G)** Ventral Amygdala. Positive effect sizes indicate ADHD>controls. Voxels in significant clusters are opaque and boxed. Subthreshold voxels are presented translucently.

TABLE S14. Significant associations between Attention Problems scores and subcortico-cortical connectivity using alternative seed definitions. n= 9890.

Cluster	X	Y	Z	Peak *partial-r*	Mean *patrial-r*	Size (voxels)	Overlap	Talairach label
Bilateral Dorsal Caudate								
1	48	-27	26	0.07	0.04	2664	21.50%	Right Superior Temporal Gyrus
							21.30%	Right Postcentral Gyrus
							20.10%	Right Insula
							14.50%	Right Inferior Parietal Lobule
							10.40%	Right Precentral Gyrus
							2.10%	Right Transverse Temporal Gyrus
							1.10%	Right Middle Temporal Gyrus
2	-61	-31	14	0.06	0.04	1311	53.40%	Left Superior Temporal Gyrus
							15.40%	Left Insula
							12.40%	Left Postcentral Gyrus
							6.50%	Left Inferior Parietal Lobule
							5.80%	Left Transverse Temporal Gyrus
							1.90%	Left Precentral Gyrus
							1.80%	Left Middle Temporal Gyrus
3	20	-43	68	0.05	0.04	919	24.00%	Right Postcentral Gyrus
							14.60%	Right Paracentral Lobule
							6.00%	Left Medial Frontal Gyrus
							5.60%	Right Medial Frontal Gyrus
							1.90%	Right Superior Parietal Lobule

							1.60%	Right Cingulate Gyrus
4	-29	-37	72	0.06	0.04	604	27.50%	Left Postcentral Gyrus
							9.20%	Left Inferior Parietal Lobule
							6.40%	Left Superior Parietal Lobule
Bilateral Ventral Caudate								
1	70	-15	12	0.06	0.04	2365	24.20%	Right Superior Temporal Gyrus
							18.80%	Right Insula
							17.00%	Right Inferior Parietal Lobule
							13.00%	Right Postcentral Gyrus
							11.50%	Right Precentral Gyrus
							2.10%	Right Transverse Temporal Gyrus
2	-61	-11	4	0.06	0.04	810	48.60%	Left Superior Temporal Gyrus
							13.70%	Left Insula
							13.20%	Left Postcentral Gyrus
							10.30%	Left Precentral Gyrus
							7.20%	Left Transverse Temporal Gyrus
3	-41	-35	24	0.05	0.04	263	38.30%	Left Inferior Parietal Lobule
							35.80%	Left Superior Temporal Gyrus
							15.60%	Left Insula
							4.20%	Left Postcentral Gyrus
Bilateral Ventral Putamen								
1	-49	-31	20	0.05	0.04	418	37.70%	Left Superior Temporal Gyrus
							25.80%	Left Insula
							25.20%	Left Inferior Parietal Lobule
							5.90%	Left Postcentral Gyrus

							2.50%	Left Supramarginal Gyrus
2	62	-31	20	0.06	0.04	358	47.50%	Right Superior Temporal Gyrus
							20.30%	Right Inferior Parietal Lobule
							14.10%	Right Insula
							8.30%	Right Transverse Temporal Gyrus
							6.80%	Right Postcentral Gyrus
							2.80%	Right Precentral Gyrus
Bilateral Dorsal Amygdala								
1	54	-45	24	0.05	0.04	198	51.50%	Right Supramarginal Gyrus
							30.60%	Right Superior Temporal Gyrus
							17.80%	Right Inferior Parietal Lobule
Bilateral Ventral Amygdala								
1	8	14	46	0.05	0.04	228	42.30%	Right Cingulate Gyrus
							28.30%	Right Superior Frontal Gyrus
							15.40%	Right Anterior Cingulate
							13.50%	Right Medial Frontal Gyrus
2	48	10	44	0.06	0.05	169	90.20%	Right Middle Frontal Gyrus
							5.60%	Right Precentral Gyrus
							4.10%	Right Inferior Frontal Gyrus

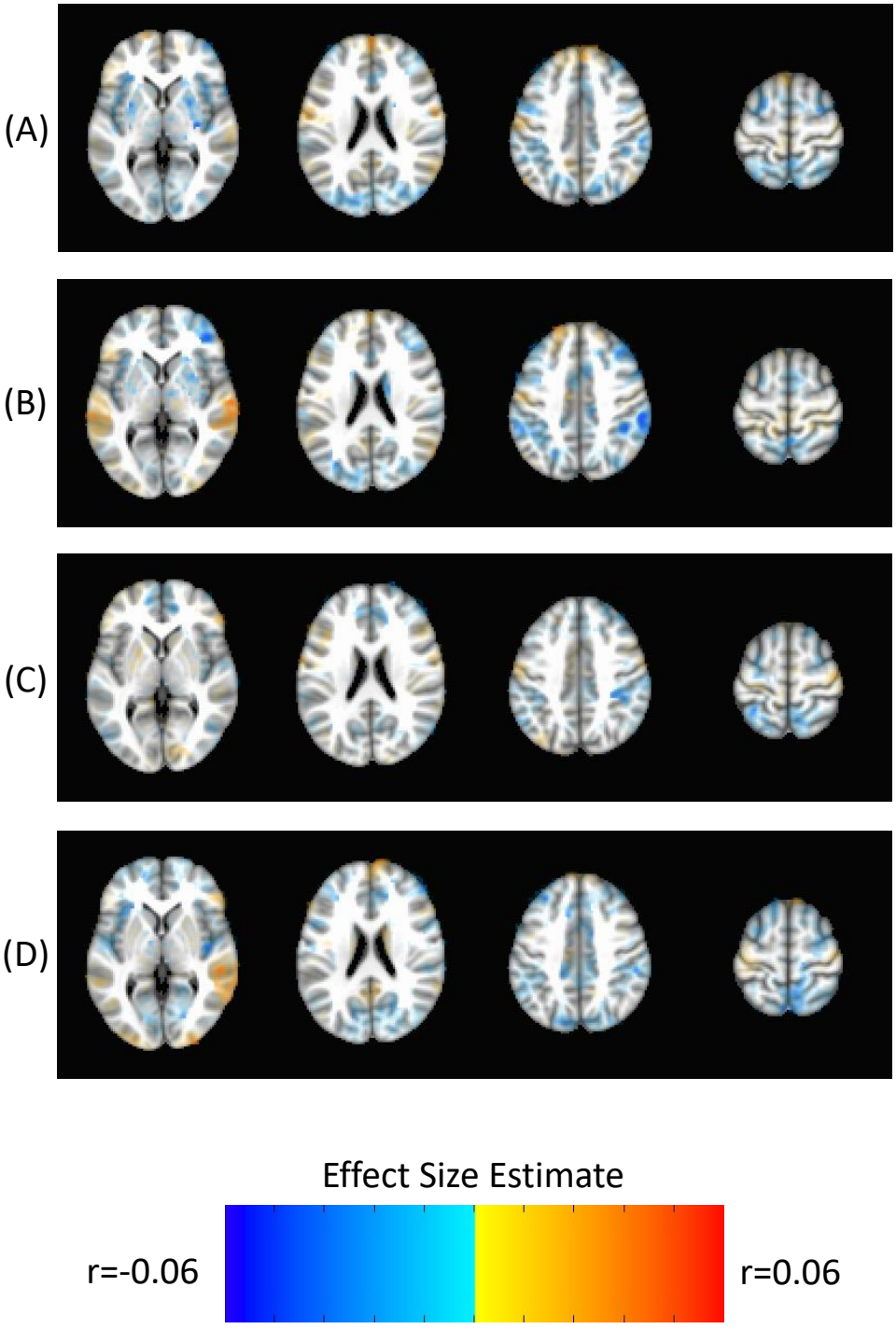

FIGURE S28. Findings from models assessing associations between seed-based subcortico-cortical connectivity and scores on the Internalizing Problems broadband scale **(A)** Caudate. **(B)** Putamen. **(C)** Nucleus Accumbens. **(D)** Amygdala. Subthreshold voxels are presented translucently.

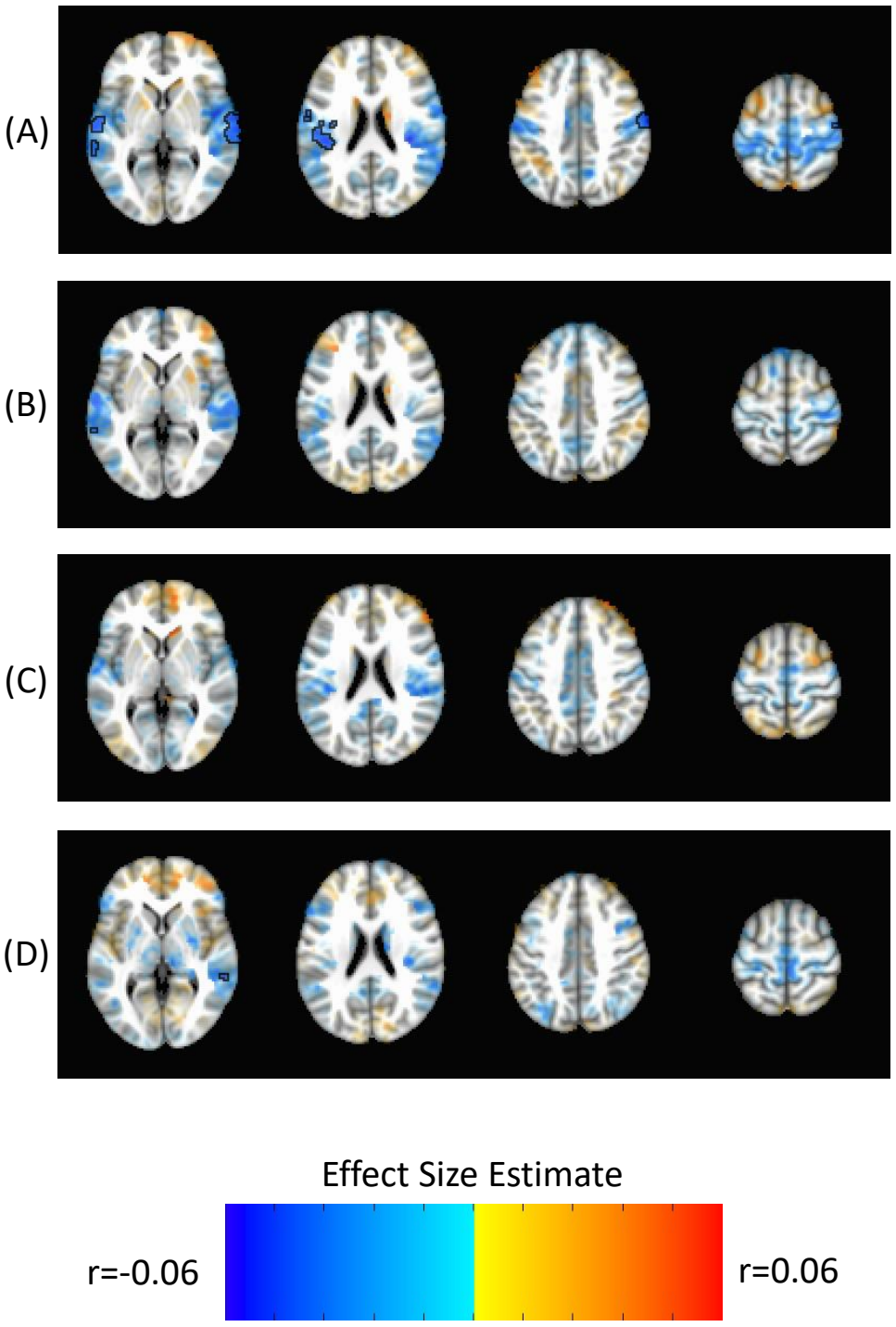

FIGURE S29. Findings from models assessing associations between seed-based subcortico-cortical connectivity and scores on the Externalizing Problems broadband scale **(A)** Caudate. **(B)** Putamen. **(C)** Nucleus Accumbens. **(D)** Amygdala. Voxels in significant clusters are opaque and boxed. Subthreshold voxels are presented translucently.

TABLE S15. Significant associations between Externalizing Problems scores and subcortico-cortical connectivity. n= 9890.

Cluster	X	Y	Z	Peak *partial-r*	Mean *patrial-r*	Size (voxels)	Overlap	Talairach label
Bilateral Caudate								
1	-57	-11	6	-0.06	-0.04	818	43.80%	Left Superior Temporal Gyrus
							15.80%	Left Postcentral Gyrus
							13.40%	Left Insula
							9.20%	Left Precentral Gyrus
							5.40%	Left Transverse Temporal Gyrus
							4.80%	Left Middle Temporal Gyrus
							2.70%	Left Inferior Parietal Lobule
2	68	-21	8	-0.06	-0.04	514	67.10%	Right Superior Temporal Gyrus
							6.10%	Right Transverse Temporal Gyrus
							5.50%	Right Middle Temporal Gyrus
3	52	-21	52	-0.05	-0.04	334	48.20%	Right Postcentral Gyrus
							26.70%	Right Precentral Gyrus
Bilateral Putamen								
1	-63	-39	10	-0.05	-0.04	199	77.90%	Left Superior Temporal Gyrus
							18.20%	Left Middle Temporal Gyrus
2	58	-9	-15	-0.05	-0.04	157	75.10%	Right Middle Temporal Gyrus
							10.10%	Right Inferior Temporal Gyrus
							5.70%	Right Superior Temporal Gyrus
							1.70%	Right Fusiform Gyrus
Bilateral Amygdala								

1	62	-49	10	-0.05	-0.04	231	54.90%	Right Middle Temporal Gyrus
							42.60%	Right Superior Temporal Gyrus
2	50	-45	-23	-0.06	-0.04	124	32.60%	Right Culmen
							28.70%	Right Fusiform Gyrus
							9.30%	Right Tuber
							5.10%	Right Inferior Temporal Gyrus

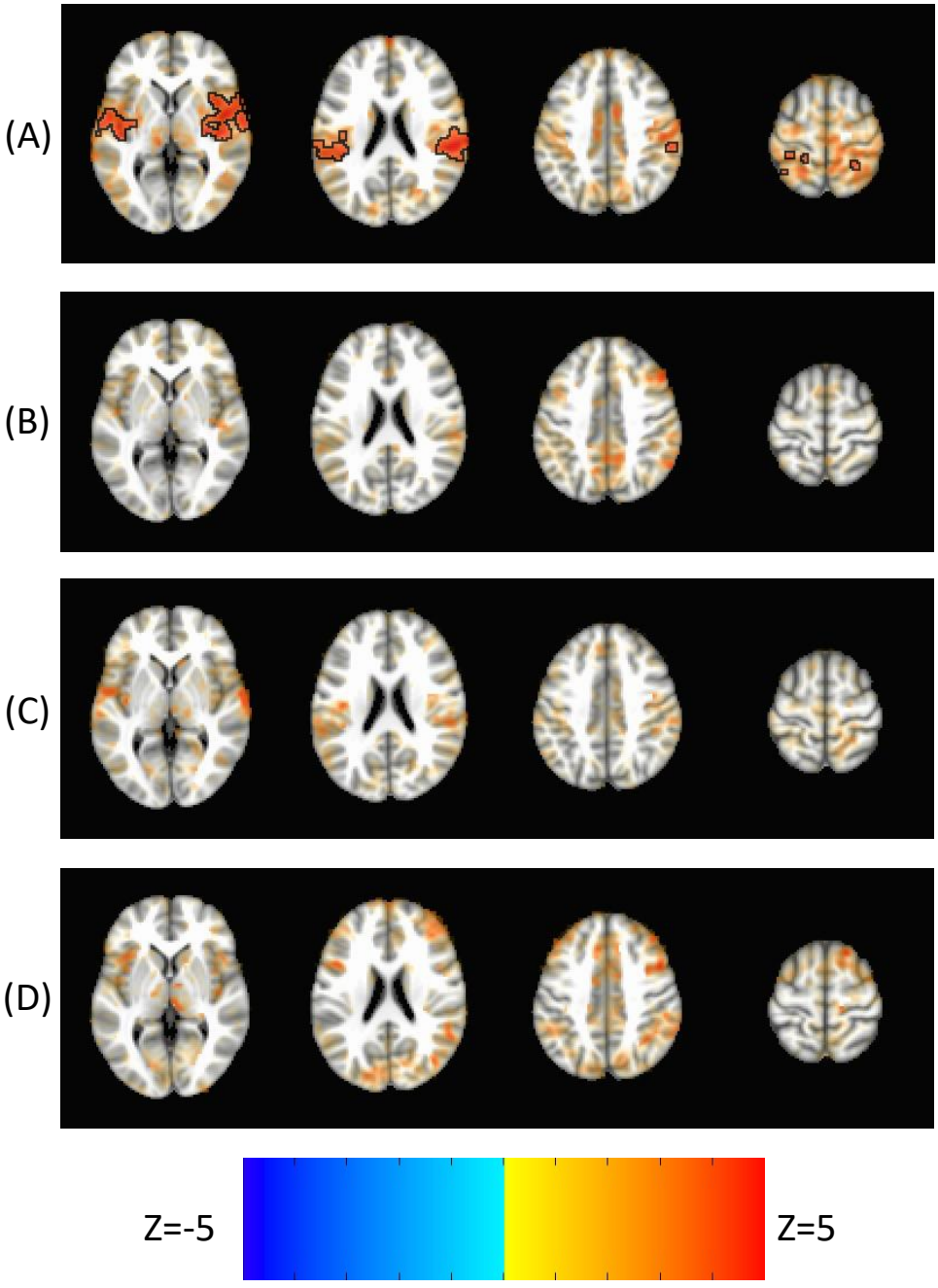

FIGURE S30. Shows regions demonstrating significantly different associations with scores on the Attention Problems subscale compared with the Internalizing Problems broadband scale. **(A)** Caudate. **(B)** Putamen. **(C)** Nucleus Accumbens. **(D)** Amygdala. Voxels in significant clusters are opaque and boxed. Subthreshold voxels are presented translucently.

TABLE S16. Regions demonstrating significantly different associations with scores on the Attention Problems subscale compared with the Internalizing Problems broadband scale (n=9980).

Cluster	X	Y	Z	Peak-Z	Mean-Z	Size (voxels)	Overlap	Talairach label
Bilateral Caudate								
1	36	4	12	5.88	4.29	2494	28.00%	Right Superior Temporal Gyrus
							22.70%	Right Insula
							16.60%	Right Inferior Parietal Lobule
							12.30%	Right Postcentral Gyrus
							9.10%	Right Precentral Gyrus
							2.00%	Right Transverse Temporal Gyrus
2	-49	-11	-3	5.72	4.14	1355	52.40%	Left Superior Temporal Gyrus
							24.00%	Left Insula
							7.90%	Left Inferior Parietal Lobule
							6.80%	Left Transverse Temporal Gyrus
							4.20%	Left Postcentral Gyrus
							1.00%	Left Precentral Gyrus
3	30	-55	56	4.75	4.02	316	22.90%	Right Superior Parietal Lobule
							5.90%	Right Postcentral Gyrus
							4.70%	Right Precuneus
							1.90%	Right Inferior Parietal Lobule
4	-35	-43	52	5.18	4.09	254	37.40%	Left Inferior Parietal Lobule
							13.30%	Left Postcentral Gyrus
							7.10%	Left Superior Parietal Lobule

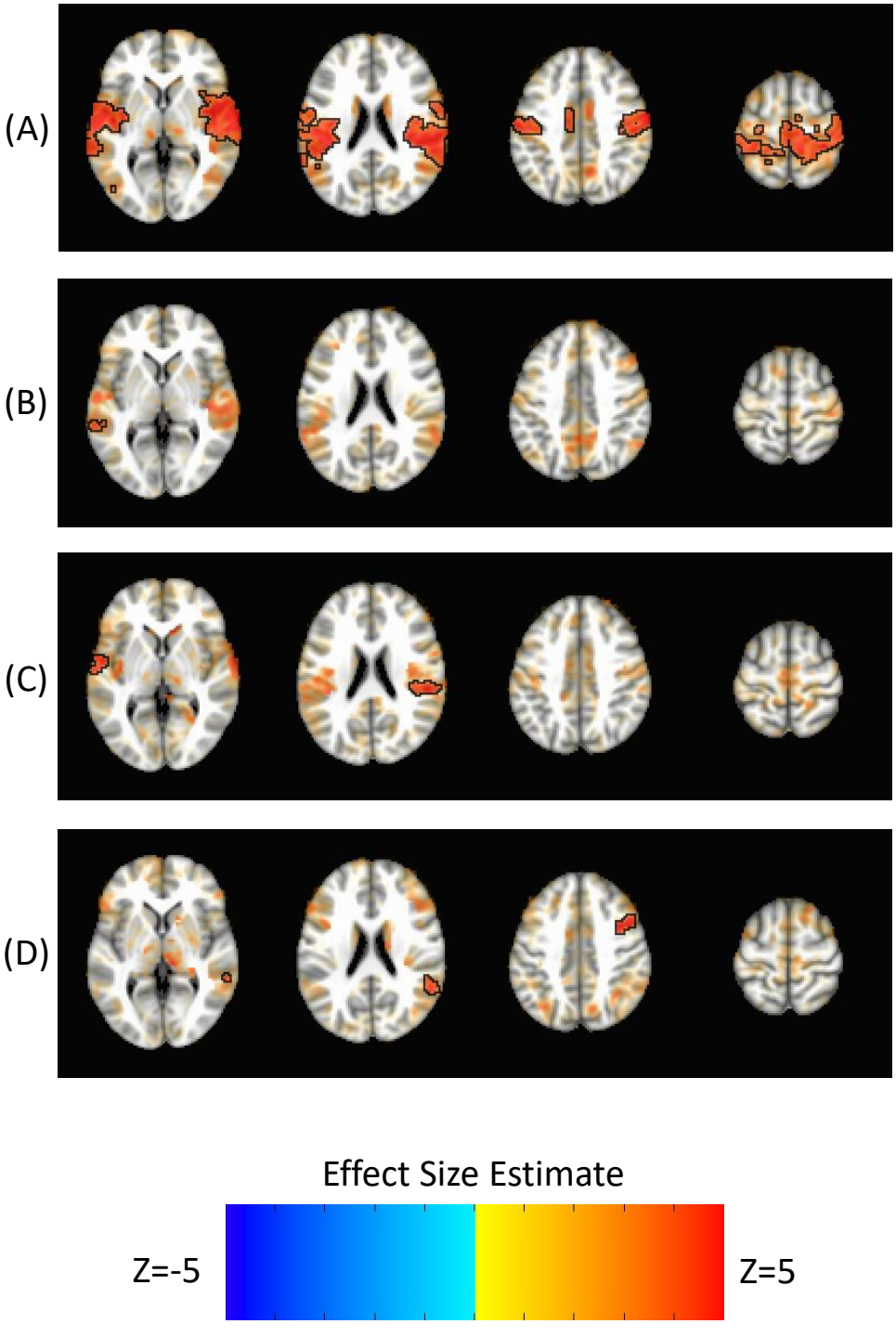

FIGURE S31. Shows regions demonstrating significantly different associations with scores on the Attention Problems subscale compared with the Externalizing Problems broadband scale. **(A)** Caudate. **(B)** Putamen. **(C)** Nucleus Accumbens. **(D)** Amygdala. Voxels in significant clusters are opaque and boxed. Subthreshold voxels are presented translucently.

TABLE S17. Regions demonstrating significantly different associations with scores on the Attention Problems subscale compared with the Externalizing Problems broadband scale (n=9980).

Cluster	X	Y	Z	Peak-Z	Mean-Z	Size (voxels)	Overlap	Talairach label
Bilateral Caudate								
1	-59	-13	6	7.74	4.47	13872	12.30%	Left Superior Temporal Gyrus
							12.00%	Right Superior Temporal Gyrus
							9.90%	Right Postcentral Gyrus
							8.10%	Right Precentral Gyrus
							7.60%	Left Postcentral Gyrus
							7.30%	Right Insula
							5.10%	Left Precentral Gyrus
							4.20%	Left Insula
							3.00%	Right Inferior Parietal Lobule
							2.60%	Left Middle Temporal Gyrus
							2.20%	Left Inferior Parietal Lobule
							1.90%	Right Paracentral Lobule
							1.60%	Right Medial Frontal Gyrus
							1.50%	Left Medial Frontal Gyrus
							1.10%	Right Middle Temporal Gyrus
							1.00%	Left Paracentral Lobule
							1.00%	Left Transverse Temporal Gyrus
Bilateral Putamen								

1	52	-11	-9	4.96	4.12	269	80.50%	Right Middle Temporal Gyrus
							7.70%	Right Inferior Temporal Gyrus
							3.80%	Right Superior Temporal Gyrus
							3.30%	Right Fusiform Gyrus
2	-67	-33	14	4.84	4.04	184	66.50%	Left Middle Temporal Gyrus
							33.10%	Left Superior Temporal Gyrus
Bilateral Nucleus Accumbens								
1	52	-31	22	5.31	4.25	470	42.10%	Right Inferior Parietal Lobule
							29.70%	Right Superior Temporal Gyrus
							11.10%	Right Insula
							10.90%	Right Postcentral Gyrus
2	-57	-5	2	5.21	4.18	325	57.10%	Left Superior Temporal Gyrus
							26.50%	Left Precentral Gyrus
							7.10%	Left Insula
							6.30%	Left Transverse Temporal Gyrus
Bilateral Amygdala								
1	48	12	44	6.03	4.34	397	84.10%	Right Middle Frontal Gyrus
							8.50%	Right Precentral Gyrus
							5.00%	Right Inferior Frontal Gyrus
2	62	-49	10	5.17	4.13	364	40.60%	Right Superior Temporal Gyrus

	34.30%	Right Middle Temporal Gyrus
	18.70%	Right Supramarginal Gyrus
	6.40%	Right Inferior Parietal Lobule

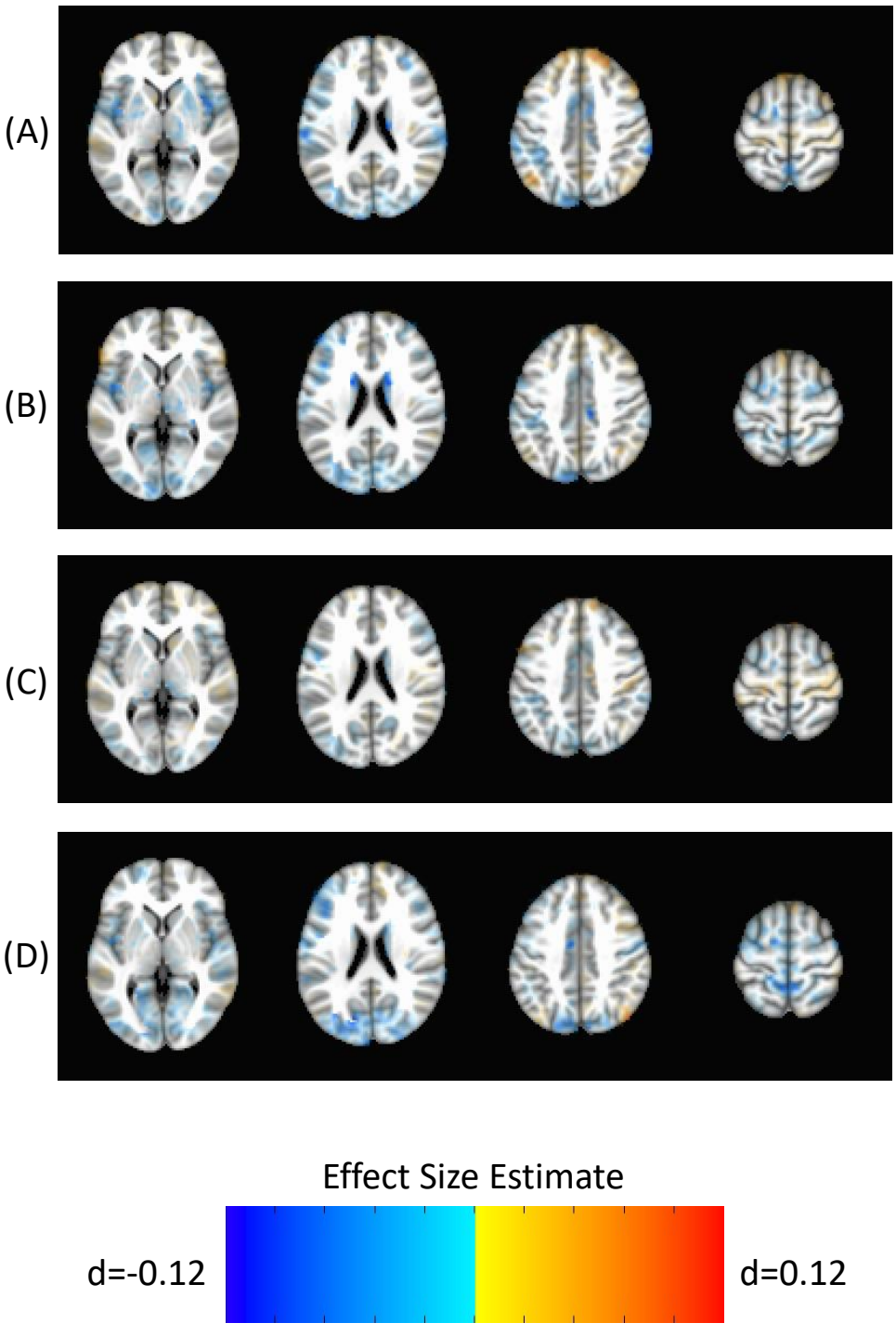

FIGURE S32. Findings from models assessing associations between seed-based subcortico-cortical connectivity and working memory performance. **(A)** Caudate. **(B)** Putamen. **(C)** Nucleus Accumbens. **(D)** Amygdala. Voxels in significant clusters are opaque and boxed. Subthreshold voxels are presented translucently.

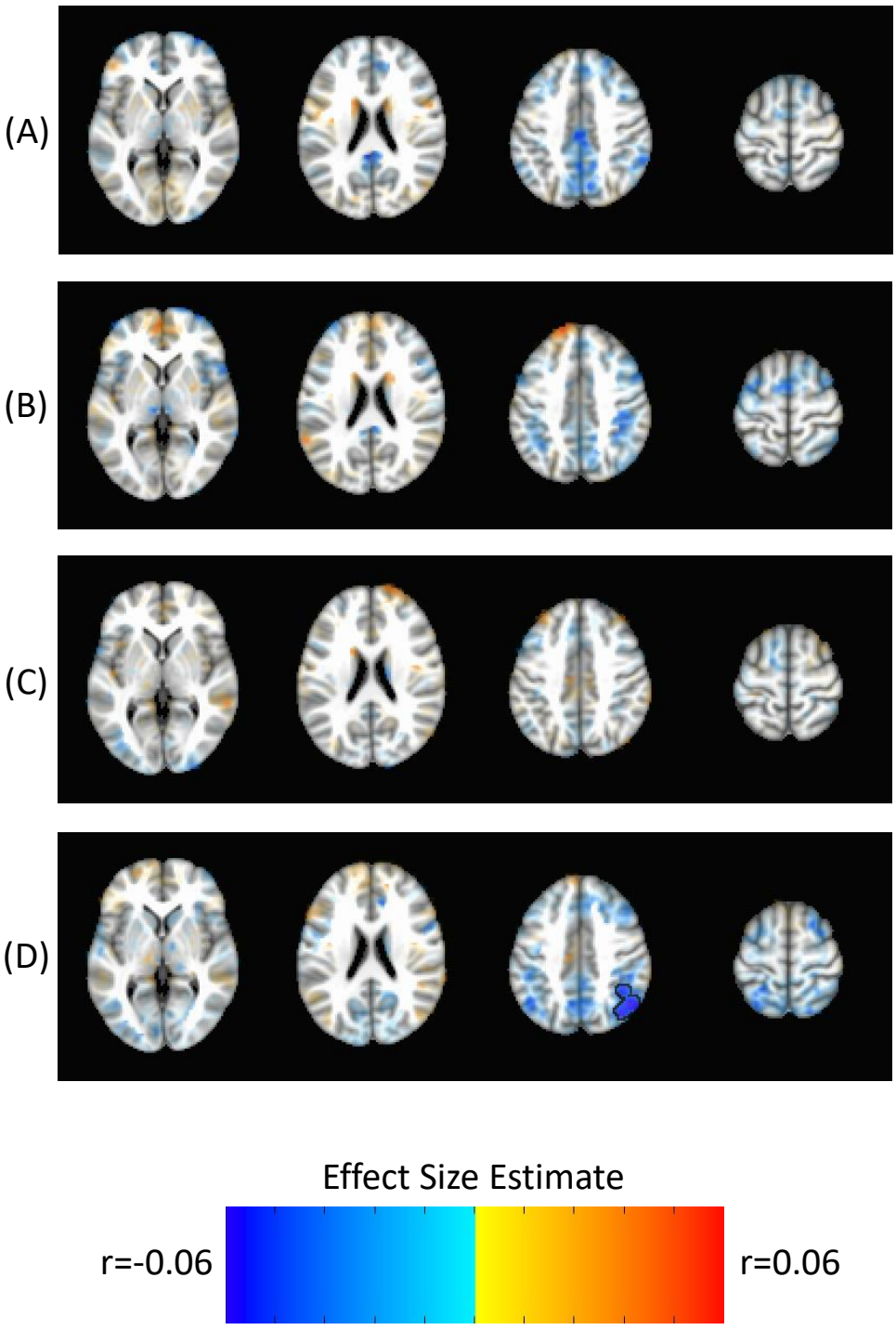

FIGURE S33. Findings from models assessing associations between seed-based subcortico-cortical connectivity and working memory performance. **(A)** Caudate. **(B)** Putamen. **(C)** Nucleus Accumbens. **(D)** Amygdala. Voxels in significant clusters are opaque and boxed. Subthreshold voxels are presented translucently.

TABLE S18. Significant associations between subcortico-cortical connectivity and working memory performance. n= 7245.

Cluster	X	Y	Z	Peak *partial-r*	Mean *patrial-r*	Size (voxels)	Overlap	Talairach label
Bilateral Amygdala								
1	48	-63	44	-0.07	-0.05	531	48.40%	Right Inferior Parietal Lobule
							10.10%	Right Precuneus
							9.00%	Right Superior Parietal Lobule
							5.40%	Right Angular Gyrus

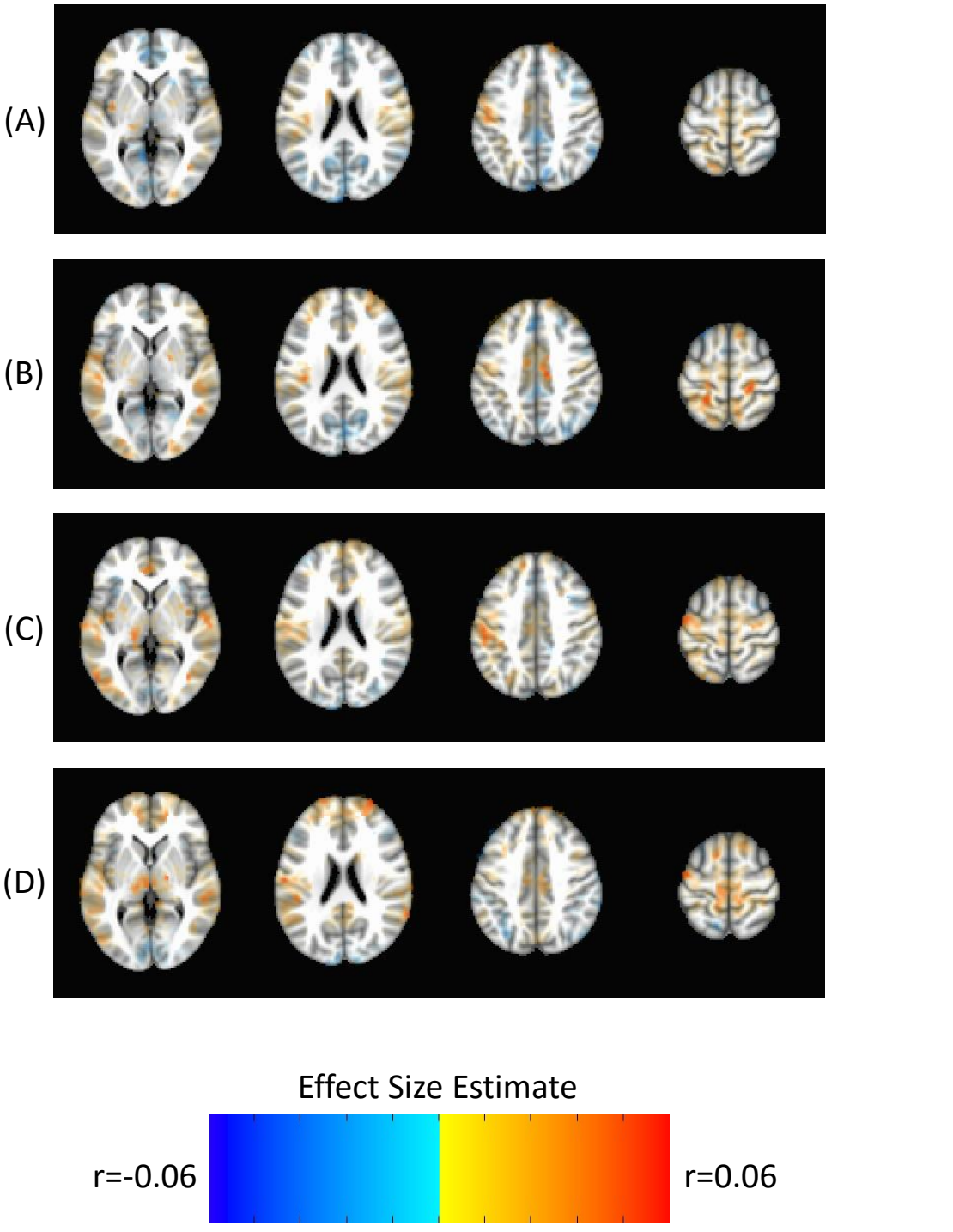

FIGURE S34. Findings from models assessing associations between seed-based subcortico-cortical connectivity and processing speed performance. **(A)** Caudate. **(B)** Putamen. **(C)** Nucleus Accumbens. **(D)** Amygdala. Subthreshold voxels are presented translucently.

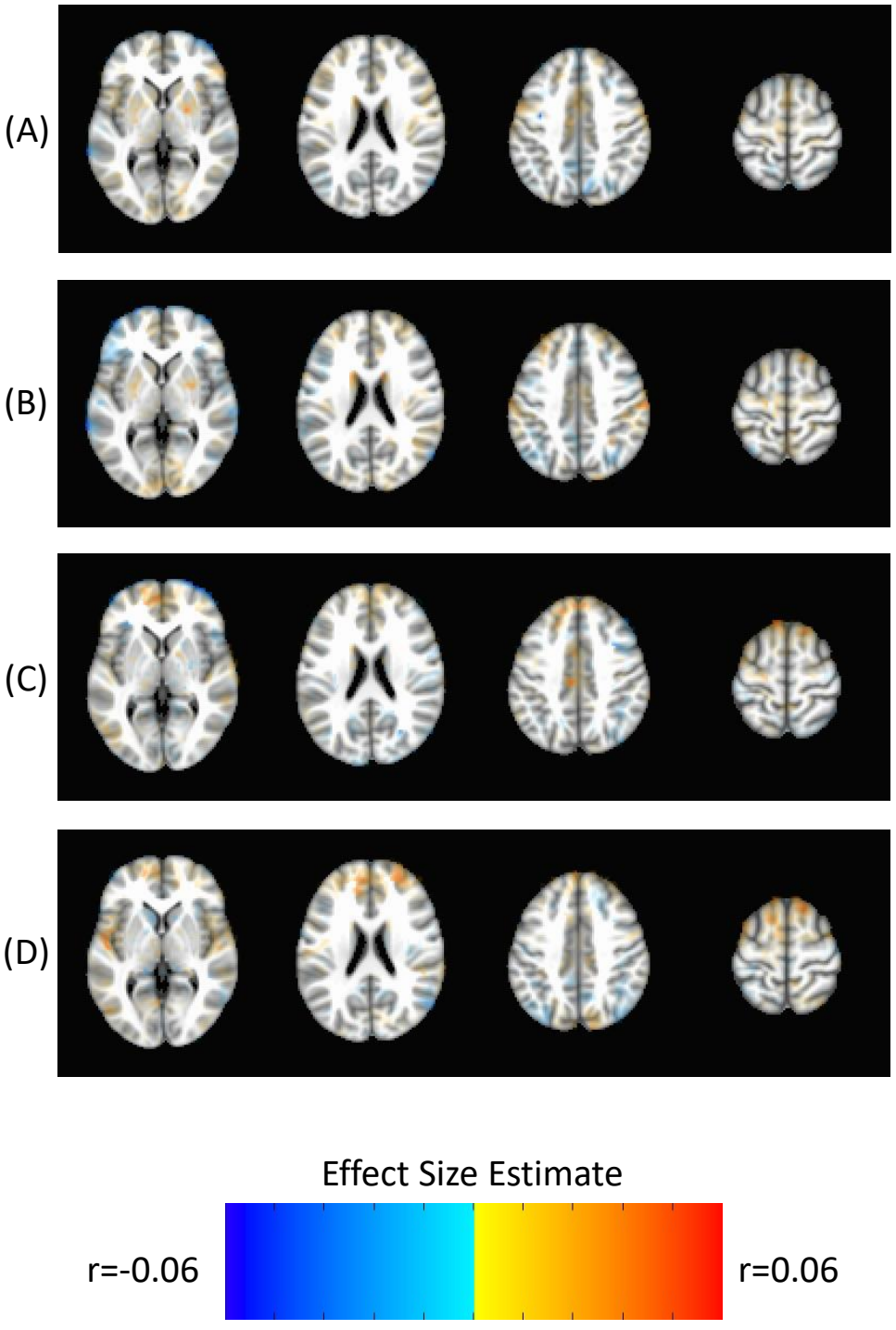

FIGURE S35. Findings from models assessing associations between seed-based subcortico-cortical connectivity and flanker task performance. **(A)** Caudate. **(B)** Putamen. **(C)** Nucleus Accumbens. **(D)** Amygdala. Subthreshold voxels are presented translucently.

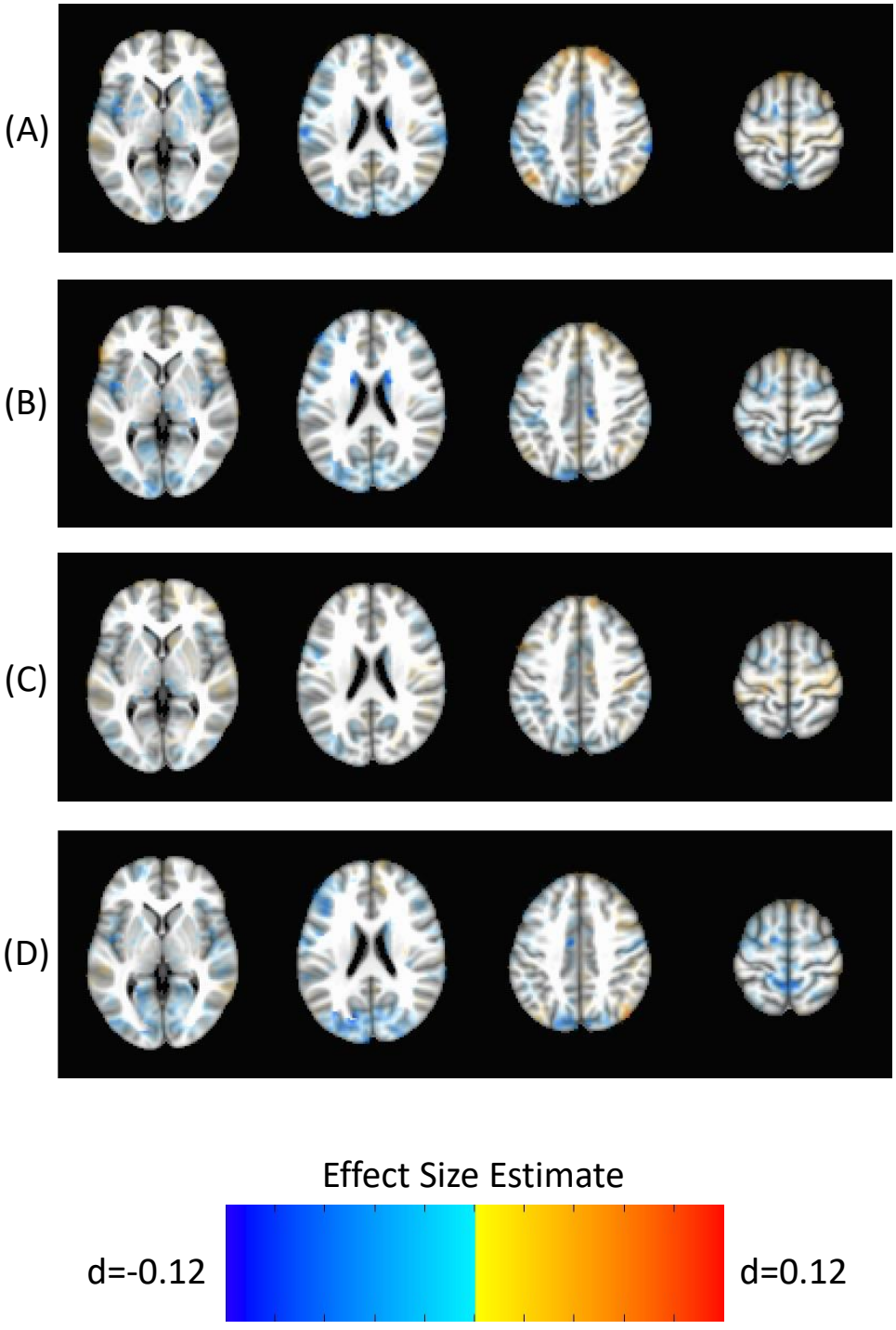

FIGURE S36. Findings from models assessing associations between seed-based subcortico-cortical connectivity and decision making on the cash choice task (3 Months >3 days). **(A)** Caudate. **(B)** Putamen. **(C)** Nucleus Accumbens. **(D)** Amygdala. Subthreshold voxels are presented translucently.

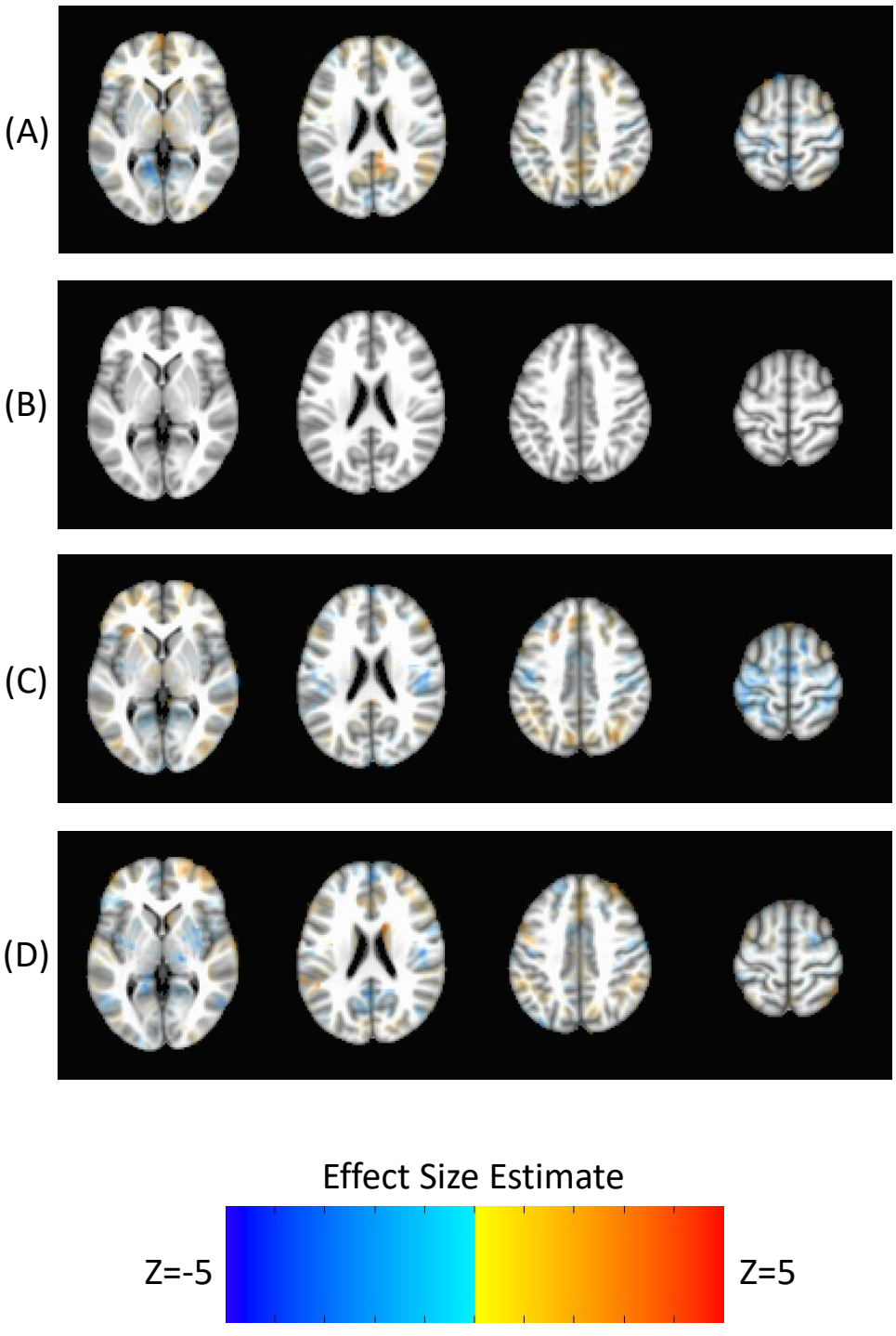

FIGURE S37. Findings from models assessing examining association between ADHD diagnosis and the linear effects of age. **(A)** Caudate. **(B)** Putamen. **(C)** Nucleus Accumbens. **(D)** Amygdala. Subthreshold voxels are presented translucently.

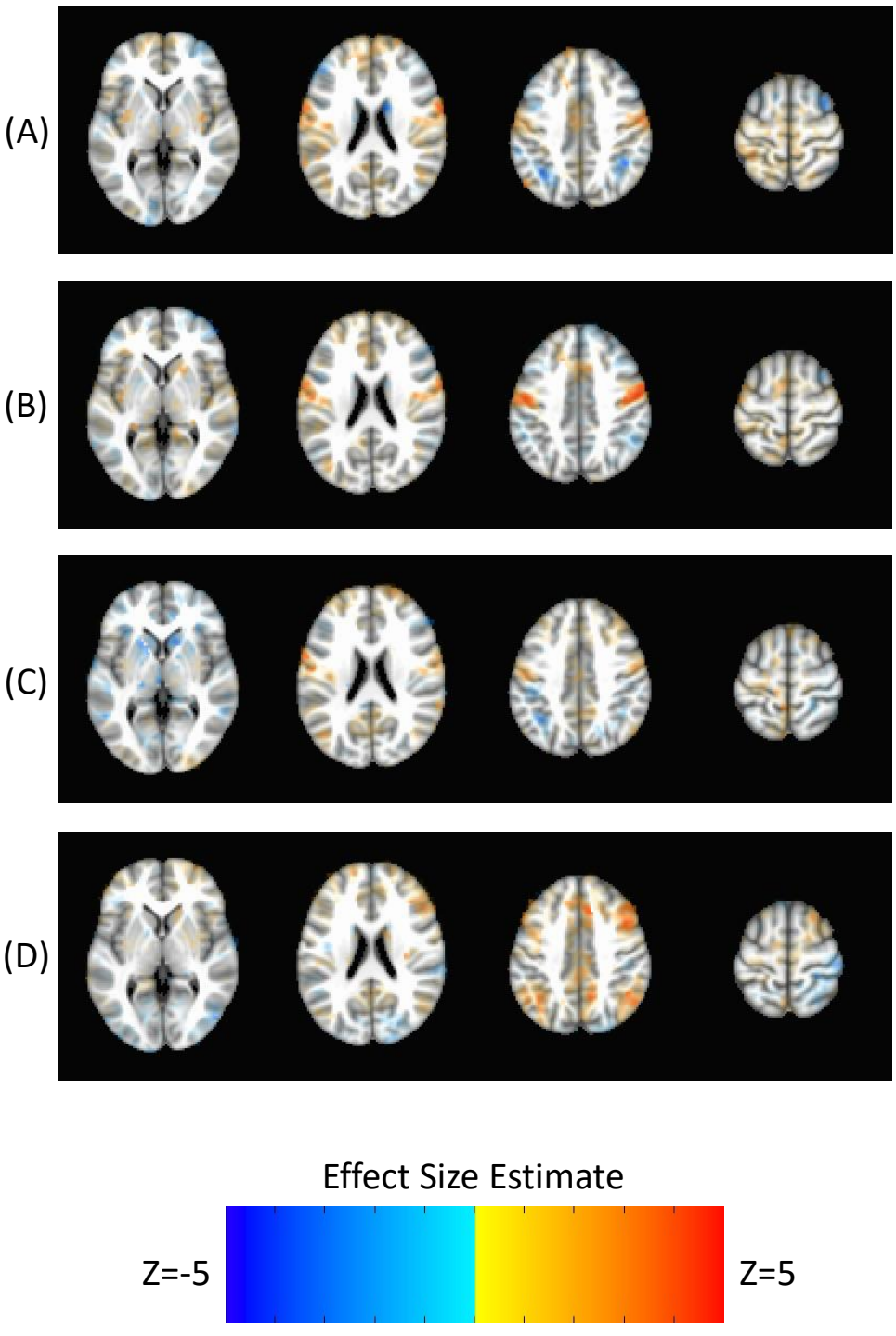

FIGURE S38. Findings from models assessing examining association between ADHD diagnosis and quadratic effects of age. **(A)** Caudate. **(B)** Putamen. **(C)** Nucleus Accumbens. **(D)** Amygdala. Subthreshold voxels are presented translucently.

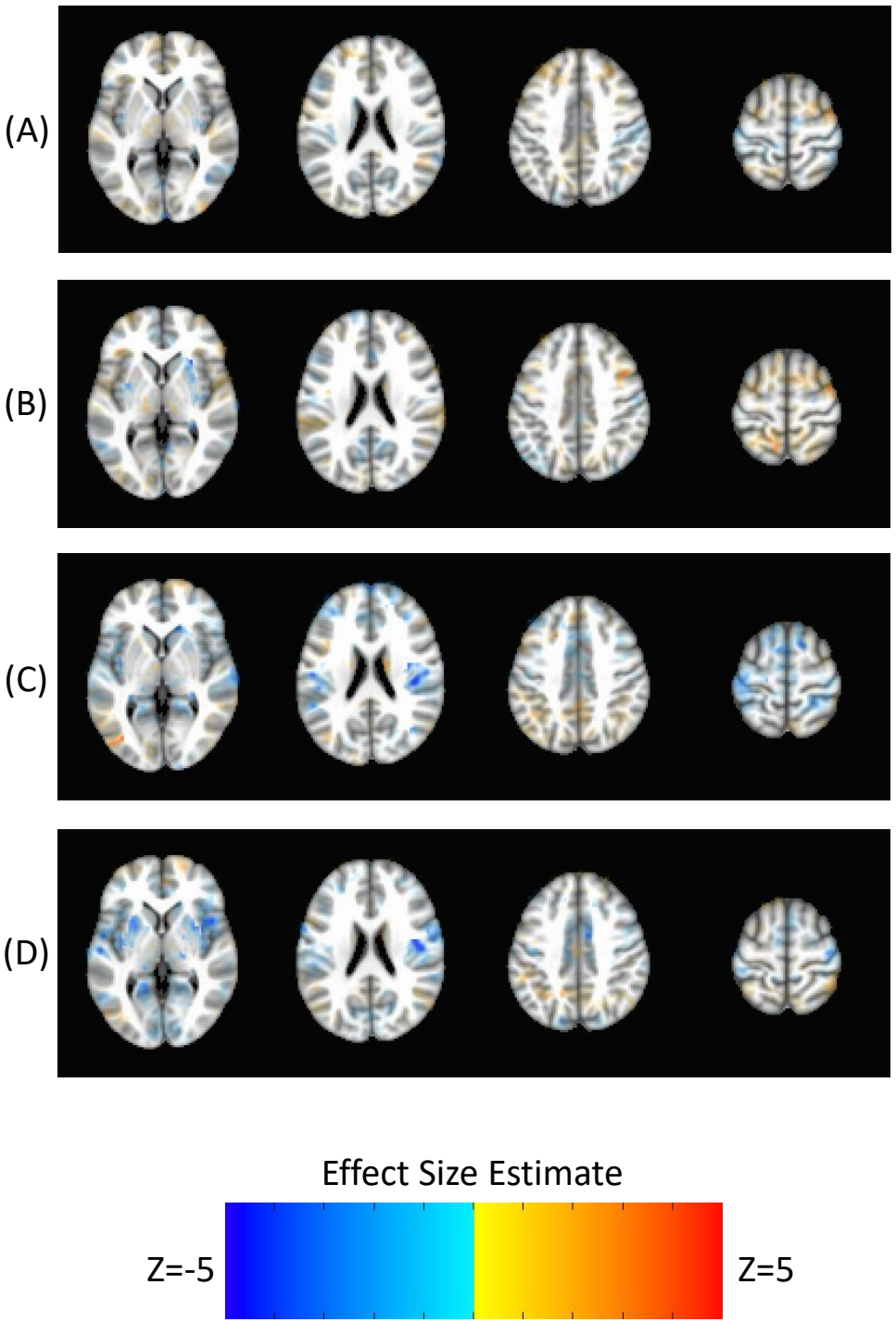

FIGURE S39. Findings from models assessing examining association between Attention Problems and the linear effects of age. **(A)** Caudate. **(B)** Putamen. **(C)** Nucleus Accumbens. **(D)** Amygdala. Subthreshold voxels are presented translucently.

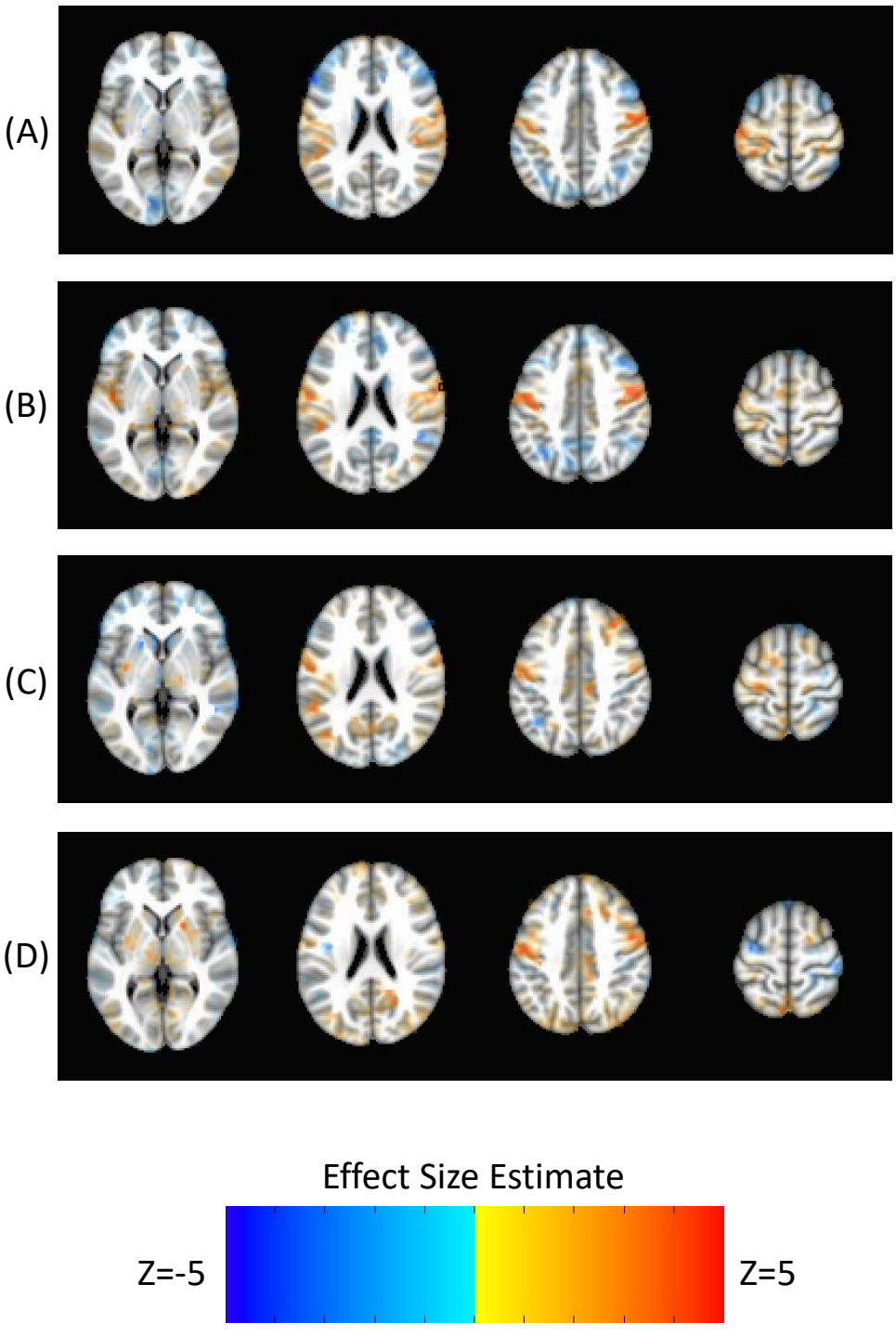

FIGURE S40. Findings from models assessing examining association between Attention Problems and the quadratic effects of age. **(A)** Caudate. **(B)** Putamen. **(C)** Nucleus Accumbens. **(D)** Amygdala. Subthreshold voxels are presented translucently.

TABLE S19. Significant interaction between Attention Problems and the quadratic effects of age on subcortico-cortical connectivity.

Cluster	X	Y	Z	Peak-Z	Mean-Z	Size (voxels)	Overlap	Talairach label
Bilateral Putamen								
1	66	-3	16	5.26	4.34	119	66.10%	Right Precentral Gyrus
							8.40%	Right Superior Temporal Gyrus
							5.20%	Right Postcentral Gyrus

Supplementary References

1. Casey BJ, Cannonier T, Conley MI, et al.: The adolescent brain cognitive development (ABCD) study: imaging acquisition across 21 sites. Developmental cognitive neuroscience 2018; 32:43–54

2. Hagler Jr DJ, Hatton S, Cornejo MD, et al.: Image processing and analysis methods for the Adolescent Brain Cognitive Development Study. Neuroimage 2019; 202:116091

3. Feczko E, Conan G, Marek S, et al.: Adolescent Brain Cognitive Development (ABCD) Community MRI Collection and Utilities. bioRxiv 2021;

4. Townsend L, Kobak K, Kearney C, et al.: Development of three web-based computerized versions of the Kiddie Schedule for affective disorders and schizophrenia child psychiatric diagnostic interview: preliminary validity data. Journal of the American Academy of Child & Adolescent Psychiatry 2020; 59:309–325

5. Cordova M, Antovich DM, Ryabinin P, et al.: ADHD: Restricted Phenotypes Prevalence, Comorbidity, and Polygenic Risk Sensitivity in ABCD Baseline Cohort2021;

6. Somerville LH, Bookheimer SY, Buckner RL, et al.: The Lifespan Human Connectome Project in Development: A large-scale study of brain connectivity development in 5–21 year olds. Neuroimage 2018; 183:456–468

7. Harms MP, Somerville LH, Ances BM, et al.: Extending the Human Connectome Project across ages: Imaging protocols for the Lifespan Development and Aging projects. Neuroimage 2018; 183:972–984

8. Norman LJ, Sudre G, Bouyssi-Kobar M, et al.: An examination of the relationships between attention/deficit hyperactivity disorder symptoms and functional connectivity over time. Neuropsychopharmacology 2021; 1–7

9. Reich W: Diagnostic interview for children and adolescents (DICA). Journal of the American Academy of Child & Adolescent Psychiatry 2000; 39:59–66

10. Brown SA, Brumback T, Tomlinson K, et al.: The National Consortium on Alcohol and NeuroDevelopment in Adolescence (NCANDA): a multisite study of adolescent development and substance use. Journal of studies on alcohol and drugs 2015; 76:895–908

11. Pfefferbaum A, Rohlfing T, Pohl KM, et al.: Adolescent development of cortical and white matter structure in the NCANDA sample: role of sex, ethnicity, puberty, and alcohol drinking. Cerebral cortex 2016; 26:4101–4121

12. Zhao Q, Sullivan EV, Honnorat N, et al.: Association of heavy drinking with deviant fiber tract development in frontal brain systems in adolescents. JAMA psychiatry 2021; 78:407–415

13. Müller-Oehring EM, Kwon D, Nagel BJ, et al.: Influences of age, sex, and moderate alcohol drinking on the intrinsic functional architecture of adolescent brains. Cerebral Cortex 2018; 28:1049–1063

14. Pohl KM, Sullivan EV, Pfefferbaum A: The NCANDA_PUBLIC_BASE_RESTINGSTATE_V01 Data Release of the National Consortium on Alcohol and NeuroDevelopment in Adolescence (NCANDA) [Internet]. Sage Bionetworks Synapse 2017; [cited 2021 Sep 9] Available from: https://dx.doi.org/10.7303/syn11605291

15. Pohl KM, Sullivan EV, Pfefferbaum A: The NCANDA_PUBLIC_BASE_STRUCTURAL_V01 Data Release of the National Consortium on Alcohol and NeuroDevelopment in Adolescence (NCANDA) [Internet]. Sage Bionetworks Synapse 2017; [cited 2021 Sep 9] Available from: https://dx.doi.org/10.7303/syn11541569

16. Tobe RH, MacKay-Brandt A, Lim R, et al.: A longitudinal resource for studying connectome development and its psychiatric associations during childhood. Scientific Data 2022; 9:300

17. Nooner KB, Colcombe SJ, Tobe RH, et al.: The NKI-Rockland sample: a model for accelerating the pace of discovery science in psychiatry. Frontiers in neuroscience 2012; 6:152

18. Wechsler D: WASI-II: Wechsler abbreviated scale of intelligence.2011;

19. Ai L, Craddock RC, Tottenham N, et al.: Is it time to switch your T1W sequence? Assessing the impact of prospective motion correction on the reliability and quality of structural imaging. NeuroImage 2021; 226:117585

20. Esteban O, Markiewicz CJ, Blair RW, et al.: fMRIPrep: a robust preprocessing pipeline for functional MRI. Nature methods 2019; 16:111–116

21. Gorgolewski K, Burns CD, Madison C, et al.: Nipype: a flexible, lightweight and extensible neuroimaging data processing framework in python. Frontiers in neuroinformatics 2011; 5:13

22. Tustison NJ, Avants BB, Cook PA, et al.: N4ITK: improved N3 bias correction. IEEE transactions on medical imaging 2010; 29:1310–1320

23. Jenkinson M, Bannister P, Brady M, et al.: Improved optimization for the robust and accurate linear registration and motion correction of brain images. Neuroimage 2002; 17:825–841

24. Ciric R, Wolf DH, Power JD, et al.: Benchmarking of participant-level confound regression strategies for the control of motion artifact in studies of functional connectivity. Neuroimage 2017; 154:174–187

25. Ciric R, Rosen AFG, Erus G, et al.: Mitigating head motion artifact in functional connectivity MRI. Nat Protoc 2018; 13:2801–2826

26. Gur RE, Moore TM, Rosen AFG, et al.: Burden of Environmental Adversity Associated With Psychopathology, Maturation, and Brain Behavior Parameters in Youths. JAMA Psychiatry 2019; 76:966–975

27. Cui Z, Li H, Xia CH, et al.: Individual variation in functional topography of association networks in youth. Neuron 2020;

28. Gu S, Xia CH, Ciric R, et al.: Unifying the Notions of Modularity and Core–Periphery Structure in Functional Brain Networks during Youth. Cerebral Cortex 2020; 30:1087–1102

29. Cox RW: AFNI: software for analysis and visualization of functional magnetic resonance neuroimages. Computers and Biomedical research 1996; 29:162–173

30. Hallquist MN, Hwang K, Luna B: The nuisance of nuisance regression: spectral misspecification in a common approach to resting-state fMRI preprocessing reintroduces noise and obscures functional connectivity. Neuroimage 2013; 82:208–225

31. Jenkinson M, Beckmann CF, Behrens TE, et al.: Fsl. Neuroimage 2012; 62:782–790

32. Desikan RS, Ségonne F, Fischl B, et al.: An automated labeling system for subdividing the human cerebral cortex on MRI scans into gyral based regions of interest. Neuroimage 2006; 31:968–980

33. Norman L, Lawrence N, Iles A, et al.: Attachment-security priming attenuates amygdala activation to social and linguistic threat. Social Cognitive and Affective Neuroscience 2015; 10:832–839

34. Norman LJ, Sudre G, Bouyssi-Kobar M, et al.: A Longitudinal Study of Resting-State Connectivity and Response to Psychostimulant Treatment in ADHD. American Journal of Psychiatry 2021; appi. ajp. 2021.20091342

35. Di Martino A, Scheres A, Margulies DS, et al.: Functional connectivity of human striatum: a resting state FMRI study. Cerebral cortex 2008; 18:2735–2747

36. Gianaros PJ, Hariri AR, Sheu LK, et al.: Preclinical atherosclerosis covaries with individual differences in reactivity and functional connectivity of the amygdala. Biological psychiatry 2009; 65:943–950

37. Kim S: ppcor: an R package for a fast calculation to semi-partial correlation coefficients. Communications for statistical applications and methods 2015; 22:665

38. Kuznetsova A, Brockhoff PB, Christensen RH: lmerTest package: tests in linear mixed effects models. Journal of statistical software 2017; 82:1–26

39. Hughett P: Accurate computation of the F-to-z and t-to-z transforms for large arguments. Journal of Statistical Software 2008; 23:1–5

40. Ben-Shachar MS, Lüdecke D, Makowski D: effectsize: Estimation of effect size indices and standardized parameters. Journal of Open Source Software 2020; 5:2815

41. Fox J, Weisberg S: An R companion to applied regression. Sage publications, 2011

42. Yan C-G, Wang X-D, Zuo X-N, et al.: DPABI: data processing & analysis for (resting-state) brain imaging. Neuroinformatics 2016; 14:339–351

43. Satterthwaite TD, Wolf DH, Ruparel K, et al.: Heterogeneous impact of motion on fundamental patterns of developmental changes in functional connectivity during youth. Neuroimage 2013; 83:45–57

44. Sudre G, Norman L, Bouyssi-Kobar M, et al.: A mega-analytic study of white matter microstructural differences across five cohorts of youth with attention deficit hyperactivity disorder. Biological Psychiatry 2022;

45. Arnsten AF, Rubia K: Neurobiological circuits regulating attention, cognitive control, motivation, and emotion: disruptions in neurodevelopmental psychiatric disorders. Journal of the American Academy of Child & Adolescent Psychiatry 2012; 51:356–367

46. Norman LJ, Carlisi C, Lukito S, et al.: Structural and functional brain abnormalities in attention-deficit/hyperactivity disorder and obsessive-compulsive disorder: a comparative meta-analysis. JAMA psychiatry 2016; 73:815–825

47. Lipszyc J, Schachar R: Inhibitory control and psychopathology: a meta-analysis of studies using the stop signal task. Journal of the International Neuropsychological Society: JINS 2010; 16:1064

48. Wright L, Lipszyc J, Dupuis A, et al.: Response inhibition and psychopathology: A meta-analysis of go/no-go task performance. Journal of Abnormal Psychology 2014; 123:429

49. Willcutt EG, Doyle AE, Nigg JT, et al.: Validity of the executive function theory of attention-deficit/hyperactivity disorder: a meta-analytic review. Biological psychiatry 2005; 57:1336–1346

50. Mowinckel AM, Pedersen ML, Eilertsen E, et al.: A meta-analysis of decision-making and attention in adults with ADHD. Journal of attention disorders 2015; 19:355–367

51. Huang-Pollock CL, Karalunas SL, Tam H, et al.: Evaluating vigilance deficits in ADHD: a meta-analysis of CPT performance. Journal of abnormal psychology 2012; 121:360

52. Martinussen R, Hayden J, Hogg-Johnson S, et al.: A meta-analysis of working memory impairments in children with attention-deficit/hyperactivity disorder. Journal of the American academy of child & adolescent psychiatry 2005; 44:377–384

53. Jackson JN, MacKillop J: Attention-deficit/hyperactivity disorder and monetary delay discounting: a meta-analysis of case-control studies. Biological Psychiatry: Cognitive Neuroscience and Neuroimaging 2016; 1:316–325

54. Amlung M, Marsden E, Holshausen K, et al.: Delay discounting as a transdiagnostic process in psychiatric disorders: a meta-analysis. JAMA psychiatry 2019; 76:1176–1186

55. Nigg JT, Willcutt EG, Doyle AE, et al.: Causal Heterogeneity in Attention-Deficit/Hyperactivity Disorder: Do We Need Neuropsychologically Impaired Subtypes? Biological Psychiatry 2005; 57:1224–1230

56. Norman LJ, Carlisi CO, Christakou A, et al.: Neural dysfunction during temporal discounting in paediatric attention-deficit/hyperactivity disorder and obsessive-compulsive disorder. Psychiatry Research: Neuroimaging 2017; 269:97–105

57. Schaefer A, Gray JR: A role for the human amygdala in higher cognition. Reviews in the Neurosciences 2007; 18:355–364

58. West HV, Burgess GC, Dust J, et al.: Amygdala activation in cognitive task fMRI varies with individual differences in cognitive traits. Cognitive, Affective, & Behavioral Neuroscience 2021; 21:254–264

59. Weintraub S, Dikmen SS, Heaton RK, et al.: Cognition assessment using the NIH Toolbox. Neurology 2013; 80:S54–S64